Tropical Cyclones (TCs) Risk Assessment in South Asia: Focusing on the Coastal Areas of Bangladesh

by

Syeda Nazifa Tasneem

A thesis submitted to the Graduate Faculty of
Auburn University
in partial fulfillment of the
requirements for the Degree of
Master of Science

Auburn, Alabama
May 06, 2023

Keywords: Tropical Cyclone, Social Vulnerability Index, Analytical Hierarchy Process, Vulnerability, Risk, Mangrove

Approved by

Chandana Mitra, Chair, Associate Professor of Geosciences
Luke Marzen, Professor of Geosciences
Ashraf Dewan, Associate Professor of School of Earth and Planetary Sciences

Abstract

Tropical cyclones recurrently batter the coastal regions of Bangladesh. It causes a lot of damage in the less resilient regions, especially the cities. This study aims to pinpoint the areas that are both physically and socially susceptible to tropical cyclones using the Analytical Hierarchy Process (AHP), Principal Component Analysis (PCA), and various geospatial techniques. The results indicated higher social vulnerability in the western and central regions of coastal Bangladesh. In addition, the areas near the Bay of Bengal exhibited higher overall social and physical risk than others. However, throughout time, the central coast showed the maximum risk level among all. Additionally, the Sundarbans mangrove forest located in the Indian territory showed poor health and degraded forest, which suggests that tropical cyclones might have disrupted the forests. The findings obtained in this study will be beneficial to the emergency responders and policymakers in coastal area management and disaster risk reduction.

Acknowledgment

The author would like to thank the Almighty for the strength and good health that He bestowed upon her to finish this study. The author is exceedingly grateful to her major professor, Dr. Chandana Mitra, who has been a great mentor; for her endless support, motivation, guidance, and valuable time to enlighten her in this endeavor. The author appreciates her committee members, Dr. Luke Marzen and Dr. Ashraf Dewan, for all their valuable knowledge, insightful comments, and guidance they provided when needed throughout her journey. The author would like to express gratitude towards them for their unconditional help.

The author is thankful enough to her UrbanPrism lab mates: Megha, Miranda, Subhasis, and Sukannya, for their constant support and motivation. A special thanks to the Department of Geosciences for all the support during her term at Auburn University.

The author is thankful to Dr. Asif Ishtiaque, Dr. Christopher Burton, Dr. Debajit Datta, and Masudur Rahman for their insightful comments on her research. The author appreciates the help of WARPO and CEGIS for providing her with valuable data for this research.

Last but not least, the author would like to thank her parents and sisters for their continuous support and encouragement.

Table of Contents

List of Tables

List of Figures

List of Abbreviations

BFD Bangladesh Forest Department

CEGIS Centre for Environmental and Geographic Information Services

EM-DAT Epidemiology of Disasters. Emergency Events Database

FEMA Federal Emergency Management Agency

UNESCO The United Nations Educational, Scientific and Cultural Organization

WMO World Meteorological Organization

CHAPTER 01

INTRODUCTION

1.1 Background

Natural hazards have always been an integral part of the Earth's system, causing damage and devastation to the environment (Agrawal, 2018; FEMA, 2023; WMO, 2022a). The frequency of natural disasters has grown five times between 1970 to 2021, with the most significant increase attributed to hydrometeorological disasters, such as storms and floods (WMO, 2021). Tropical cyclones (TCs) are also referred to as typhoons and hurricanes, depending on their forming locations on the globe (Shultz et al., 2014). TCs are one of the most catastrophic and deadliest hydrometeorological natural disasters in tropical and sub-tropical latitudes (Hoque et al., 2018; Regnier & Harr, 2006). Even in their initial period of development, TCs batter many shore and sea-surrounded regions across the world (Hoque et al., 2018; Peduzzi et al., 2012; WMO, 2022b). The intensity and impact of this natural disaster are alarming. Often tropical cyclones are accompanied by multi-hazards such as gusty winds, torrential rainfall triggering floods and landslides, and intensive storm surges that mainly hit the coastal regions (UNDRR, 2017; WMO, 2022b; Zhou et al., 2018). They have the ability to collapse the communication network and cause many causalities and massive property and environmental damages (Dube et al., 2009; Gaona et al., 2018; Hoque et al., 2018; Peduzzi et al., 2012; Zhou et al., 2018). TCs are low-pressure weather systems, and warm tropical oceans are one of the key prerequisites (Fig 1.1) for the formation of these storms that can cause terrible damage when they make landfall (Mohapatra et al., 2014). As illustrated in Fig. 1.1, additional key formation factors

include atmospheric instability and pre-existing near-surface disturbance, moderately moist air, a vertical wind speed of roughly 23 mph, and the Coriolis force (Gray, 1998).

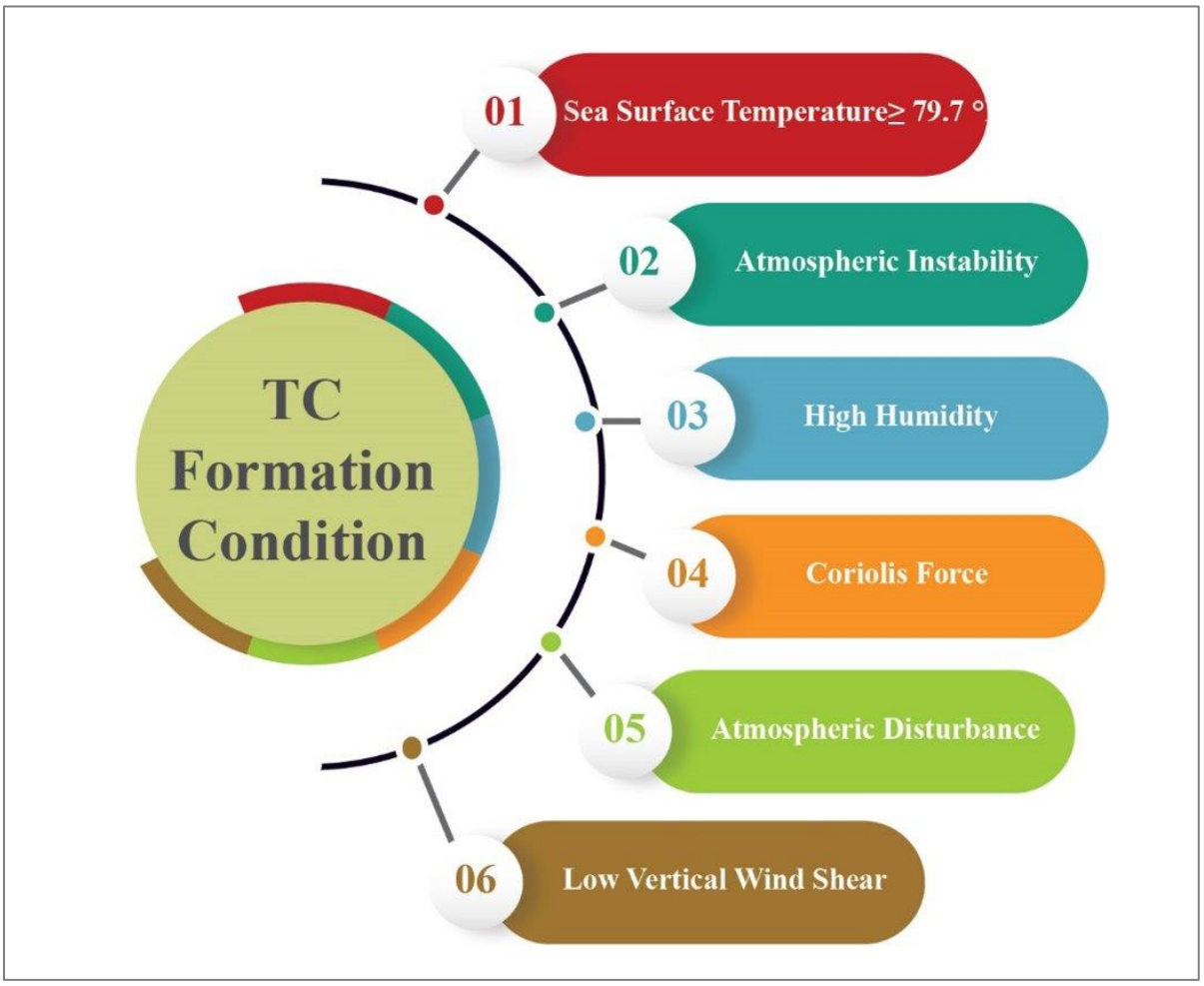

Fig 1.1: Tropical cyclone formation conditions

TCs are the second most prevalent global disaster, representing 17% of all disasters (WMO, 2021). It is documented that, over the past five decades (1970 – 2019), they have consistently taken a toll on human lives, accounting for 779,324 or 38% of disaster-related mortality (Hoque et al., 2016; Pielke et al., 2008; WMO, 2021). Moreover, a financial loss of about 1.4 trillion USD was caused by 1,942 TCs during the same period (WMO, 2022b).

Worldwide, oceans in tropical latitudes produce 80 to 90 tropical cyclones per year on average; however, only around 40 to 50 of them make landfall with a wind speed of at least 33 ms^{-1}, which correspondents to the strength of hurricanes, typhoons, or severe TCs (Frank & Young, 2007). From 1970 to 2019, economic losses in North America, Central America, and the Caribbean region reached a peak (Fig. 1.2), while Asia recorded the highest number of cyclonic mortality and frequency (WMO, 2021).

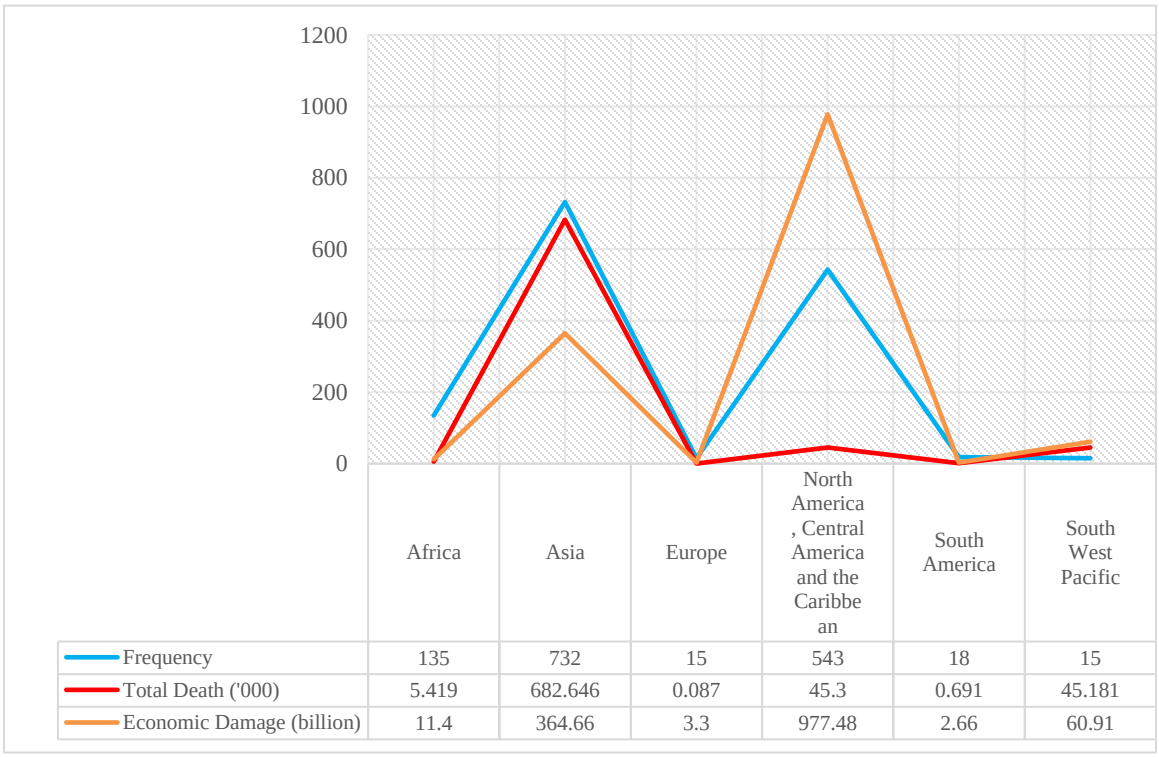

	Africa	Asia	Europe	North America, Central America and the Caribbean	South America	South West Pacific
Frequency	135	732	15	543	18	15
Total Death ('000)	5.419	682.646	0.087	45.3	0.691	45.181
Economic Damage (billion)	11.4	364.66	3.3	977.48	2.66	60.91

Fig 1.2: Casualties caused by tropical cyclones from 1970 to 2019 (adapted from WMO (2021)

Bangladesh and India - two South Asian nations are at grave risk of tropical cyclones in the North Indian Ocean (NIO), which is also recognized as one of the breeding grounds for cyclogenesis activity (Mohapatra et al., 2014; Wahiduzzaman & Yeasmin, 2019). The Bay of Bengal (BoB), which is a sub-basin in the eastern part of the NIO, is one of the deadliest TCs

hotspots, with an average of 4 out of 5 TCs originating every year, putting coastal nations at risk of cyclonic mortality (Mohapatra et al., 2014; Sharma et al., 2022). It forms around 5.5% of global TCs, and Bangladesh is struck by approximately 1% of them (Alam & Dominey-Howes, 2015; Rahman & Rahman, 2015). Despite experiencing relatively fewer TCs than its neighboring country India (Fig. 1.3), Bangladesh alone encountered 60% of the global mortality caused by TCs from 1990 to 2010 (Rahman & Rahman, 2015; Rana, 2013; WMO, 2021). According to the chronological records, among the ten deadliest TCs, seven were in South Asia, where

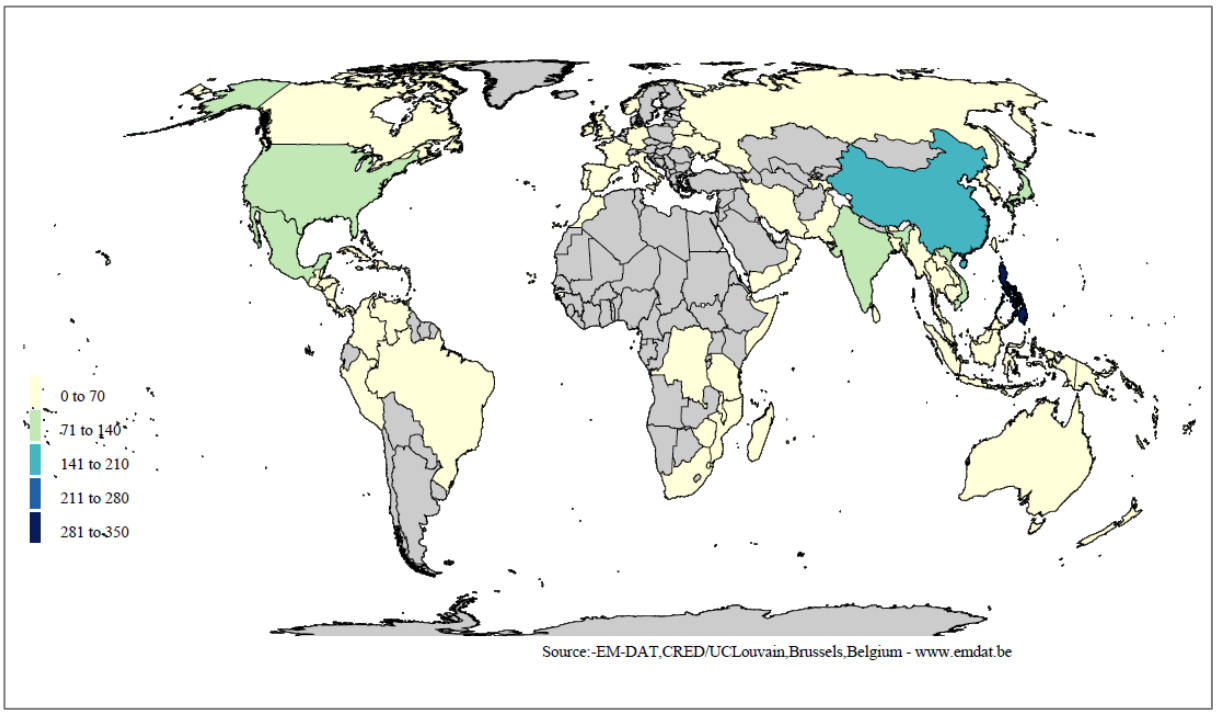

Fig 1.3: Tropical cyclone frequencies around the globe from 1970-2023 (Source: EM-DAT)

Bangladesh was the most vulnerable country, with more than half a million cyclonic deaths attributed to only two tropical cyclones from 1970 to 2008 (Defu et al., 2013). Overpopulation, flat coastal terrain, deltaic systems, and inadequate disaster preparedness exacerbate disaster damage in the NIO basin, even though TCs are relatively rare compared to other basins. Whether

climate change will increase the number of TCs is still up for debate; however, a positive trend with regard to TCs intensity and extreme cyclonic flooding might be possible in the future (Mitchell et al., 2022; Woodruff et al., 2013).

Bangladesh is in the Ganges-Brahmaputra-Meghna (GBM) delta, which is highly vulnerable to disasters due to the concentrated population and its exposure to environmental challenges like natural hazards (Gain et al., 2022; Rahman et al., 2020). Moreover, Bangladesh is at the frontline of the battle against climate change. According to the long-term global climate risk index (CRI) 2020, Bangladesh ranked seventh among the ten most affected countries from 2000-2019 regarding extreme weather events (Eckstein et al., 2021). Nevertheless, Bangladesh has implemented and emphasized mitigation strategies that have cut cyclone-related mortality down by over 100-folds in the past 38 years (Haque et al., 2012). This is exemplified by the differences in mortality in the 1970 Bhola cyclone, which experienced 500,000 deaths, compared to the Sidr cyclone in 2007, which experienced 4234 deaths. However, cyclone Sidr, a category-4 storm with a high tidal surge, left millions of people homeless despite the fact that a large-scale evacuation of about 3 million people was carried out prior to its landfall (Haque et al., 2012). It also caused long-term damage, like salinity intrusion, and destroyed millions of acres of crops and livestock (Haque et al., 2012). The damages escalate in these regions mainly because of inaccurate warning systems and poor city planning (Quader et al., 2017).

Catastrophic disturbances, such as TCs, can damage the structure and function of coastal forests, which serve as a key component in attenuating storm intensity and protecting coastal communities (Alongi, 2008; Everham & Brokaw, 1996; Hochard et al., 2019; Xi, 2015). Globally, the extent of mangroves has decreased by approximately 524,524 ha between 1996 and 2020, and studies showed that tropical cyclones over six decades are responsible for around 45%

of the reported global mangrove destruction (Bunting et al., 2022; Sippo et al., 2018). The Sundarbans mangrove forest, rich in biodiversity and a UNESCO World Heritage Site, is one of the areas most affected by TCs in Southeast Asia. This is the world's largest continuous mangrove forest (~3861 sq mi), covering around 2323 sq mi areas of Bangladesh and 1358 sq mi areas in India (West Bengal) (BFD, 2023; Ghosh et al., 2015; Mahmood et al., 2021). Super cyclone Sidr alone damaged around 21% of the total area of the Sundarbans mangrove forest, where around 965 sq mi areas of Bangladesh's Sundarbans were impacted (Bhowmik & Cabral, 2013; Khan, 2016). After cyclone Sidr, approximately 618 sq mi of Sundarbans forest were damaged by cyclone Amphan (Sen, 2020). Not only are the mangroves resourceful for the economy, but they also act as a natural barrier, reducing the intensity of natural calamities like TCs and tsunamis which in turn protect the coastal communities.

1.2 Goal and Objectives

This research focused on two main components of disaster management: place-based risk assessment and the health of the mangrove forest. The specific objectives of this study are the following:

A. **The first research objective** is to develop a social vulnerability map for the coastal regions of Bangladesh emphasizing TCs.

   The tasks performed to create the risk map are-

i. Developing an index to assess social vulnerability focusing on (a) demographic, (b) socio-economic, and (c) special need criteria.

B. **The second research objective** is to develop a physical vulnerability and TCs risk map for the coastal regions of Bangladesh.

   The steps were followed to develop the risk map -

i. Assessing physical vulnerability considering (a) elevation, (b) slope, (c) population density, (d) land cover, (e) proximity to cyclone track, and (f) proximity to the coastline.

ii. Analyzing hazard by (a) TCs frequency, (b) TCs wind speed, (c) storm surge height, and (d) rainfall.

iii. Observing mitigation capacity with the proximity to (a) cyclone shelter, (b) health facility, and (c) paved road network

iv. Preparing a cyclone risk map by integrating physical and social vulnerability parameters

C. **The third research objective** is to analyze the vegetation and degradation status of the Sundarbans Mangrove forests.

The tasks performed to analyze these are-

i. Analyzing short-term pre and post-cyclone periods and long-term yearly average NDVI to monitor the changes in the forest's vegetation health caused by the disaster.

ii. Observing the immediate disturbance of tropical cyclones in the forest by using the modified Radar Forest Degradation Index (mRFDI)

1.3 Study Area

The 19 coastal districts (Fig 1.4) of Bangladesh account for 32 percent of the country's geographic area and occupy approximately 18224 sq miles which is the residence of around 35 million people, or 28% of the country's population (BBS, 2011; Moslehuddin et al., 2015; World Bank, 2019). This entire coastal zone of Bangladesh is divided into two distinct regions considering the proximity to the Bay of Bengal. The most vulnerable coastal region to climate change is the exposed coastal region (Fig 1.4) which includes 12 coastal districts and 48 local government territories or upazilas (counties) and converges with the sea directly. On the other hand, 67% of upazilas (counties) are in the interior region (Fig 1.4), that is impacted by tidal

functions, and do not meet the sea or lower estuary directly (Moslehuddin et al., 2015; Parvin et al., 2010). Based on their geomorphic and topographic criteria, both exposed and interior coastal areas are further subdivided into western, central, and eastern parts (Fig 1.4) (Quader et al., 2017).

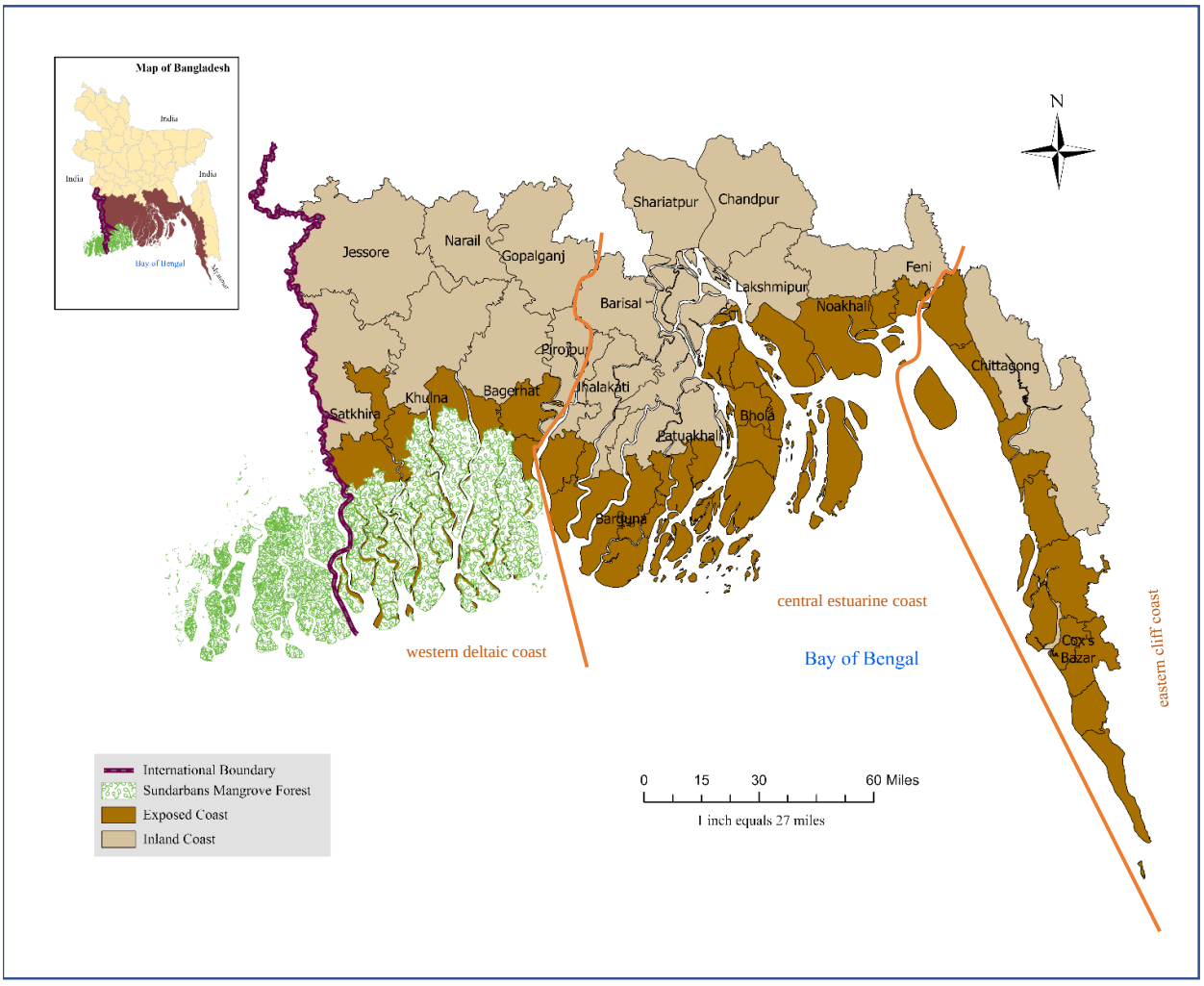

Fig 1.4: Study Area Map

The western region or western deltaic coast is highly vulnerable to natural disasters such as cyclonic storms associated with tidal floods because of several reasons, such as its exposure to the Bay of Bengal, a relatively low elevation with an average of 1.5 m, primarily located in the

Ganges Tidal Floodplain, and higher rates of poverty (Murshed et al., 2022). In addition, with a range of coastal features including tidal flats, mangrove swamps, natural levees, and the Sundarbans mangrove forest in the southwest of the area, this semi-active delta extends from Jashore to Pirojpur districts (Fig. 1.4) (Akter et al., 2019; Brammer, 2012; Murshed et al., 2022).

The central coastal region or the central estuarine coast covers the areas from Barishal to Feni districts (Fig. 1.4), and most of them fall under the highly active Meghna Estuarine Floodplains (Brammer, 2012; Murshed et al., 2022; Rahman & Rahman, 2015). This region is characterized by a narrow strip of land with geomorphological active offshore islands. Unlike the western part, this region does not have any mangrove forest; therefore, it suffers the direct impacts of storm surges and cyclones (Murshed et al., 2022; Quader et al., 2017).

The Chattogram and Cox's Bazar districts are included in the eastern region, often known as the eastern cliff coast (Fig. 1.4), which is mostly part of the Chittagong Coastal Plains (Brammer, 2012; Murshed et al., 2022). The eastern part of this region contains the Chittagong Hill Tracts, which makes this region the steepest among the three coastal regions by reaching a maximum elevation of 327 meters above the mean sea level (Murshed et al., 2022). Due to socioeconomic conditions and geophysical qualities, the southern part of the eastern coast is highly susceptible to tropical cyclones (Quader et al., 2017).

1.4 Significance of this Research

Coastal areas are highly populated across the world, and around 37% of the global inhabitant was documented in 2017 within 100 km of the coastline (UNEP, 2023). Climate change will have a substantial impact in the future, posing a threat to coastal lives, resources, and ecosystems, and Bangladesh will not be spared. Bangladesh is subjected to several natural disasters on a regular basis. Multiple environmental hazards, including hydro-meteorological

natural disasters like cyclones, storm surges, flooding, etc., exert mounting pressure on the coastal communities of Bangladesh. It is augmented by the country's geographical location, agrarian economy, and huge population (McGranahan et al., 2007). Despite a significant decline in cyclone fatalities, Bangladesh continues to struggle protecting livelihood and property among vulnerable coastal populations, making economic damage evident. Though the government has improved the early warning systems, evacuation before a cyclone is still challenging due to key issues like illiteracy, inadequate cyclone shelter, awareness, and poor communication (Haque et al., 2012).

Protecting a region or community fully from disaster attacks is not possible, but it is important to build disaster-resilient communities to withstand and recover from the disaster. Therefore, identifying location-based potential risks and the vulnerable population along with their mitigation capacity through an appropriate risk assessment approach is essential. An effective risk assessment must consider several components, such as exposure, population sensitivity to hazards, and the community's ability to fight back against the casualty (Cutter, 2011; Dewan, 2013). Cutter et al. (2003) pointed out that socially disadvantaged individuals are subjected to get the severe brunt of disasters since they have a lower likelihood of recuperating and a higher likelihood of dying. By understanding social vulnerability effectively, it is possible to protect the communities without disrupting livelihood and damaging properties (Flanagan et al., 2011). Besides evaluating physical and social vulnerability, it is important to seek the status of the highly threatened mangrove forest since it plays a vital role in mitigating the disaster damage.

The primary purpose of this research is to show the current degree of susceptibility and risk of the coastal areas and communities to TCs impacts, as well as the condition of the

mangrove, which has been shielding the coast by obstructing the powerful cyclonic wind and storm surges for years. Several studies have been carried out on coastal cyclone vulnerability, but studying physical and social vulnerability in detail and integrating them still needs to be popular among researchers. Furthermore, the immediate impact on the Sundarbans mangrove forests using optical remote sensing data in most of the studies has been noticed, which can give an inaccurate result of the vegetation health due to a number of factors. In order to avoid significant data gaps in the presence of high cloud cover before and after the cyclones, this research also analyzed radar data to observe the forest disturbance, which is not found in other researchers' work. This study developed and evaluated a spatial multi-criteria approach using the AHP method for comprehensively mapping physical vulnerability to tropical cyclones and risk. This study also analyzed social vulnerability using the social vulnerability index (SoVI) and created risk maps for the entire coast. The major findings of the research will aid in depicting the existing scenario and predicting the foreseeable impact of tropical cyclones in the coastal regions and the mangrove forest. The research will also be helpful in developing risk management strategies and policies to make a better and climate-adaptive future.

References

Agrawal, N. (2018). Defining natural hazards - Large scale hazards. *Advances in Natural and Technological Hazards Research*, 49, 1-40. https://doi.org/10.1007/978-94-024-1283-3_1

Akter, M., Jahan, M., Kabir, R., Karim, D. S., Haque, A., Rahman, M., & Salehin, M. (2019). Risk assessment based on fuzzy synthetic evaluation method. *Science of the Total Environment*, *658*, 818–829. https://doi.org/10.1016/j.scitotenv.2018.12.204

Alam, E., & Dominey-Howes, D. (2015). A new catalogue of tropical cyclones of the northern Bay of Bengal and the distribution and effects of selected landfalling events in Bangladesh. *International Journal of Climatology*, 35 (6), 801–835. https://doi.org/10.1002/joc.4035

Alongi, D. M. (2008). Mangrove forests: Resilience, protection from tsunamis, and responses to global climate change. *Estuarine, Coastal and Shelf Science*, *76*(1), 1–13. https://doi.org/10.1016/j.ecss.2007.08.024

Rahman, M. A., & Rahman, S. (2015). Natural and traditional defense mechanisms to reduce climate risks in coastal zones of Bangladesh. *Weather and Climate Extremes*, *7*, 84–95. https://doi.org/10.1016/j.wace.2014.12.004

BBS. (2011). Population & Housing Census 2011 (Zila Series & Community Series).

BFD. (2023). Natural Mangrove Forest (Sundarban).

Bhowmik, A. K., & Cabral, P. (2013). Cyclone Sidr Impacts on the Sundarbans Floristic Diversity. *Earth Science Research*, *2*(2), 62. https://doi.org/10.5539/esr.v2n2p62

Brammer, H. (2012). Physical Geography of Bangladesh. The University Press Ltd.

Bunting, P., Rosenqvist, A., Hilarides, L., Lucas, R. M., Thomas, N., Tadono, T., Worthington, T. A., Spalding, M., Murray, N. J., & Rebelo, L. M. (2022). Global Mangrove Extent

Change 1996–2020: Global Mangrove Watch Version 3.0. Remote Sensing, 14(15). https://doi.org/10.3390/rs14153657

Cutter, S. L. (2011). A ciência da vulnerabilidade: modelos, métodos e indicadores. *Revista Crítica de Ciências Sociais, 93*, 59–69. https://doi.org/10.4000/rccs.165

Cutter, S. L., Boruff, B. J., & Shirley, W. L. (2003). Social Vulnerability to Environmental Hazards. *Social Science Quarterly*, *84*(2), 242–261. https://doi.org/10.1111/1540-6237.8402002

Defu, L., Huajun, L., Guilin, L., Hongda, S., & Fengqing, W. (2013). Typhoon/hurricane/tropical cyclone disasters: Prediction, prevention and mitigation. *Natural Disasters: Prevention, Risk Factors and Management*, 1–72. https://doi.org/10.4236/gep.2019.75003

Dewan, A. M. (2013). Vulnerability and Risk Assessment. *Floods in a Megacity* (pp. 139–177). Springer Netherlands. https://doi.org/10.1007/978-94-007-5875-9_6

Dube, S. K., Jain, I., Rao, A. D., & Murty, T. S. (2009). Storm surge modelling for the Bay of Bengal and Arabian Sea. *Natural Hazards*, *51*(1), 3–27. https://doi.org/10.1007/s11069-009-9397-9

Eckstein, D., Künzel, V., & Schäfer, L. (2021). Global Climate Risk Index 2021. Germanwatch e.V. https://www.germanwatch.org/en/19777

Everham, E. M., & Brokaw, N. V. L. (1996). Forest Damage and Recovery from Catastrophic Wind. *Botanical Review*, *62*(2), 113–185. https://doi.org/10.1007/BF02857920

FEMA. (2023). Natural Hazards. https://hazards.fema.gov/nri/natural-hazards.

Flanagan, B. E., Gregory, E. W., Hallisey, E. J., Heitgerd, J. L., & Lewis, B. (2011). A Social Vulnerability Index for Disaster Management. *Journal of Homeland Security and Emergency Management*, *8*(1). https://doi.org/10.2202/1547-7355.1792

Frank, W. M., & Young, G. S. (2007). The interannual variability of tropical cyclones. *Monthly Weather Review*, *135*(10), 3587–3598. https://doi.org/10.1175/MWR3435.1

Gain, A. K., Rahman, M. M., Sadik, M. S., Adnan, M. S. G., Ahmad, S., Ahsan, S. M. M., Ashik-Ur-Rahman, M., Balke, T., Datta, D. K., Dewan, C., Huq, N., Khan, M. S. A., Large, A., Mallick, B., Mohibbullah, M., Mondal, M. S., Narayan, S., Rabbani, G., Rahman, R., Renaud, F. G., Rogers, K. G., & van Loon-Steensma, J. M. (2022). Overcoming challenges for implementing nature-based solutions in deltaic environments: Insights from the Ganges-Brahmaputra delta in Bangladesh. *Environmental Research Letters*, *17*(6). https://doi.org/10.1088/1748-9326/ac740a

Gaona, M. F. R., Villarini, G., Zhang, W., & Vecchi, G. A. (2018). The added value of IMERG in characterizing rainfall in tropical cyclones. *Atmospheric Research*, *209*, 95–102. https://doi.org/10.1016/j.atmosres.2018.03.008

Ghosh, A., Schmidt, S., Fickert, T., & Nüsser, M. (2015). The Indian Sundarban mangrove forests: History, utilization, conservation strategies and local perception. *Diversity*, *7*(2), 149–169. https://doi.org/10.3390/d7020149

Gray, W. M. (1998). Meteorology, and Atmospheric Physics the Formation of Tropical Cyclones. *Meteorol. Atmos. Phy*, *67*.

Hochard, J. P., Hamilton, S., & Barbier, E. B. (2019). Mangroves shelter coastal economic activity from cyclones. *Proceedings of the National Academy of Sciences of the United States of America*, *116*(25), 12232–12237. https://doi.org/10.1073/pnas.1820067116

Hoque, M. A. A., Phinn, S., Roelfsema, C., & Childs, I. (2016). Assessing tropical cyclone impacts using object-based moderate spatial resolution image analysis: a case study in Bangladesh. *International Journal of Remote Sensing*, *37*(22), 5320–5343.

https://doi.org/10.1080/01431161.2016.1239286

Hoque, M. A. A., Phinn, S., Roelfsema, C., & Childs, I. (2018). Assessing tropical cyclone risks using geospatial techniques. *Applied Geography*, *98*, 22–33. https://doi.org/10.1016/j.apgeog.2018.07.004

Khan, M. (2016). Disaster Impact on Sundarbans-a Case Study on Sidr Affected Area. *IMPACT: International Journal of Research in Applied, Natural and Social Sciences (IMPACT: IJRANSS), Special Edition.* http://www.impactjournals.us/index.php/download/conference/conf--1480141354-2.

Mahmood, H., Ahmed, M., Islam, T., Uddin, M. Z., Ahmed, Z. U., & Saha, C. (2021). Paradigm shift in the management of the Sundarbans mangrove forest of Bangladesh: Issues and challenges. *Trees, Forests and People*, *5*, 100094. https://doi.org/10.1016/j.tfp.2021.100094

McGranahan, G., Balk, D., & Anderson, B. (2007). The rising tide: Assessing the risks of climate change and human settlements in low elevation coastal zones. *Environment and Urbanization*, *19*(1), 17–37. https://doi.org/10.1177/0956247807076960

Mitchell, D., Hawker, L., Savage, J., Bingham, R., Lord, N. S., Khan, M. J. U., Bates, P., Durand, F., Hassan, A., Huq, S., Islam, A. S., Krien, Y., Neal, J., Sampson, C., Smith, A., & Testut, L. (2022). Increased population exposure to Amphan-scale cyclones under future climates. *Climate Resilience and Sustainability*, *1*(2). https://doi.org/10.1002/cli2.36

Mohapatra, M., Bandyopadhyay, B. K., & Tyagi, A. (2014). Status and plans for operational tropical cyclone forecasting and warning systems in the North Indian Ocean region. *Monitoring and Prediction of Tropical Cyclones in the Indian Ocean and Climate*

Change, 149–168. https://doi.org/10.1007/978-94-007-7720-0_14

Moslehuddin, A. Z. M., Abedin, M. A., Hossain, M. A., & Habiba, U. (2015). Soil Health and Food Security: Perspective from Southwestern Coastal Region of Bangladesh. *Food security and risk reduction in Bangladesh*, 187–212. https://doi.org/10.1007/978-4-431-55411-0_11

Murshed, S., Griffin, A. L., Islam, M. A., Wang, X. H., & Paull, D. (2022). Assessing multi-climate-hazard threat in the coastal region of Bangladesh by combining influential environmental and anthropogenic factors. *Progress in Disaster Science*, *16*. https://doi.org/10.1016/j.pdisas.2022.100261

Parvin, G. A., Ahsan, S. R., & Shaw, R. (2010). Community-Based Coastal Zone Management in Bangladesh. *Community and Coastal Zone Management*, 165-184. https://www.researchgate.net/publication/274075743

Peduzzi, P., Chatenoux, B., Dao, H., De Bono, A., Herold, C., Kossin, J., Mouton, F., & Nordbeck, O. (2012). Global trends in tropical cyclone risk. *Nature Climate Change*, *2*(4), 289–294. https://doi.org/10.1038/nclimate1410

Pielke, R. A., Gratz, J., Landsea, C. W., Collins, D., Saunders, M. A., & Musulin, R. (2008). Normalized Hurricane Damage in the United States: 1900–2005. *Natural Hazards Review*, *9*(1), 29–42. https://doi.org/10.1061/(asce)1527-6988(2008)9:1(29)

Quader, M. A., Khan, A. U., & Kervyn, M. (2017). Assessing risks from cyclones for human lives and livelihoods in the coastal region of Bangladesh. *International Journal of Environmental Research and Public Health*, *14*(8). https://doi.org/10.3390/ijerph14080831

Rahman, M. A., & Rahman, S. (2015). Natural and traditional defense mechanisms to reduce

climate risks in coastal zones of Bangladesh. *Weather and Climate Extremes*, *7*, 84–95. https://doi.org/10.1016/j.wace.2014.12.004

Rahman, Md. M., Ghosh, T., Salehin, M., Ghosh, A., Haque, A., Hossain, M. A., Das, S., Hazra, S., Islam, N., Sarker, M. H., Nicholls, R. J., & Hutton, C. W. (2020). Ganges-Brahmaputra-Meghna delta, Bangladesh and India: a transnational mega-delta. *Deltas in the Anthropocene*, 23-51.

Rana, M. H. (2013). Shelter from Storms in Bangladesh. World Bank.

Regnier, E., & Harr, P. A. (2006). A dynamic decision model applied to hurricane landfall. *Weather and Forecasting*, *21*(5), 764-780. https://doi.org/10.1175/WAF958.1

Sen, S. (2020). Sunderban mangroves, post Amphan: An overview. *International Journal of Creative Research Thoughts, 8.* www.ijcrt.org

Sharma, S., Suwa, R., Ray, R., Shamim, M., & Mandal, H. (2022). Successive Cyclones Attacked the World's Largest Mangrove Forest Located in the Bay of Bengal under Pandemic. *Sustainability, 14*(9), 5130.

Shultz, J. M., Shepherd, J. M., Bagrodia, R., & Espinel, Z. (2014). Tropical cyclones in a year of rising global temperatures and a strengthening El Niño. *Disaster Health, 2*(3–4), 151–162. https://doi.org/10.1080/21665044.2014.1111722

Sippo, J. Z., Lovelock, C. E., Santos, I. R., Sanders, C. J., & Maher, D. T. (2018). Mangrove mortality in a changing climate: An overview. *Estuarine, Coastal and Shelf Science, 215*, 241–249. https://doi.org/10.1016/j.ecss.2018.10.011

UNDRR. (2017a). Hazard.

UNEP. (2023). Coastal zone management.

Wahiduzzaman, M., & Yeasmin, A. (2019). Statistical forecasting of tropical cyclone landfall

activities over the North Indian Ocean rim countries. *Atmospheric Research*, *227*, 89–100. https://doi.org/10.1016/j.atmosres.2019.04.034

WMO. (2021). WMO Atlas of Mortality and Economic Losses from Weather, Climate and Water Extremes (1970–2019). https://library.wmo.int/index.php?lvl=notice_display&id=21930#.Y2fm2nbMI7e

WMO. (2022a). Natural hazards and disaster risk reduction. https://public.wmo.int/en/our-mandate/focus-areas/natural-hazards-and-disaster-risk-reduction

WMO. (2022b). Tropical Cyclones.

Woodruff, J. D., Irish, J. L., & Camargo, S. J. (2013). Coastal flooding by tropical cyclones and sea-level rise. *Nature*, *504*(7478), 44–52. https://doi.org/10.1038/nature12855

World Bank. (2019). Coastal Resilience in Bangladesh: Protecting Coastal Communities from Tidal Flooding and Storm Surges.

Xi, W. (2015). Synergistic effects of tropical cyclones on forest ecosystems: a global synthesis. *Journal of Forestry Research*, *26*(1), 1–21. https://doi.org/10.1007/s11676-015-0018-z

Zhou, Y., Matyas, C., Li, H., & Tang, J. (2018). Conditions associated with rain field size for tropical cyclones landfalling over the Eastern United States. *Atmospheric Research*, *214*, 375–385. https://doi.org/10.1016/j.atmosres.2018.08.019

CHAPTER 2

Social Vulnerability Assessment of the Coastal Communities of Bangladesh using the Social Vulnerability Index (SoVI)

2.1 Background

Globally, natural hazards are becoming more frequent, with the year 2021 alone experiencing 13% more natural disasters compared to the year 1991 (UNDRR, 2022). Advanced disaster preparedness strategies have helped individuals to defend themselves through time; however, the economic loss rocketed by 80%, exerted financial pressure on the affected people and made their life difficult (UNDRR, 2022). Hydrometeorological disasters were attributed to 50% of all disasters in the past 50 years (1970-2019), and more than 91% of the 45% of disaster mortality occurred in developing countries (WMO, 2021). Based on recent statistical data, Asia emerged as the forefront region in terms of disaster-induced fatality, with the highest number of disasters struck there in 2021, including around 60% of deaths caused by 78% of hydrometeorological disasters, notably floods and storms (UNDRR, 2022). There has been a wide range of effects on society due to disasters, depending on factors such as poverty, education, income and so forth (Cutter et al., 2003). Rudimentary facilities which could safeguard individuals and their assets from disaster damage are often lacking in deprived poor communities. Furthermore, access to recovery assets by these groups is limited, a phenomenon that can be seen throughout developing and developed countries (Fothergill & Peek, 2004). Hazards accelerate poverty in poor communities, rendering them more susceptible to the next

disaster. For instance, hurricane Stan in 2005 compelled children from 7.3% of affected households in Guatemala to engage in child labor instead of attending school (GFDRR, 2023).

When a community or group of people have potential exposure to threats, whether natural or anthropogenic disasters or disease epidemics, it is termed social vulnerability (CDC, 2020; FEMA, 2023). A crucial determining factor for social vulnerability is the resilience of such a group (Cutter & Finch, 2008). Therefore, assessing social vulnerability is essential in identifying communities in need of assistance before or after a disaster to limit disaster damages. To define and evaluate socioeconomic disparities, a number of social vulnerability indices have been developed within the framework of disaster vulnerability, which are still being debated in order to establish best practices for determining how disasters can turn into societal catastrophe and validating their outcomes (Goodman et al., 2021; Rufat et al., 2019). The social vulnerability index (SoVI) is widely used, reliable, and frequently cited by researchers and governmental organizations (Enderami & Sutley, 2022).

As a place-based technique, the SoVI approximates social vulnerability within a particular geographic area by integrating several variables into a single score that is indicative of the probability that a community is more vulnerable than others around the country in terms of social vulnerability (Cutter & Finch, 2008; Goodman et al., 2021; FEMA, 2023; Flanagan et al., 2011; Wilson, 2019). The SoVI score is proportional to the community's vulnerability, with the upper and lower scores of the index corresponding to the highest and lowest levels of vulnerability (FEMA, 2023; Spielman et al., 2020). Since Cutter et al. (2003) developed SoVI for the US, it has been modified and adapted for many studies to analyze and present different aspects of spatiotemporal vulnerabilities (Cutter & Finch, 2008; Goodman et al., 2021; Rabby et al., 2019). However, the standard inductive approach to reduce dimensionality in SoVI is

Principal Component Analysis (PCA), because of the ambiguity of the relationship between the variables and vulnerability (Bucherie et al., 2022; Heß, 2017; Mavhura et al., 2017; Rabby et al., 2019; Tasnuva et al., 2021).

Worldwide coastal communities are prone to natural hazards, specifically hydrometeorological hazards such as cyclones, floods, and storm surges (Bathi & Das, 2016). In addition to physical vulnerability to potential hazards, socioeconomic factors may affect coastal communities' resilience. According to a study conducted by the United States Census Bureau, based on the social vulnerability index and multidimensional deprivation index, coastal areas are more deprived and at higher risk than inland areas (Glassman & Devore, 2023). This mounting vulnerability and societal inequality are common in the global south.

Storms are the one of major natural disasters in Bangladesh, which recurrently inflict damage on human lives and livelihoods. Coastal communities in developing countries like Bangladesh confront serious consequences during tropical cyclones due to a range of factors, including poverty, poor infrastructure, and lack of access to resources (Haque et al., 2012). Although cyclonic mortality decreased in this country, the maximum economic loss climbed by approximately 57 times, skyrocketing from 86 million in the 1970s to 4942 million US dollars in the 2000s (ADB, 2015). Cyclones Sidr (2007) and Aila (2009) devastated coastal Bangladesh, resulting in a 44% decrease in average income and a rise in poverty (Roy & Sultana, 2010). In a world where natural disasters are becoming more prevalent because of changing climate and increased population, studying socioeconomic vulnerability is becoming immensely important because risk multiplies proportionally as population increases in vulnerable areas (Gu, 2019).

Despite the impacts mentioned above, relatively few studies were conducted on social vulnerability assessment in the coastal areas of Bangladesh. For quantifying social vulnerability,

academics previously relied on questionnaire surveys and focus group discussions (Mallick et al., 2011; Mudasser et al., 2020). A social vulnerability index was calculated by Rabby et al. (2019) at the Union level covering the entire coastal areas of Bangladesh. Tasnuva et al. (2021), on the other hand, examined a small area at the Ward level using this index. Both of them used more than 25 indicators to construct the index. Alternatively, Miah et al. (2020) assigned only four demographic and socioeconomic factors to the Chittagong district to determine social vulnerability. However, they have done it for overall natural hazards, whereas vulnerability is hazard-specific (Cardona et al., 2012). For this reason, a composite index for emergency response must consider variables that might exacerbate the condition caused by a natural disaster, as changes in variable and geographical scale might ultimately have a profound effect on the outcome (Bucherie et al., 2022; Tate & Emrich, 2021). The variables were selected at the upazila or county level considering a particular hazard- TCs to construct SoVI for the entire coastal zone of Bangladesh. The index can prove beneficial for cyclone-related disaster preparedness, emergency responders during tropical cyclones, and during cyclonic recovery actions.

2.2 Materials and Methods

2.2.1 Data Required

SoVI is constructed using census data at various scales (national, county, union, ward) around the world (Flanagan et al., 2011; Rabby et al., 2019; Tasnuva et al., 2021). To conduct this study, the most recent Population and Housing Census of 2011 at the upazila (county) level was used, which was provided by the Bangladesh Bureau of Statistics (BBS). The study employed 19 variables, many of which are related to vulnerability. Researchers have modified this index depending on geographical conditions, hazard context, and data availability. However,

Cutter et al. (2003) assessed the country's social vulnerability at the same geographic scale (county) as this study.

2.2.2 Rationale of Variable Selection

Factors are crucial in the execution of SoVI and possess the potential to alter the outcome in the same catastrophic setting. From a vast database of the BBS 2011 census, 19 variables (as shown in Table. 2.1) were taken into account for 131 upazilas (county) across 19 coastal districts. Demographic, economic, social, housing structure, composition, and facilities were some of the main themes of these indicators.

Table 2.1: SoVI variables and other information

Theme	Cardinality	Variance Explained (%)	Variables Description	Loading
Demography, Dependent population, Ethnic, Marital Status, Education, Housing structure and facilities, Employment status	+	52.416	% of total rural population	0.938
			% of total female population	0.908
			% age below 5 years (0-4)	0.900
			% of total disabled population	0.903
			% of total ethnic population	0.499
			% of total widowed and divorced population aged 10 years and above)	0.911
			% of literacy of population aged 7 years & above	0.858
			% of total kacha and jhupri household	0.805
			% of total household without safe drinking source	0.454
			% of total household without electricity	0.944
			% of total household with non-sanitary and no toilet	0.828

			% of total population looking for work and don't work (10 years & above)	0.872
			% of total Population works in primary sector (10 years & above)	0.960
			% of total Population works in service sector and industry (10 Years & above)	0.703
Vulnerable Population	+	15.532	% of total homeless population	0.893
			% of total rented household	0.899
Total population, Aged population, and Housing composition	+	14.368	% of total population	0.831
			% of age 65 and over	0.864
			% of total households more than 5 people	0.820

As part of the demographic analysis, rural and female population proportions were included. The rural population tends to be more vulnerable because of their limited access to basic facilities, disaster resources, and reliance on agriculture. As a result of social, cultural, and economic inequalities, along with their involuntary evacuation behavior, women are more susceptible to cyclones than men, particularly in developing nations like Bangladesh. Women's mortality rates during cyclone Gorky (1991) resulted in 14 times higher than men's, followed by five times higher mortality rates during cyclone Sidr (2007) (Rahman & Rahman, 2015). Hence, including these demographic variables can provide a better understanding of the social vulnerability to cyclones in the coastal areas of Bangladesh. Coastal areas are highly populated, which increases vulnerability. Therefore, the total population was included as a variable.

The percentage of people under five years (0-4) and above 65 years old for each county was incorporated in this study. The inclusion of these variables was justified by the fact that

people dependent on others are more vulnerable in the event of a disaster (Martin, 2015). Children are particularly vulnerable due to their physical and physiological vulnerability, which increase their risk of mortality (UNICEF, 2021). In Bangladesh, the average life expectancy was 72 years in 2020 and was around 68 years in 2011 (BBS, 2011; World Bank, 2023). Persons aged 60 or above are considered elderly in Bangladesh, and those over 65 are deemed more susceptible to cyclones because of their reduced physical strength and weakened mental capacity (Hossain, 2016; Malak et al., 2020). The same reasoning is applicable to the disabled population.

The ethnic community, also referred to as the tribal or indigenous community, is very small in Bangladesh, sharing only 1.25% of this country's population (Macdonald, 2021). This variable was considered because, often, they can amplify social vulnerability. For example, evidence shows that since the community lacks access to fundamental rights and disaster awareness, ethnic women are more vulnerable (The Business Standard, 2020). Thus, including this variable is crucial for identifying and considering vulnerable populations that might otherwise go unnoticed.

The populations of widowed and divorced people were considered under marital characteristics. Cvetkovic (2016) studied how married individuals perceive disaster preparedness differently than divorced and widowed ones. His finding showed that married persons exhibit greater liability towards their family and community, whereas a dilemma was noticed in taking precautions among divorced people.

Households with more than five members were considered due to their effectiveness in responding to and recovering from the crisis together with higher capital (Rabby et al., 2019). Moreover, literacy is another factor that might reduce sensitivity. A positive relationship exists between literacy and adaptive capacity, a vulnerability attribute capable of attenuating social

vulnerability. It allows people to make decisions at their discretion, respond to warning systems, and promote positive behavior toward evacuation (Samhsa, 2017). Although there is debate regarding the effectiveness of formal education versus the traditional method in cyclonic disaster preparedness, education is more likely to indirectly pave the path to employment, giving individuals more control over disaster impact (Muttarak & Lutz, 2014; Sharma et al., 2013). In this case, the literacy rate of men and women aged 7 years and above is included in the literacy variable.

For employment, three types were added: the unemployed community, people who work in primary sectors, and people engaged in service sectors and industries. The first two categories are assumed to be increasing vulnerability as they do not have any money or little money to recover and reconstruct (Hallegatte et al., 2017). Conversely, people with solvency who work in the third category have better control over recovery and strategies. The unemployed population includes the percentage of people from 10 years old looking for a job or who do not work.

Variables within the category of housing structures and types were used to build SoVI. Traditional houses or low-cost housing like Kutcha and Jhupri houses are constructed with substandard and unsustainable materials such as mud, bamboo, straws, and CI sheets. Alam et al. (2017) investigated 300 houses in their study, of which around 147 dwellings had very low structural quality. In coastal Bangladesh, the majority of homes are substandard and non-engineered. The rationale behind selecting this variable is that kutcha and jhupri houses are not physically sound enough to withstand the strong winds and downpours that accompany TCs, which can heighten the casualties during the disaster. In addition, rented homes are also notably at risk of cyclones and other natural hazards. Tenants might not have the standard level of building protection which is common in areas with poor law enforcement (Lee & van Zandt,

2019). Moreover, people experiencing homelessness in the coastal regions are often exposed to vulnerability because of their ignorance of impending storms, as well as a lack of permanent housing and amenities, such as healthcare, sanitation, and clean drinking water.

In the realm of housing facilities, no electricity, inaccessibility to safe drinking water, and non-sanitary toilets were considered. Having no power connection in a dwelling unit restricts people's networks and makes their lives more difficult. Households without safe drinking water included people who use sources like the pond, which is highly exposed to contamination during cyclonic flooding, leading to water-borne diseases. Regarding toilet facilities, the household percentage using non-sanitary toilets and no toilets were derived from the census. These are signs of poor sewage facilities, which might hasten the spread of illness following a natural disaster.

2.2.3 Data Preparation

Prior to computing the complex matric, SoVI, it is essential to check the suitability of data. To this end, this study followed the steps shown in Fig. 2.1 to preprocess the dataset for factor analysis. First, the analysis of the selected variables was conducted using the Statistical Package for Social Science (SPSS) software. Next, all variables were converted to percentages to normalize the data. The next step involves the verification of data accuracy by scrutinizing the minimum and maximum values, along with the mean and standard deviation. In this dataset, there were three missing values for Sanagazi upazila under Feni District, which were substituted by the mean value.

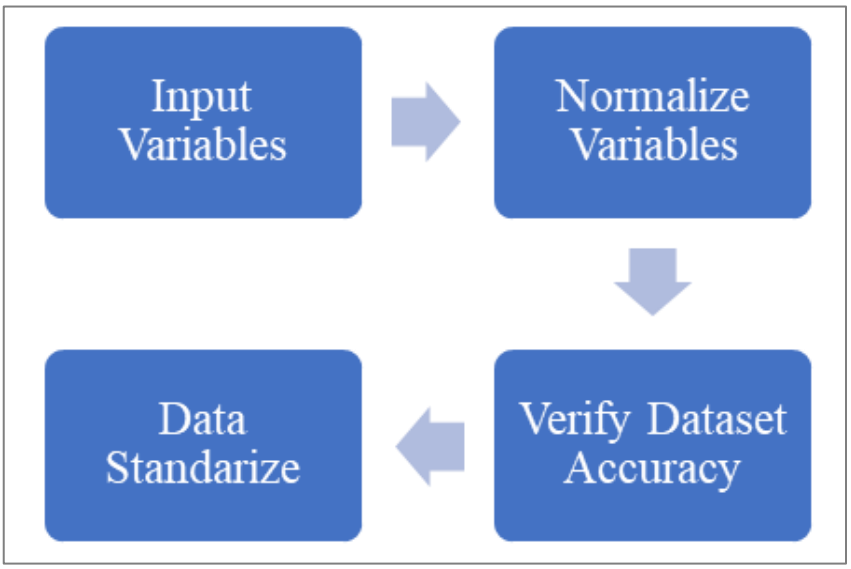

Fig. 2.1: Flowchart of Data pre-processing for PCA analysis

Since all variables do not have the same scale, standardizing the data is essential. All variables are uniformly rescaled with an average of 0 and a standard deviation of 1 after z-score standardization (Dinc et al., 2014). To calculate the z score, a following equation (1) was used:

$$z = \frac{Raw\ Value - Mean}{Standard\ Deviation} \quad (1)$$

In this study, SoVI was constructed using the methods used by Rabby et al. (2019) and Tasnuva et al. (2021).

2.2.4 Calculation of PCA and SoVI

PCA is done to simplify a large multidimensional dataset into a simple index. Fig. 2.2 shows a scree plot of the eigenvalues and only the components with an eigenvalue greater than one are kept for further analysis.

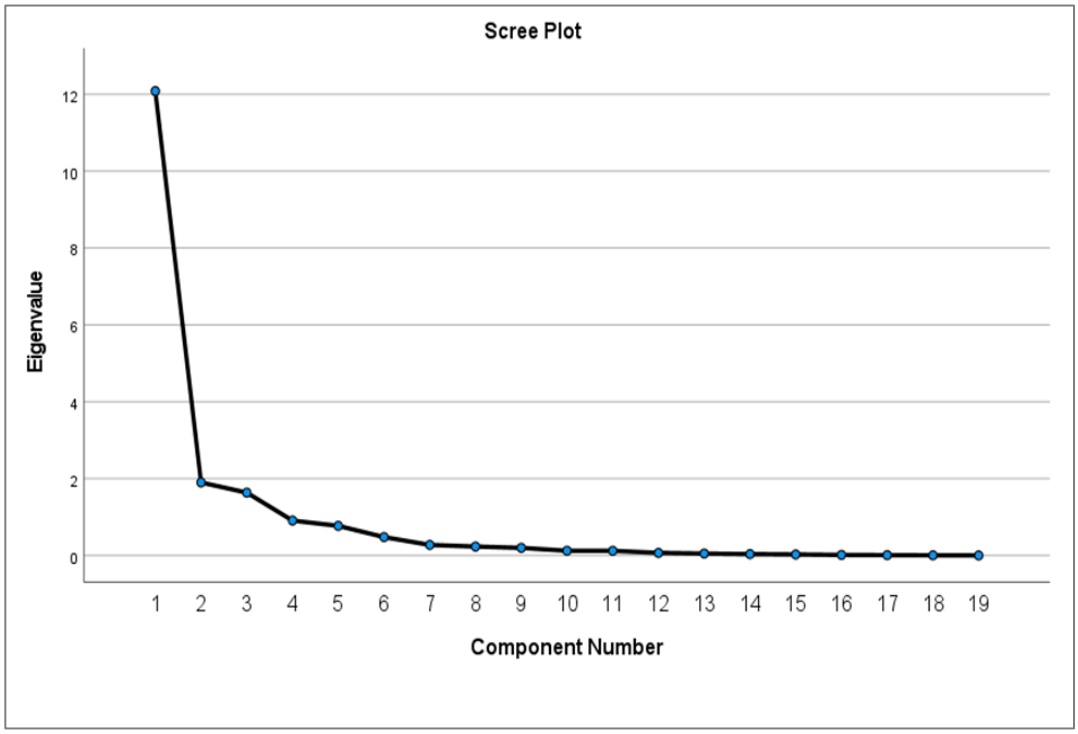

Fig. 2.2: Scree plot with eigenvalue of the studied variables

The variables that passed the Kaiser-Meyer-Olkin (KMO) test for sample adequacy were reduced by performing a varimax rotation with 100 iterations. Based on the recommendation of Kaiser (1974), a range of values (Fig. 2.3a) was employed to verify the quality of the solution and interpretability of the result. A value below 0.50 indicates the futility of factor analysis.

(a)

in the .90s, marvelous
in the .80s, meritorious
in the .70s, middling
in the .60s, mediocre
in the .50s, miserable
below .50, unacceptable

(b)

KMO and Bartlett's Test[a]

Kaiser-Meyer-Olkin Measure of Sampling Adequacy.	.898

Fig. 2.3: KMO score (a) Kaiser's (1974) sampling suitability table (b) Present study's result

By examining the maximum factor loadings, variables from the rotated component matrix were grouped and given a cardinality. For this study, all three groups increased vulnerability, so a positive sign was used to execute the additive approach to construct SoVI. Finally, the formula (2) below was used to calculate the composite SoVI scores for each county:

$$\text{SoVI} = \text{Factor 1} + \text{Factor 2} + \text{Factor 3} \quad (2)$$

2.2.5 Mapping Social Vulnerability

An effective mapping can provide direct attention to people as well as provide information on geographic differences (Rabby et al., 2019). ArcGIS Pro was used to depict the spatial distribution of the SoVI score (Raduszynski & Numada, 2023). To facilitate the illustration of communities with varying levels of vulnerability, the standard deviation classification method was used to create four distinct classes. In Figure 2.4, areas with extremely high to extremely low levels of vulnerability are identified with a value ranging from less than -0.5 to over 1.5 standard deviation.

2.3 Result and Discussions

Of the 19 variables examined in this study, only three variables had an eigenvalue greater than 1, explaining approximately 82% of the total variance in the dataset (Table. 2.1). KMO score of 0.898 (Fig. 2.3b) indicates that subsequent factor analysis would be highly suitable for the dataset generated by this study. Table 2.1 shows that the maximum loading in the first component or Factor 1 was 0.960, and the minimum was 0.454. This group contained demographic characteristics, dependent population, ethnic community, marital and employment status, education, housing structure, and facilities. Vulnerable populations in terms of housing possession were grouped together in Factor 2, where the loading varied from 0.893 to 0.899

(Table 2.1). According to Table 2.1, Factor 3's loading values ranged from 0.820 to 0.864, which includes the percentage of the aged population, the percentage of the total population, and the percentage of the housing composition. A total of 14 variables are in Factor 1, two in Factor 2, and three in Factor 3, which explained 52.416%, 15.532%, and 14.368% of data variance, respectively (Table 2.1). All the values, except the percentage of the total household without safe drinking source and the percentage of the total ethnic population, have a very high loading which indicates a strong influence of these variables on their components (Burstyn, 2004).

Fig. 2.4 shows the spatial distribution of social vulnerability of the coastal community of Bangladesh where the maximum composite SoVI score was assigned to Feni upazila (11) in Feni district, and the minimum was attributed to Chittagong Metro in the Chittagong district (-1.59). The entire eastern coast, encompassing Chittagong and Cox's Bazar districts, showed a very low to low vulnerability (<-0.50 Std. Dev.) (Fig. 2.4).

The central estuarine coast exhibited considerable variability in the spatial distribution of social vulnerability score, varying from very high (>1.5 Standard Deviation) to very low (<-0.50 Standard Deviation) (Fig. 2.4). Feni district close to the eastern coast, demonstrates moderate to high vulnerability, apart from Feni Sadar Upazila which exhibits very high social vulnerability (Fig. 2.4). Exposed coasts showed mostly higher vulnerability on the central coast (Fig. 2.4). Among the 12 districts investigated, only the entire Barisal and Noakhali districts showed lower vulnerability. On the other hand, the remaining ten districts exhibited low to very highly vulnerable communities. Notably, the maximum number of very highly vulnerable communities were concentrated in the central region. Feni upazila in Feni district, Amtali and Barguna upazila in Barguna district, Chandpur upazila in Chandpur district, Charfasson and Bhola upazila in Bhola district (Fig. 2.4) need immediate attention from the disaster resilience authorities because

of their latent ability to change TCs strike into a social catastrophe.

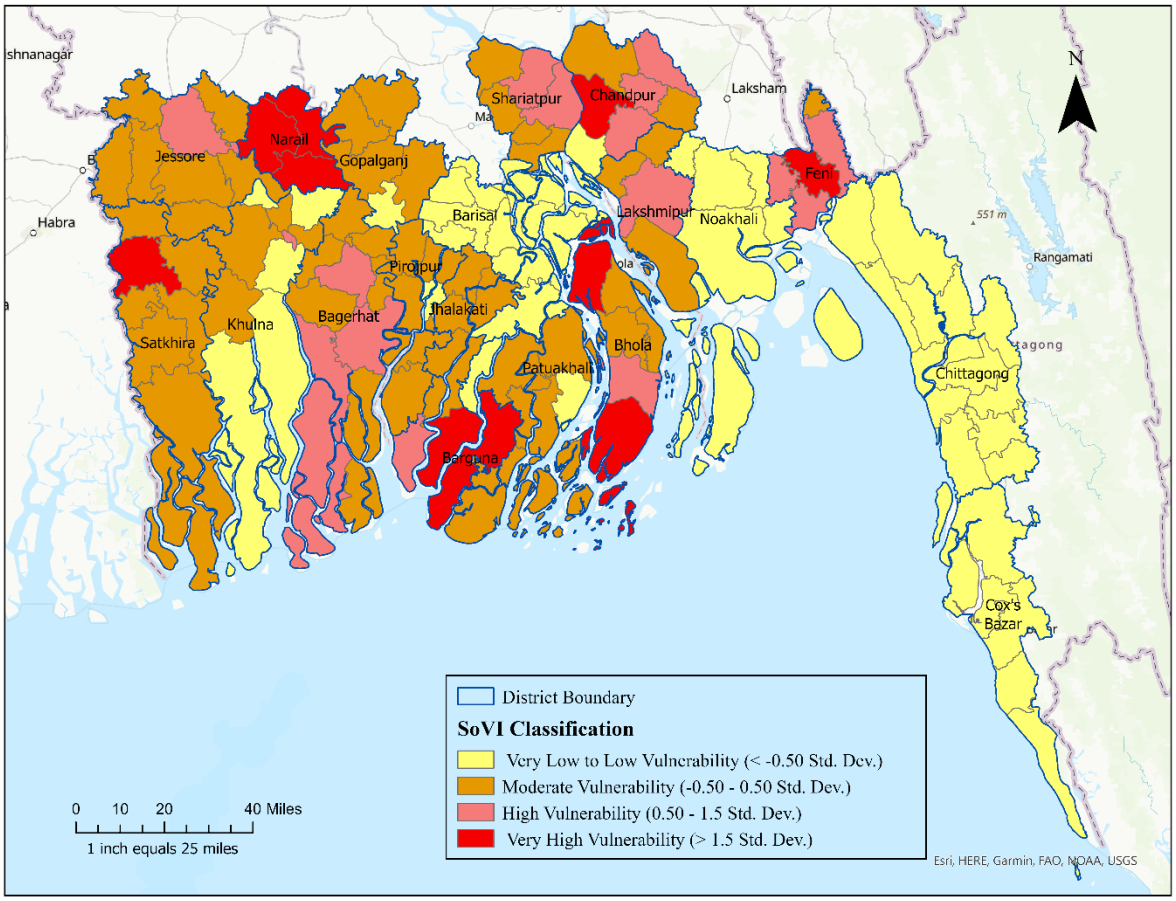

Fig. 2.4: Spatial distribution of social vulnerability at the county level

In this study, the maximum vulnerability on the western coast was noticed in Narail, Kalia, and Lohagara upazila in Narail district and Satkhira upazila in Satkhirra district (Fig. 2.4). Moderate vulnerability predominates near West Bengal, India, which is a frequent TCs landfall area. Most of the upazilas in the Khulna district demonstrate very low to low vulnerability whereas the adjacent district Bagerhat showed high vulnerability (Fig. 2.4). Among 131 counties across the coast, 26 counties were susceptible to high and very high social vulnerability (Fig. 2.4), where ten upazilas were the Sadar or metropolitan cities of the districts. Cutter et al. (2003)

also found metropolitan cities highly vulnerable in their study. Other researchers assessed social vulnerability on the Bangladesh coast using different parameters and geographic scales which makes it impossible to compare this study's result with theirs. One of the major limitations of this study is that all the data used to construct SoVI was from Population and Housing Census 2011 because the 2021 census data has not yet been published. The total population increased by

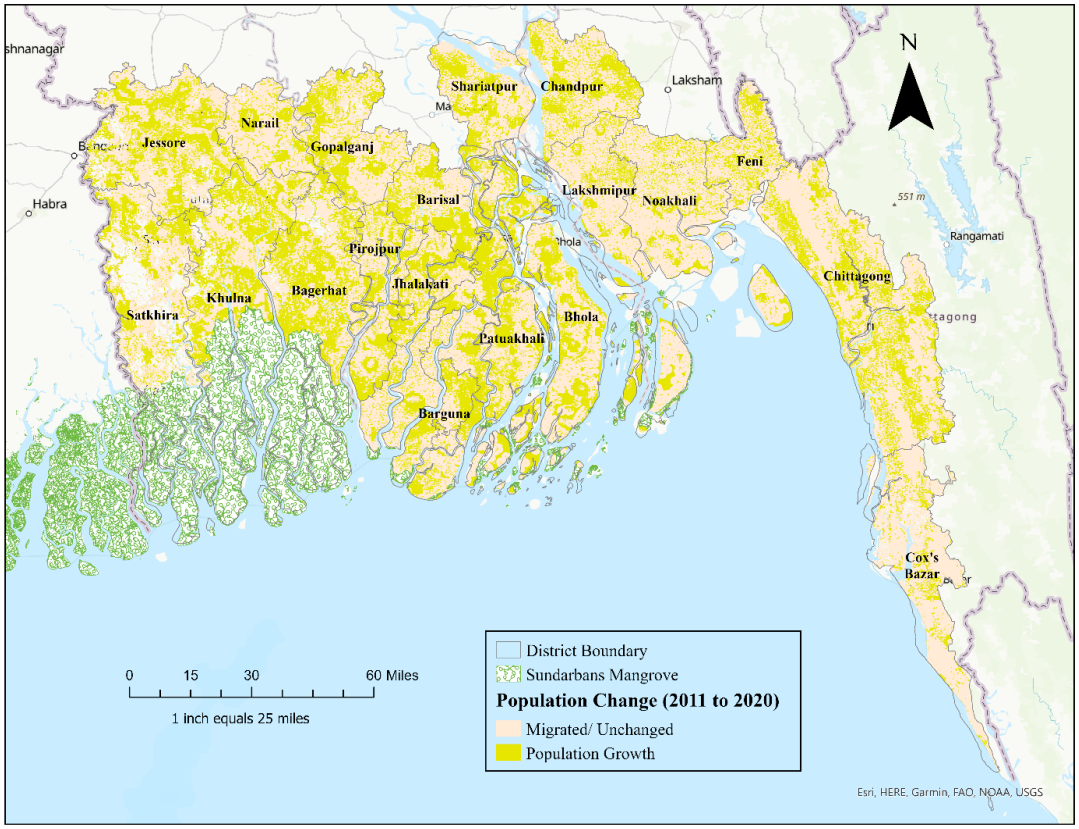

Fig. 2.5: Change in total population from 2011 to 2020

around 26% in 2020 from 2011, which was extracted from World Pop raster layers. Fig. 2.5 shows that almost all over the coast population increased, including the areas with very low vulnerability. It is assumed that with the increasing population, social vulnerability will increase too.

2.4 Conclusion

Studying social vulnerability is essential in the context of Coastal Bangladesh because although Bangladesh has touched the milestone in reducing disaster-related death, it is lagging in terms of economic loss, and the number keeps rising. The population increased rapidly since 2011 on the coast, which will eventually change the current vulnerability from this study's findings. However, keeping this data limitation aside, the study provides valuable insights into the areas at higher risk of cyclones in the future. The study highlights the exposed central coastal areas as particularly vulnerable, and their proximity to the Bay of Bengal influences their socio-economic condition. Another significant outcome of the study is that the metropolitan areas, which are highly populated areas, are at higher risk. The findings of this study will help decision-makers in implementing disaster preparedness measures in high-risk zones also, the low-risk areas, which are in touch with highly vulnerable areas, should be taken under consideration for increasing social resiliency and adaptive capacity. As the population in Bangladesh continues to grow and socio-economic conditions evolve, it is essential to conduct regular and updated assessments of social vulnerability to ensure that disaster management efforts remain effective. Ultimately, this study contributes to ongoing efforts to increase social resiliency and adaptive capacity in Bangladesh and similar regions worldwide.

References:

ADB. (2015). Bangladesh: Capacity Building for Disaster Risk Finance in Bangladesh.

Alam, M. R., Kaish, A. B. M. A., Zain, M. F. M., Dev, S. K., & Mahzabin, M. S. (2017). Vulnerability assessment and construction recommendations of local houses in the cyclone prone coastal areas of Bangladesh. *International Journal of Disaster Risk Reduction*, *21*, 118–130. https://doi.org/10.1016/j.ijdrr.2016.10.010

Bathi, J. R., & Das, H. S. (2016). Vulnerability of coastal communities from storm surge and flood disasters. *International Journal of Environmental Research and Public Health*, *13*(2). https://doi.org/10.3390/ijerph13020239

BBS. (2011). Population & Housing Census 2011 (Zila Series & Community Series).

Bucherie, A., Hultquist, C., Adamo, S., Neely, C., Ayala, F., Bazo, J., & Kruczkiewicz, A. (2022). A comparison of social vulnerability indices specific to flooding in Ecuador: principal component analysis (PCA) and expert knowledge. *International Journal of Disaster Risk Reduction*, *73*. https://doi.org/10.1016/j.ijdrr.2022.102897

Burstyn, I. (2004). Principal component analysis is a powerful instrument in occupational hygiene inquiries. *Annals of Occupational Hygiene, 48*(8), 655–661. https://doi.org/10.1093/annhyg/meh075

Cardona, O.-D., Aalst, M. K. van, Birkmann, J., Fordham, M., McGregor, G., Perez, R., Pulwarty, R. S., Schipper, E. L. F., & Sinh, B. T. (2012). Determinants of risk: exposure and vulnerability. *Managing the Risks of Extreme Events and Disasters to Advance Climate Change Adaptation*.

CDC. (2020). CDC Social Vulnerability Index (SVI).

Cutter, S. L., Boruff, B. J., & Shirley, W. L. (2003). Social Vulnerability to Environmental

Hazards. *Social Science Quarterly*, *84*(2), 242–261. https://doi.org/10.1111/1540-6237.8402002

Cutter, S. L., & Finch, C. (2008). Temporal and spatial changes in social vulnerability to natural hazards. *Proceedings of the National Academy of Sciences of the United States of America*, *105*(7), 2301–2306. https://doi.org/10.1073/pnas.0710375105

Cvetkovic, V. (2016). Marital status of citizens and floods: Citizen preparedness for response to natural disasters. *Vojno Delo*, *68*(8), 89–116. https://doi.org/10.5937/vojdelo1608089c

Dinc, I., Sigdel, M., Dinc, S., Sigdel, M. S., Pusey, M. L., & Aygun, R. S. (2014). Evaluation of normalization and PCA on the performance of classifiers for protein crystallization images. *IEEE SOUTHEASTCON 2014*, 1–6. https://doi.org/10.1109/SECON.2014.6950744

Enderami, S. A., & Sutley, E. J. (2022). Social Vulnerability Score: A Scalable Index for Representing Social Vulnerability in Virtual Community Resilience Testbeds. https://doi.org/10.21203/rs.3.rs-2113725/v1

FEMA. (2023). Social Vulnerability.

Flanagan, B. E., Gregory, E. W., Hallisey, E. J., Heitgerd, J. L., & Lewis, B. (2011). A Social Vulnerability Index for Disaster Management. *Journal of Homeland Security and Emergency Management*, *8*(1). https://doi.org/10.2202/1547-7355.1792

Fothergill, A., & Peek, L. A. (2004). Poverty and Disasters in the United States: A Review of Recent Sociological Findings. *Natural Hazards*, *32*

GFDRR. (2023). Breaking the link between extreme weather and extreme poverty.

Glassman, B., & Devore, A. (2023). By Two Government Measures, 526 Counties — Mostly in the South — Are Economically and Socially Deprived and Vulnerable. *United States*

Census Bureau.

Goodman, Z. T., Stamatis, C. A., Stoler, J., Emrich, C. T., & Llabre, M. M. (2021). Methodological challenges to confirmatory latent variable models of social vulnerability. *Natural Hazards*, *106*(3), 2731–2749. https://doi.org/10.1007/s11069-021-04563-6

Gu, D. (2019). Population Division Exposure and vulnerability to natural disasters for world's cities. www.unpopulation.org.

Hallegatte, S., Vogt-Schilb, A., Bangalore, M., & Rozenberg, J. (2017). Unbreakable: Building the Resilience of the Poor in the Face of Natural Disasters. *Unbreakable: Building the Resilience of the Poor in the Face of Natural Disasters*. Washington, DC: World Bank. https://doi.org/10.1596/978-1-4648-1003-9

Haque, U., Hashizume, M., Kolivras, K. N., Overgaard, H. J., Das, B., & Yamamoto, T. (2012). Reduced death rates from cyclones in Bangladesh: What more needs to be done? *Bulletin of the World Health Organization*, *90*(2), 150–156. https://doi.org/10.2471/BLT.11.088302

Heß, V. D. C. (2017). Weigh(t)ing the dimensions of social vulnerability based on a regression analysis of disaster damages. *Natural Hazards and Earth System Sciences Discussions*. https://doi.org/10.5194/nhess-2017-74

Hossain, M. M. (2016). Projection on Elderly Population in Bangladesh. https://www.researchgate.net/publication/281149148

Kaiser, H. F. (1974). An Index of Factorial Simplicity.

Lee, J. Y., & Van Zandt, S. (2019). Housing Tenure and Social Vulnerability to Disasters: A Review of the Evidence. *Journal of Planning Literature*, *34*(2), 156–170. https://doi.org/10.1177/0885412218812080

Macdonald, G. (2021). The Challenges Facing Plainland Ethnic Groups in Bangladesh: Land, Dignity and Inclusion. *International Republican Institute*. https://www.iri.org/resources/new-bangladesh-report-examines-needs-of-plainland-ethnic-groups/

Malak, M. A., Sajib, A. M., Quader, M. A., & Anjum, H. (2020). "We are feeling older than our age": Vulnerability and adaptive strategies of aging people to cyclones in coastal Bangladesh. *International Journal of Disaster Risk Reduction, 48*. https://doi.org/10.1016/j.ijdrr.2020.101595

Mallick, B., Rubayet Rahaman, K., & Vogt, J. (2011). Social vulnerability analysis for sustainable disaster mitigation planning in coastal Bangladesh. *Disaster Prevention and Management: An International Journal*, *20*(3), 220–237. https://doi.org/10.1108/09653561111141682

Martin, S. A. (2015). A framework to understand the relationship between social factors that reduce resilience in cities: Application to the City of Boston. *International Journal of Disaster Risk Reduction, 12*, 53–80. https://doi.org/10.1016/j.ijdrr.2014.12.001

Mavhura, E., Manyena, B., & Collins, A. E. (2017). An approach for measuring social vulnerability in context: The case of flood hazards in Muzarabani district, Zimbabwe. *Geoforum, 86*, 103–117. https://doi.org/10.1016/j.geoforum.2017.09.008

Miah, J., Khandaker, T. H., Mallik, A. H., & Najia, S. I. (2020). Assessing coastal vulnerability of Chittagong District, Bangladesh using geospatial techniques. *Journal of Coastal Conservation*. https://doi.org/10.1007/s11852-020-00784-2/Published

Mudasser, M., Hossain, Md. Z., Rahaman, K. R., & Ha-Mim, N. M. (2020). Investigating the Climate-Induced Livelihood Vulnerability Index in Coastal Areas of Bangladesh. *World*,

1(2), 149–170. https://doi.org/10.3390/world1020012

Muttarak, R., & Lutz, W. (2014). Is education a key to reducing vulnerability to natural disasters and hence unavoidable climate change? In *Ecology and Society, 19*(1). https://doi.org/10.5751/ES-06476-190142

Rabby, Y. W., Hossain, M. B., & Hasan, M. U. (2019). Social vulnerability in the coastal region of Bangladesh: An investigation of social vulnerability index and scalar change effects. *International Journal of Disaster Risk Reduction*, *41*. https://doi.org/10.1016/j.ijdrr.2019.101329

Raduszynski, T., & Numada, M. (2023). Measure and spatial identification of social vulnerability, exposure and risk to natural hazards in Japan using open data. *Scientific Reports*, *13*(1). https://doi.org/10.1038/s41598-023-27831-w

Rahman, M. A., & Rahman, S. (2015). Natural and traditional defense mechanisms to reduce climate risks in coastal zones of Bangladesh. *Weather and Climate Extremes*, *7*, 84–95. https://doi.org/10.1016/j.wace.2014.12.004

Roy, K., & Sultana, U. T. (2010). Climate Change Disasters and Rural Poverty: Case of Coastal Bangladesh. *3rd International Conference on Bangladesh Environment*. https://doi.org/10.13140/RG.2.1.1000.6244

Rufat, S., Tate, E., Emrich, C., & Antolini, F. (2019). How Valid Are Social Vulnerability Models? *Annals of the American Association of Geographers*, *109*(4), 1131–1153. https://doi.org/10.1080/24694452.2018.1535887ï

Samhsa. (2017). Greater Impact: How Disasters Affect People of Low Socioeconomic Status.

Sharma, U., Patwardhan, A., & Patt, A. G. (2013). Education as a determinant of response to cyclone warnings: Evidence from coastal zones in India. *Ecology and Society*, *18*(2).

https://doi.org/10.5751/ES-05439-180218

Spielman, S. E., Tuccillo, J., Folch, D. C., Schweikert, A., Davies, R., Wood, N., & Tate, E. (2020). Evaluating social vulnerability indicators: criteria and their application to the Social Vulnerability Index. *Natural Hazards*, *100*(1), 417–436. https://doi.org/10.1007/s11069-019-03820-z

Tasnuva, A., Hossain, M. R., Salam, R., Islam, A. R. M. T., Patwary, M. M., & Ibrahim, S. M. (2021). Employing social vulnerability index to assess household social vulnerability of natural hazards: an evidence from southwest coastal Bangladesh. *Environment, Development and Sustainability*, *23*(7), 10223–10245. https://doi.org/10.1007/s10668-020-01054-9

Tate, E., & Emrich, C. (2021). Assessing Social Equity in Disasters.

The Business Standard. (2020, August 27). Ethnic women hit hardest in natural disasters.

UNDRR. (2022). Global Natural Disaster Assessment Report. https://www.preventionweb.net/publication/2021-global-disaster-assessment-report

UNICEF. (2021). The climate crisis is a child rights crisis: Introducing the Children's Climate Risk Index.

Wilson, B. S. (2019). Overrun by averages: An empirical analysis into the consistency of social vulnerability components across multiple scales. *International Journal of Disaster Risk Reduction*, *40*. https://doi.org/10.1016/j.ijdrr.2019.101268

WMO. (2021). WMO Atlas of Mortality and Economic Losses from Weather, Climate and Water Extremes (1970–2019). https://library.wmo.int/index.php?lvl=notice_display&id=21930#.Y2fm2nbMI7e

World Bank. (2023). Life expectancy at birth, total (years) - Bangladesh.

CHAPTER 3

Physical Vulnerability and Tropical Cyclones Risk Assessment in the Coastal Areas of Bangladesh

3.1 Background

The widespread impact of climate-related disasters is apparent around the world. There is no doubt that TCs are the most destructive of all the climate-related disasters, taking a heavy toll on lives and livelihoods (Mansour, 2019; Quader et al., 2017; Sahoo & Bhaskaran, 2018). The Global Climate Risk Index 2021 identifies Bangladesh as among the most vulnerable countries to climate change's adverse effects (Eckstein et al., 2021). Bangladesh is a cyclone-prone region, and TCs frequently occur in the coastal areas of the country between April and May, and October and November (Dasgupta et al., 2010). Since this region has a dense population, many communities along the coast of the BoB increase the propensity of being affected by cyclones. The BoB, also known as a hotbed of TCs, is witnessing a six-fold surge in the catastrophic potential of TCs (Murty et al., 2016). In addition, an uptick in cyclone size and maximum sustained wind speed was also observed compared to the previous decadal records (Sahoo & Bhaskaran, 2016). Historical data indicates that Bangladesh is hit by severe cyclones every three years (Ahammad et al., 2013; MoEF, 2009). This is why it is vital that a systematic spatial assessment is conducted to identify the potentially vulnerable areas along the coast.

Natural hazards are increasing globally, and a growing interest in quantifying risk and vulnerability has been observed among researchers over time. Vulnerability is a concept that refers to a group or region’s propensity to experience numerous stressors, such as social and

environmental stresses, and their inability to cope with the stresses (Adger, 2006; Kelman et al., 2016). It was introduced within the discourse of hazard and disaster in the late seventies (Flanagan et al., 2011; Wisner et al., 2003). Vulnerability is a multidimensional notion composed of several components like exposure, sensitivity, potential impact, and adaptive capacity (Fig. 3.1), where a change in one factor can influence another (Thomas et al., 2019). Exposure is the extent to which individuals or assets are susceptible to injury or unfavorable results (Viner et al., 2020). There are many factors that influence stress exposure, such as region, demographics, and socioeconomic status (Nikkanen et al., 2021; UNDRR, 2017). It is important to note that exposure does not always equate to vulnerability, as highlighted by Cardona et al. (2012).

The ability of a system to respond to a particular stress without undergoing a significant change is referred to as sensitivity (Adger, 2006; Engle, 2011; Füssel & Klein, 2006). Adaptive capacity, on the other hand, refers to the system's capability to endure stress, cope with it, and lessen the negative impact by adjusting exposure and sensitivity (Adger, 2006; Füssel & Klein, 2006). This can be influenced by various factors, such as education, access to information, resources, technology, and wealth. Adaptive capacity of a system is inversely related to susceptibility. Susceptibility decreases as adaptive capacity increases (Engle, 2011; Thomas et al., 2019). Risk is defined as the exposure of vulnerable elements to hazards or extreme events which have the potential to damage, while hazards are the events that can potentially affect lives and livelihoods (Dewan, 2013; Hoque et al., 2017; Zhu et al., 2022).

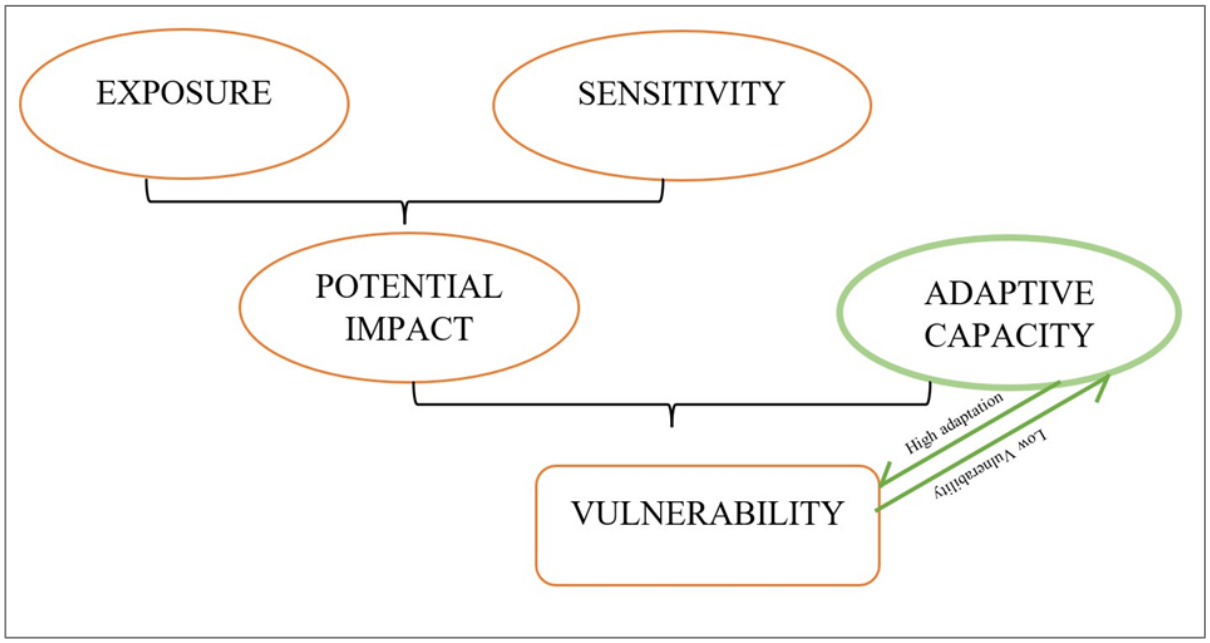

Fig 3.1: Principal components of vulnerability adapted from Engle (2011) and Glick et al. (2011)

Quantifying risk and vulnerability are the groundwork for promoting community resilience and building disaster mitigation strategies. In the past few decades, satellite imagery and geospatial techniques have made it easier to assess and map the vulnerability of cyclones (Pathak et al., 2020; Rana et al., 2010; Yin et al., 2013). In the field of hazard analysis, researchers around the world employed numerous single and multi-criteria approaches. It is, however, necessary to use the latter approach in order to understand the spatial distribution of risk in a comprehensive manner (Hoque et al., 2019; Mansour, 2019; Rana et al., 2010; Sahoo & Bhaskaran, 2018). In order to map TCs risks, one of the most popular and efficient ways to do so is to integrate multi-criteria risk evaluations of individual risk components and combine them into a spatial decision-making process (Hoque et al., 2018a; Rahman et al., 2019). Saaty (1977) introduced the Analytical Hierarchy Process (AHP) for this purpose. A number of researchers (Mondal et al., 2021; Murali et al., 2013; Rahman et al., 2019; Rajakumari et al., 2022; Sinaga et

al., 2011; Tempa, 2022) used this method to evaluate complex decisions, where hierarchical structures were used to assign weights based on the priorities of the user (Mahapatra et al., 2015; Tempa, 2022).

Bangladesh's coast is one of the major cyclone-prone areas. Approximately 30 catastrophic TCs have made landfall on this country's coast from 1960 to 2017, causing massive damage (Quader et al., 2017). Nevertheless, there are few studies on assessing vulnerability and risk in depth. Most of the researchers focused on one section of the coast to assess cyclone vulnerability and risk. Hoque et al. (2018 and 2019) analyzed the spatial distribution of cyclone risk using the AHP method. Their study primarily focused on the physical vulnerability of one upazila (county) and the eastern coast of Bangladesh. As for wind speeds, both studies focused on only one cyclone, which might bias the overall results of coastal vulnerability as a result of TCs. Hoque et al. (2021) assessed the socioeconomic and physical vulnerability on the western coast of Bangladesh. However, they used different parameters from studies mentioned above, and the weighting method was also different, which was fuzzy AHP. A major surge amplification region, the Meghna estuarine region, is overlooked in their study (Dasgupta et al., 2010). In addition, the population density of 2011, which increased sharply from 2011 to 2020, has been used in all studies (WorldPop, 2023). Mallick et al. (2017) studied southwestern coastal communities' experience and their strategies for dealing with cyclones. The entire coast was examined for tropical cyclone vulnerability by Quader et al. (2017), with a major focus on the social aspects of vulnerability. Despite this, they ignored a number of key factors that make tropical cyclones destructive, such as the height of storm surges, the speed of the cyclonic wind, and the amount of rainfall in the affected area (Hoque et al., 2019; Swain, 2022). Furthermore, the allocation of equal weighting to all indicators during an overlay analysis is a significant

limitation in their study. As far as assessing risk and vulnerability is concerned, not all variables are equally important. For instance, population density is more critical compared to land cover for cyclone vulnerability assessment. Considering cyclones, the study addresses the void and prepares a comprehensive risk map. The purpose of this study is to evaluate the risk of TCs along the Bangladesh coast through a multi-criteria and geospatial techniques.

3.2 Materials and Methods

3.2.1 Dataset and Sources

A well-prepared spatial assessment can provide valuable insights to offset the damage. Based on a literature review, the parameters of three principal risk components have been chosen: hazard, vulnerability, and mitigation capacity (Hoque et al., 2018 and 2021; Quader et al., 2017; Zhou et al., 2021). In this study, a wide range of sources, including local and global datasets, have been used (Table 3.1).

Table 3.1: Dataset Information

Name	**Source**	**Spatial Resolution**	**Time**	**Data Layer**	**Data Format**
DEM	WARPO	50m		Elevation, Slope	Raster
Population Density	World Pop	1 km	2020	Population Density	Raster
Cyclone Tracks	IBTrACS	-	1970-2022	Proximity to cyclone tracks, Frequency of cyclone	Vector

Coastline	International Steering Committee for Global Mapping	-	2016	Coastline proximity	Vector
Land Cover	ESRI	10 m	2022	Land Cover Classification	Raster
Cyclone Frequency	IBTrACS	-	1970-2022	Cyclone frequency	Vector
Cyclone Wind Speed	IBTrACS	-	1970-2022	Cyclone Wind Speed	Vector
Storm Surge Height	Reports	-	1970-2020	Storm Surge Height	Report
Rainfall	Dewan et al. (2022)	1 km	1901-2018	Rainfall Intensity	NetCDF
Cyclone Shelter	Bangladesh Bureau of Statistics (BBS)	-	Until 2009	Cyclone Shelter proximity	Vector
Health Centers	LGED	-	-	Health Center proximity	Vector
Road Type	LGED	-	-	Proximity to Paved Road	Vector

Before analysis, all layers were projected onto the WGS 1984 datum and a UTM zone 45 N coordinate system. In order to classify the layers, natural break and manual interval methods

were used, based on published studies and user judgment, to classify them into five classes ranging from very low to very high (Hoque et al., 2019; Zhou et al., 2021).

3.2.2 Methods

3.2.2.1. Vulnerability and Exposure Mapping

Topography plays a significant role in influencing disaster vulnerability (Westen et al., 2008). Low-elevated land territories on the coast are likely to be less disaster-resilient to hydro-meteorological disasters, particularly TCs, sea level rise, etc., compared to high lands (Murali et al., 2013). The digital representation of the surface or Digital Elevation Model (DEM) is an important feature for spatial modeling, which was collected from WARPO (Table 3.1). However, the original DEM data contained several data voids, mostly in the mountainous regions, which were corrected using the Inverse Distance Weighted (IDW) algorithm (Qiu et al., 2019). Later the corrected DEM data was processed using the geospatial tool (clip) and raster calculator for this study. Likewise, elevation, a flat slope is more susceptible to flooding than a steep slope (Li & Li, 2013; Mullick et al., 2019). The degree of the slope was calculated using the corrected DEM data in ArcGIS Pro. While elevation and slope are susceptible to cyclonic flooding, similarly mountainous regions with a high elevation and slope are vulnerable to landslides because of tropical rainstorms (Antinao & Farfán, 2013; Rahman et al., 2019; Zhuang et al., 2022). In the context of disaster vulnerability analysis, population plays an important role. In 2000, about 49% of Bangladesh's total population lived in the low-elevated coastal zones, making it the highest in Eastern, South-Central, and South-Eastern Asia (Neumann et al., 2015). Coasts are exposed to extreme climatic events, and densely populated areas tend to intensify the risk (Nicholls et al., 2007). The Government of Bangladesh last conducted a census to measure population density in 2011. However, the WorldPop Hub's most recent population-

gridded data was used in this study, which was obtained from https://hub.worldpop.org/.

For the assessment of physically vulnerability to TCs, factors such as proximity to cyclone tracks and coastal areas have been considered because these factors intensify the vulnerability (Alam et al., 2020). The tracks of cyclones and coastline were obtained from the International Best Track Archive for Climate Stewardship (IBTrACS) and the Princeton University Library (available at: https://maps.princeton.edu/catalog/stanford-rz344pd6047), respectively. For both criteria, multiple buffer zones were created using a geoprocessing tool in ArcGIS Pro to map the proximity to the tracks and coastline. The risk of TCs varies according to land cover, where certain types likely to increase the vulnerability (Hoque et al., 2021). Hence, knowing the coastal regions' land cover is essential to map vulnerability. The raster layer of landcover was downloaded from ESRI (available at: https://livingatlas.arcgis.com/landcover/), which had nine classes and an average accuracy of 85% at the global level (Karra et al., 2021). Further, the image was clipped according to the shapefile of coastal Bangladesh and reclassified into five classes.

3.2.2.2 Hazard Mapping

Around 30 category-one to five hurricanes passed through the coastal area of Bangladesh from 1970-2021, with numerous in the tropical storm category. Observing the pattern of the destructive nature of cyclones, notably wind speed, storm surge, and precipitation, are an essential criterion in evaluating vulnerable areas (Emanuel et al., 2006; Hoque et al., 2016; Mansour, 2019). With the information available in the IBTrACS attribute, cyclone frequency was calculated at the district level, and the natural break method was followed to classify them into five classes. The wind data was processed using the IDW data interpolation method and clipped in accordance with the area of interest. By analyzing the pattern of major TCs, storm

surge altitude was mapped and classified into five classes using the corrected DEM data (UN-Spider, 2023). The gridded monthly rainfall data from 1901-2018 was used to observe the precipitation trend.

3.2.2.3. Adaptive Capacity Mapping

The key plan to mitigate the possible adverse impact of such a hazard is reflected in the adaptive capacity of that place and the community (Mansour, 2019). A variety of structural mitigation measures were assessed in this study including distance to cyclone shelters, health infrastructures, and road networks. In the wake of cyclone disasters, a cyclone shelter serves as an ideal infrastructural mitigation measure for cyclone-affected communities to provide temporary shelter (Mallick, 2014). Furthermore, emergency health care for individuals affected by cyclones is supported by health infrastructure (Ali et al., 2020). Health center data included only hospital and clinic locations, whereas road networks analyzed paved roads only. For this study, these data were collected from the Local Government Engineering Department (LGED). Afterward, proximity analysis was performed.

3.2.2.4 Data Standardization

In order to achieve a composite result from a multi-criteria decision-making approach, all data layers must be scored at the same level (Yin et al., 2013). All raster layers were converted to 10 m spatial resolution. According to equation (1), a linear scale transformation was used to convert the alternative ranking values into a conventional range from 0 to 1 (Hoque et al., 2019):

$$p = \frac{x - min}{max - min} \quad (1)$$

Here a dataset's standardized score is indicated by p, while its individual cell value is indicated

by x, and its maximum and minimum values are indicated by min and max, respectively.

3.2.2.5. Weight Calculation using AHP Method

To weigh the parameters of risk components, the AHP method was used as a multicriteria decision-making approach. The hierarchy's overall priorities were developed by aggregating and integrating pair-wise comparison matrices (Sinaga et al., 2011). In this case, the scale ranges from 1 to 9, where 1 corresponds to equal importance and 9 corresponds to the utmost importance of the issue (Saaty, 1977). The weights for each criterion were then calculated by normalizing the pairwise comparison matrixes. The consistency ratio (CR) in the AHP technique aids in comprehending how consistently the user's judgment was used when constructing the pair-wise matrices. Using equations (2) and (3), the consistency index (CI) as well as the consistency ratio (CR) have been calculated (Mondal et al., 2021):

$$\mathrm{CI} = \frac{\lambda \max - n}{n-1} \tag{2}$$

Where λ_{max} represents the highest or principal eigenvalue of the matrix and n is the total number of variables (Khan et al., 2021).

$$\mathrm{CR} = \frac{CI}{RI} \tag{3}$$

In this case, RI represents the random index calculated by the matrix order (n) that Saaty (1980) determined. CR value over 10% indicates that the weights of the parameters cannot be used for further analysis, and the entire process should be redone (Hoque et al., 2021; Tempa, 2022). The AHP method was found to be effective in this type of complex decision-making aspect.

3.2.2.6. Overall Coastal Risk Assessment for TCs

Using the AHP method, a pair-wise comparison matrix was built for vulnerabilities,

exposures, and mitigations criteria. Then, the weighted overlay was conducted to get the overall physical vulnerability of the coast by assigning weight. Finally, social vulnerability output, which is discussed in Chapter 2, was rasterized for overall risk analysis. The following formula (4) was employed in the raster calculator with and without integrating social vulnerability to calculate risk in the coast of Bangladesh, which gives the spatial distribution of coastal vulnerability for tropical cyclones.

$$Risk = \frac{Hazard \times Vulnerability}{Mitigation} \quad (4)$$

3.3 Results and Discussion

3.3.1 Physical Vulnerability Mapping

Physical vulnerability was achieved by integrating six parameters: elevation, slope, population density, land cover, proximity to cyclone track, and coastline. A majority of the landmass in the coastal region is very low-elevated, with only 41% having an elevation higher than 6.5 feet (Fig. 3.2a). Most of the landmass (~45%) is occupied by the 6.5-16.5 feet elevation range. Based on Hoque et al. (2021)'s findings, 42% of coastal regions are classified as very high or highly vulnerable zones, with elevations up to 8 feet in the western coastal region. Almost all the regions in the western and central coasts showed this low elevation, putting these regions and communities at grave risk of cyclonic flooding. The north-western part, mainly the Jessore district and a small part of the central coast, showed a rise in elevation where the value ranged from 16.5 to 26.5 feet (Fig. 3.2a). The hilly region with an elevation of approximately 40 to 959 feet is mainly seen on the eastern coast, indicating low to very low vulnerability. However, the entire eastern cliff region is not out of cyclone risk; as seen in Fig. 3.2a, the areas near the Bay of Bengal have a lower elevation. Besides, the slope is proportionally related to elevation. Almost

the entire western and central coast had a flat slope, mostly attributed to less than 3 percent rise in the slope. In contrast, the eastern cliff coast shows variation in their slope, with a maximum slope of approximately 489 percent gradient (Fig 3.2b).

A glimpse of the concentrated population on the coast of Bangladesh can be visible in Fig. 3.2c. This is the result of the latest dataset on Bangladesh population density provided by the WorldPop research program (WorldPop, 2023). On the western coast of Bangladesh, Jessore, Khulna, and Satkhira districts showed a dense population, and the southern part of the west coast showed minimum population density because of the presence of Sundarbans mangrove forest (Fig. 3.2c). In terms of population density, the eastern coast is highly vulnerable because of the spatial distribution of high population density close to the coast (Fig. 3.2c). Besides, Chandpur, Noakhali, Lakhsmipur, and Feni districts in the central coast are highly vulnerable because of massive population density despite being inland. Based on reports and newspaper articles, cyclonic mortality was highest in the Noakhali district on the central coast from 1970-2009. According to UNEP (2002), the high population density in Asia is likely a contributor to the larger death toll caused by extreme events.

Dense vegetation has the ability to offset the intensity of tropical cyclones by working as a shield. Here in this study, dense vegetation includes forests and large patches of trees. Except for the Meghna estuarine coast, the majority of the other two coasts are guarded by dense vegetation, such as mangrove forests and hill forests, exposing the central coast to higher risk. The western part of the coast is characterized by low-lying deltaic plains dominated by wide rivers and estuaries, making it susceptible to flooding when cyclonic storm surges occur, which

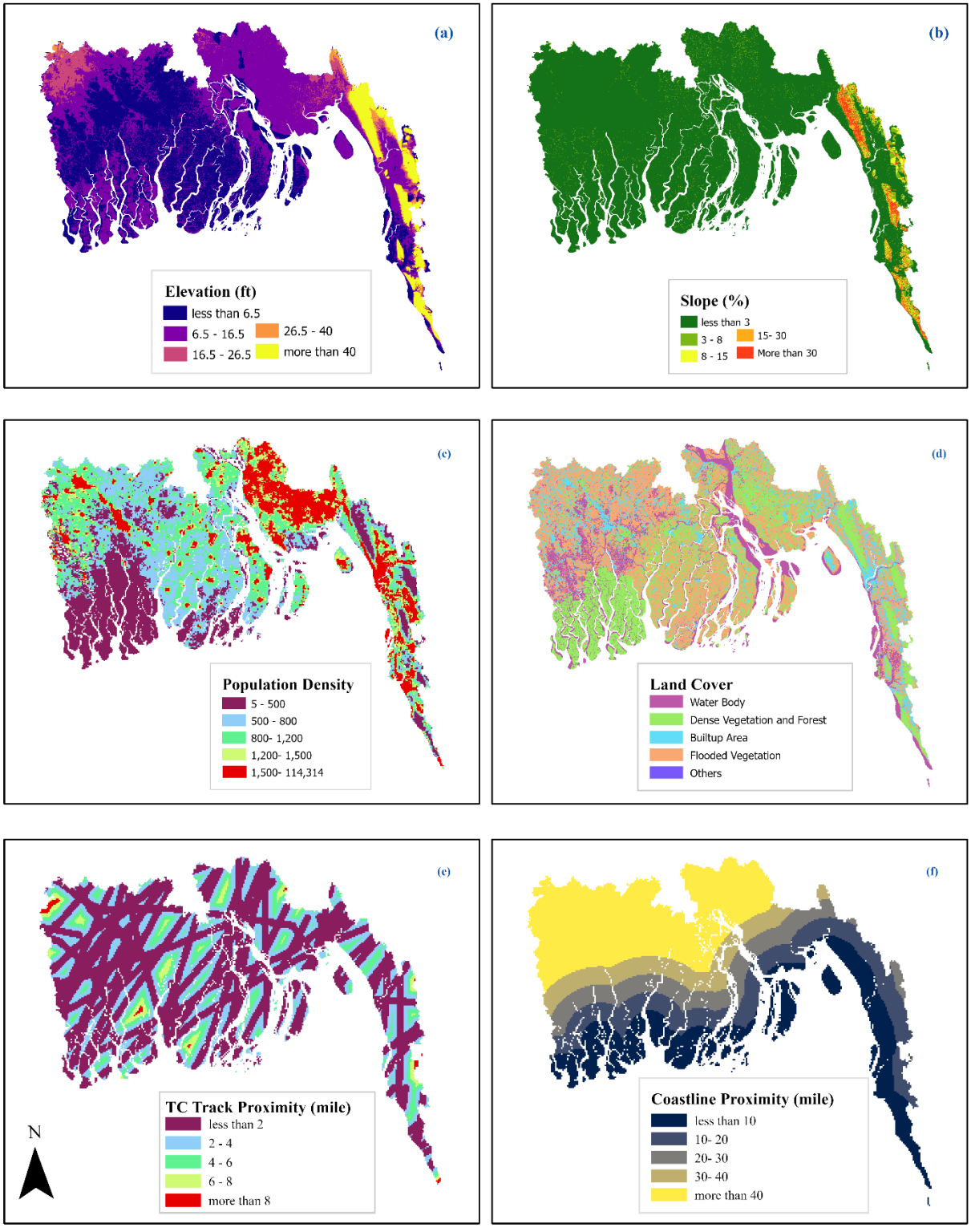

Fig.3.2. Vulnerability and exposure parameters: a) elevation, b) slope, c) population density, d) land cover, e) proximity to cyclone track, and f) proximity to coastline

is seen in Fig 3.2a and 3.2d (Barua, 1991; Karim & Mimura, 2008). Agricultural land or flooded vegetation has little resistance to cyclones' destructive impact. Fig. 3.2d represents that most of the coastal zone belongs to agricultural land, with the maximum share in the western districts.

TCs are a frequent event on the Bangladesh coast. Cyclones passed through almost all over the coastal districts from 1970-2022, making this entire zone highly vulnerable (Fig. 3.2e). Tropical cyclones mainly originate over the warm ocean; thus, proximity to the coastline should be measured. Eastern Cliff is in alarming condition because of their location, mostly within 20 miles of the coastline. A very low vulnerability was observed only in some regions in the north, particularly Jessore and Narial districts (Fig. 3.2f).

The consistency ratio (CR) for vulnerability and exposure criteria using the AHP technique was 0.06, which is below 0.10 and makes the judgment acceptable for this study. The maximum priority was given to coastline proximity, followed by cyclone track proximity, elevation, population density, slope, and land cover (Fig. 3.3). These weights were then assigned to build a composite vulnerability and exposure map using the weighted overlay tool.

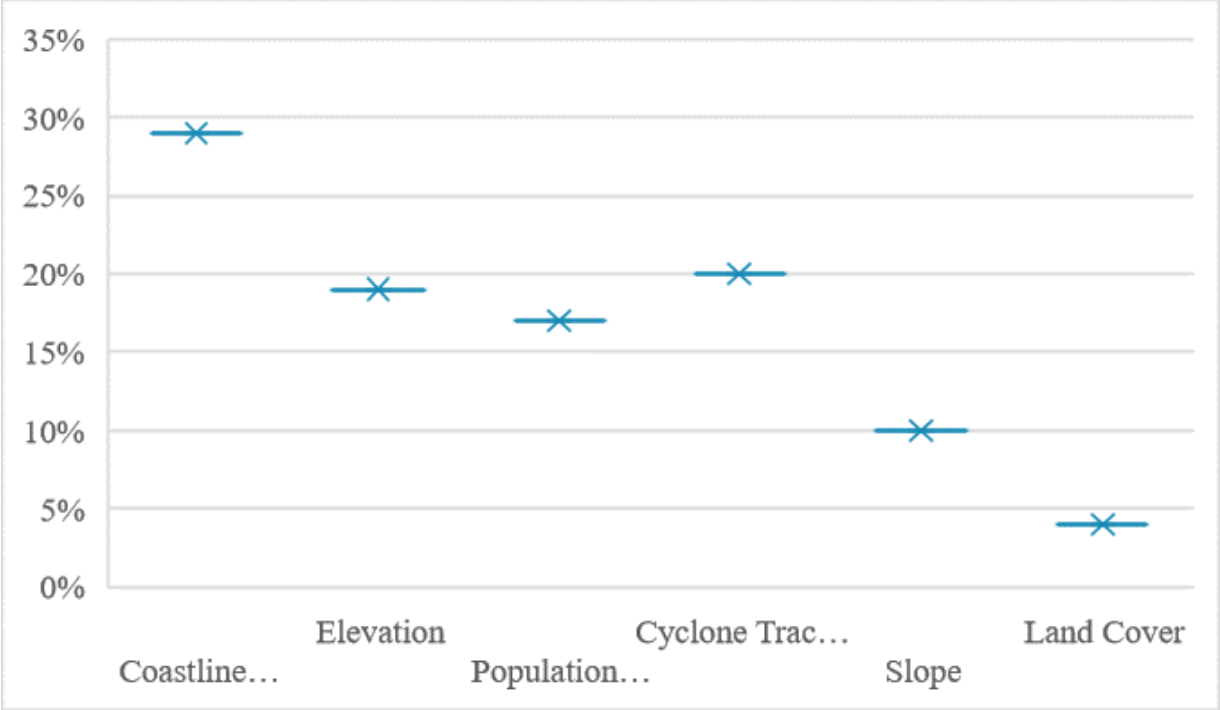

Fig. 3.3: Vulnerability and Exposure criteria weight

The composite result of vulnerability and exposure using these six parameters shows that almost the entire exposed coast was at risk. Vulnerability mostly varied from high (~50%) to very high (~3%) in this area (Fig. 3.4). Very high vulnerability was exhibited mainly in the Noakhali district on the central and Cox's Bazar and Chittagong districts on the eastern coast. This indicates the role of Sundarbans as a shield for offsetting the vulnerability on the western coast. The inland areas are within moderate vulnerability. Low vulnerability belongs to only 0.7% of the areas, whereas very low vulnerable areas were absent on the coast.

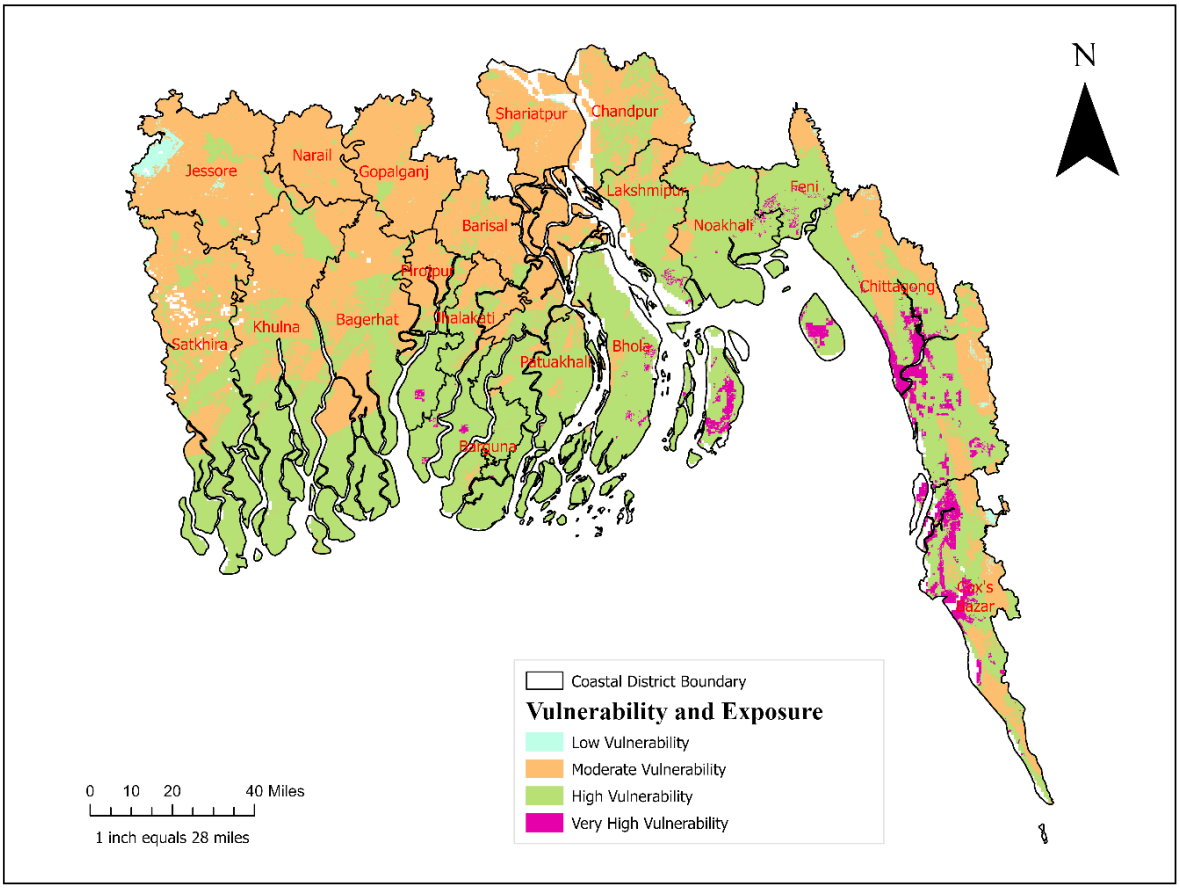

Fig. 3.4 Spatial distribution of Vulnerability and Exposure

3.3.2. Hazard Mapping

For understanding TCs patterns, four parameters were taken into account under the Hazard component: precipitation, TC cyclone frequency, TC wind speed, and storm surge height (Fig. 3.5) (Zhou et al., 2021). The western coast shows (Fig 3.5a) that higher rainfall was noticed in the districts with very high to high cyclone frequency (Fig 3.5b). However, the eastern coast and parts of the central coast do not follow this. After examining historical data from 1970 to 2022, it was revealed that although the western zone had the highest frequency of TCs (Fig. 3.5b), it also had the lowest cyclonic wind speed (Fig. 3.5c). The Sundarbans mangrove forest's ability to reduce wind speed may be one factor contributing to this low wind speed.

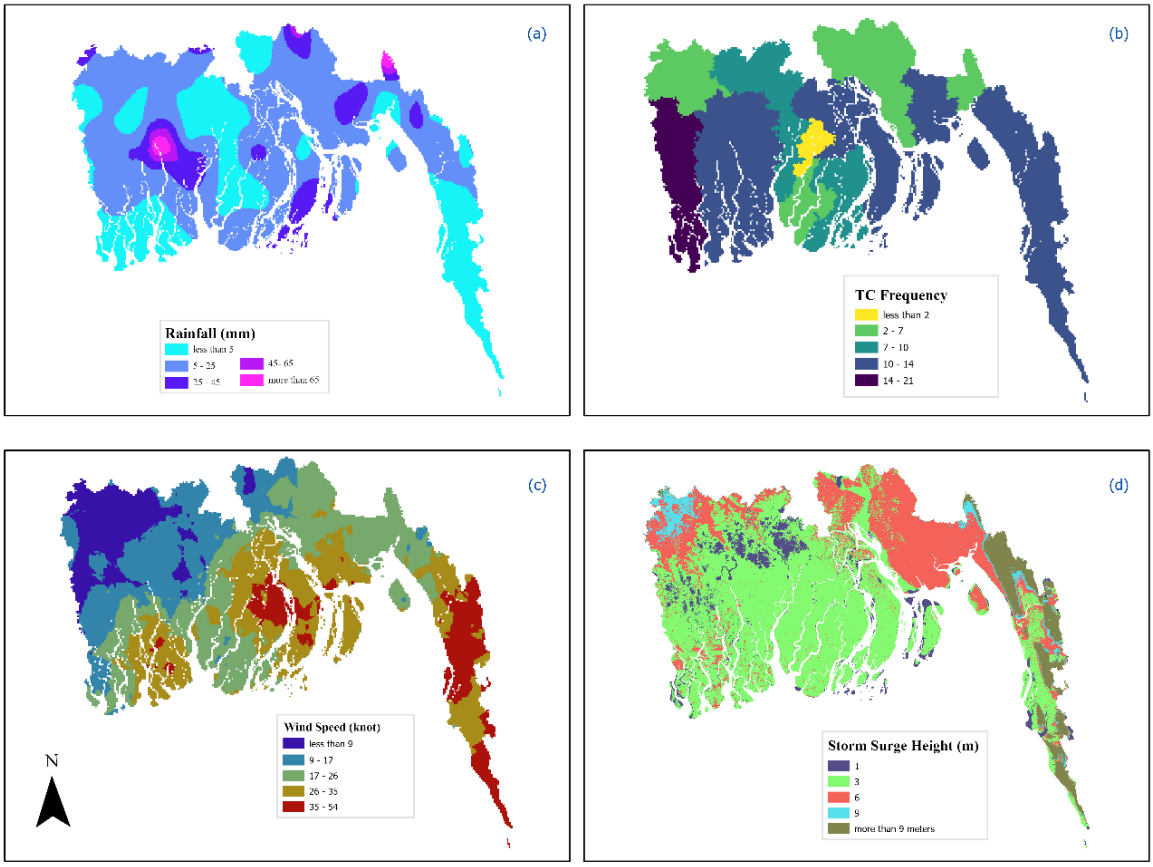

Fig.3.5. Hazard parameters: a) rainfall, b) TCs frequency, c) TCs wind speed, and d) Storm surge height

Storm surge is considered as the most destructive attribute of tropical cyclones in coastal Bangladesh (Rana et al., 2010). Records show that the highest number of cyclone fatalities in Bangladesh have been caused by storm surges (Alam et al., 2020). The height map in Fig 3.4d shows the areas that will be flooded when the storm surge reaches a certain altitude. Fig 3.5d shows the landmass that will be inundated when the storm surge will reach a certain altitude. More than half (~58%) of the coastal areas will be inundated if the storm surge height reaches 3 meters, including most of the western coast (Fig. 3.5d). Based on historical data, storm surge height caused by severe cyclones ranged from 1.5 to 9 meters (Dasgupta et al., 2010). Therefore,

except for the hilly region on the eastern coast, almost all the areas are vulnerable to cyclonic flooding. Only around 7% of areas on the eastern coast and ~3% of areas on the western coast have respectively very low and low vulnerability in terms of cyclonic flooding (Fig. 3.5d). This study supports the findings of Alam et al. (2020) that Ukhia and Ramu would suffer a lesser impact from a surge of ten meters.

The consistency ratio (CR) for Hazard criteria using the AHP technique was 4%. The maximum priority was given to storm surge height, followed by TCs frequency and windspeed, and rainfall (Fig. 3.6). These weights were then assigned to build a composite map for hazard.

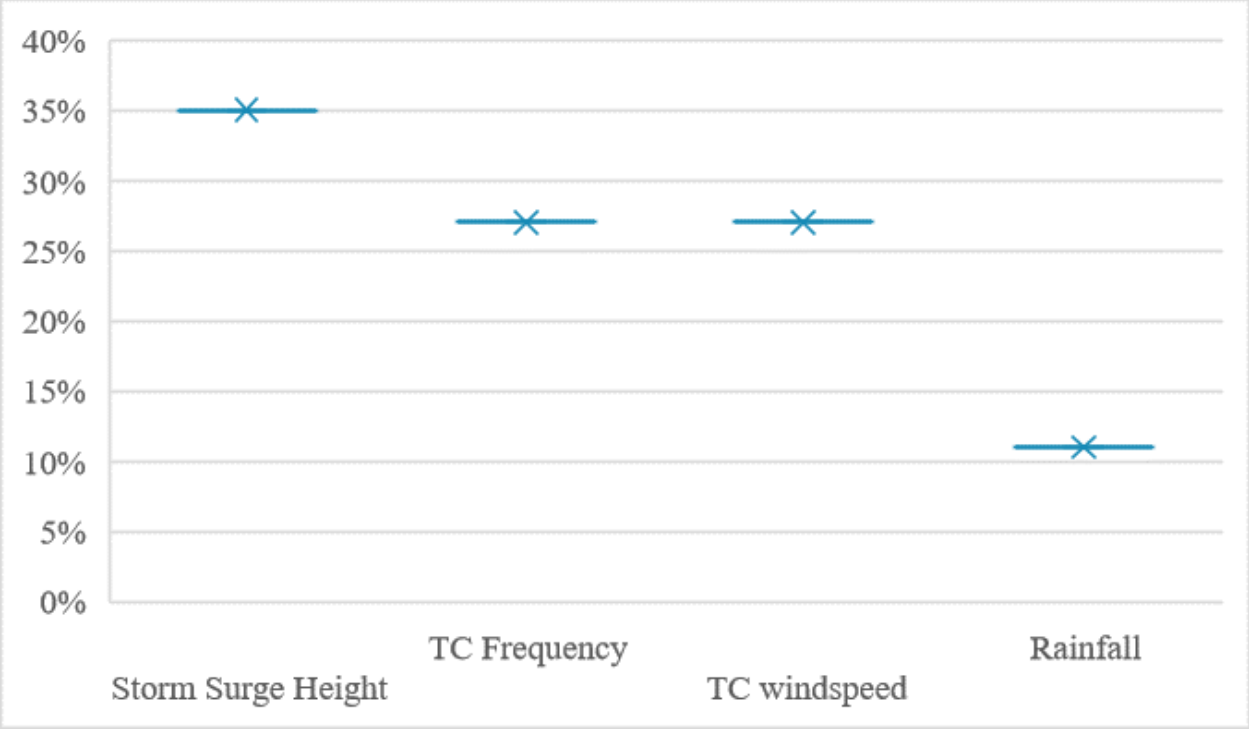

Fig 3.6: Weightage for Hazard criteria

The area with a moderate hazard category account for 22.08% of the total area, mainly distributed in the south-central exposed coast and eastern coast. The hazard map (Fig. 3.7)

reveals that the hazard level is relatively low in the western zone compared to the eastern and central coasts. The areas with moderate hazard levels (Fig. 3.7) strongly correlate with the highly vulnerable areas (Fig 3.4).

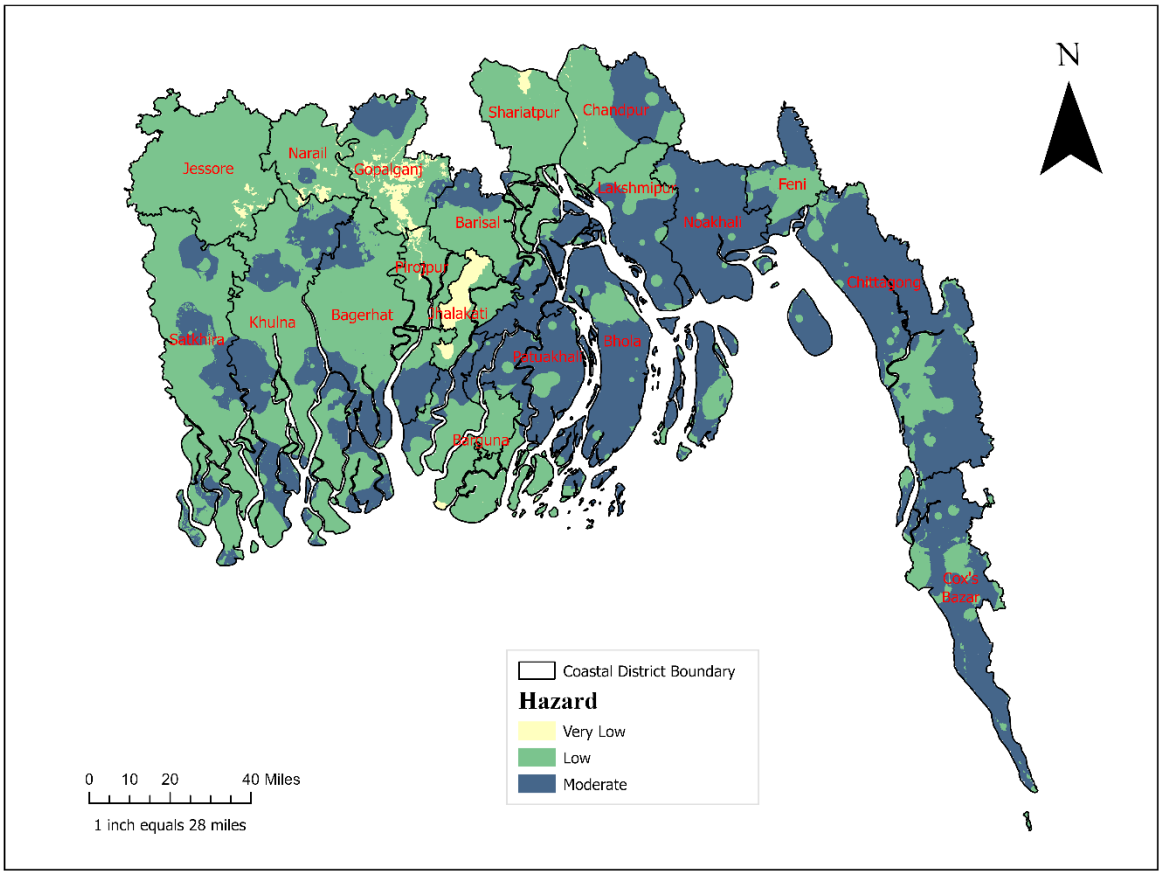

Fig. 3.7: Spatial distribution of Hazard

3.3.3 Adaptive Capacity Mapping

Nearly all of the exposed coastal areas, as shown in Fig. 3.8, are located 4 miles or less from the cyclone shelters. Around 45% of the landmass is within 1 mile of the shelter. After the deadly consequence of the Bhola cyclone in 1970, about 2,500 cyclone shelters were constructed along the coast to protect the coastal community (Faruk et al., 2018). The result of these

enormous number of cyclone shelters is reflected in the recent data where the death rate decreased by more than 100 times than in 1970. In addition, healthcare facilities are necessary for the management of the aftermath of extreme events. However, most people live outside the 4 miles buffer of health centers. Only around 27% are within one mile of the facilities, which makes the community highly vulnerable during and after a disaster. In Fig 3.8b, improper allocation of health centers can also be seen in which the eastern zone is less accessible to nearby healthcare facilities.

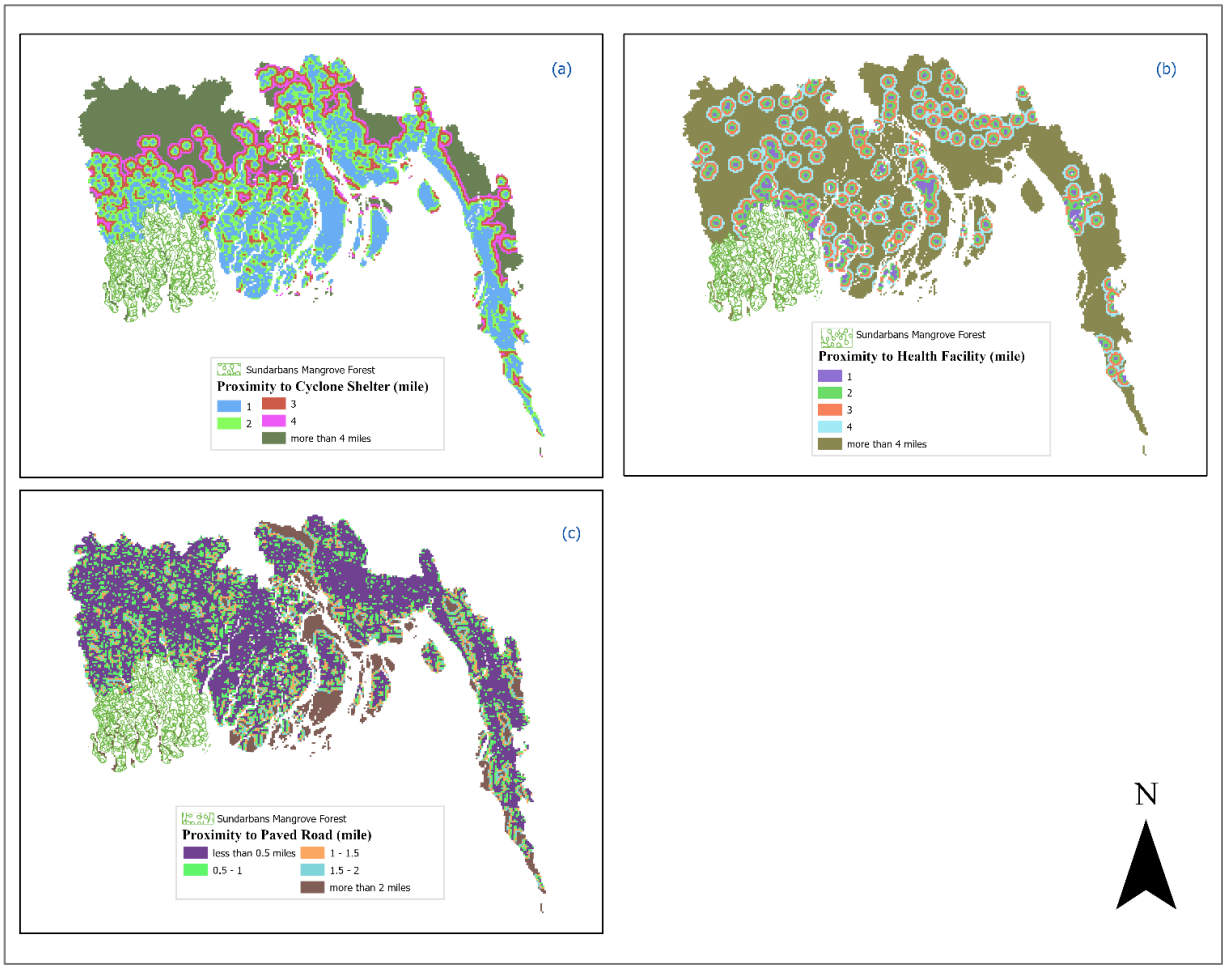

Fig. 3.8. Mitigation parameters: a) Cyclone Shelter, b) Health Center, and c) Road Network

In both the evacuation phase before a disaster and the rescue, relief, and recovery phase

afterwards, roads play a vital role (Amin et al., 2019; Zhu et al., 2022). Non-paved roads were discarded from the analysis as cyclones often bring rainfall, and that type of road will make transportation harder. Some parts of the central coasts, exposed to the Bay of Bengal, do not have access to paved roads in their proximity which puts the community in the very highly vulnerable group (Fig 3.8c).

The consistency ratio (CR) in the AHP model for mitigation criteria was 0.03, illustrates the validity of the user's choice to create a pairwise comparison matrix. The maximum priority was given to cyclone shelters, followed by coastal vegetation, health centers, and road networks (Fig. 3.9). These weights were then assigned to build a composite mitigation map using the weighted overlay tool.

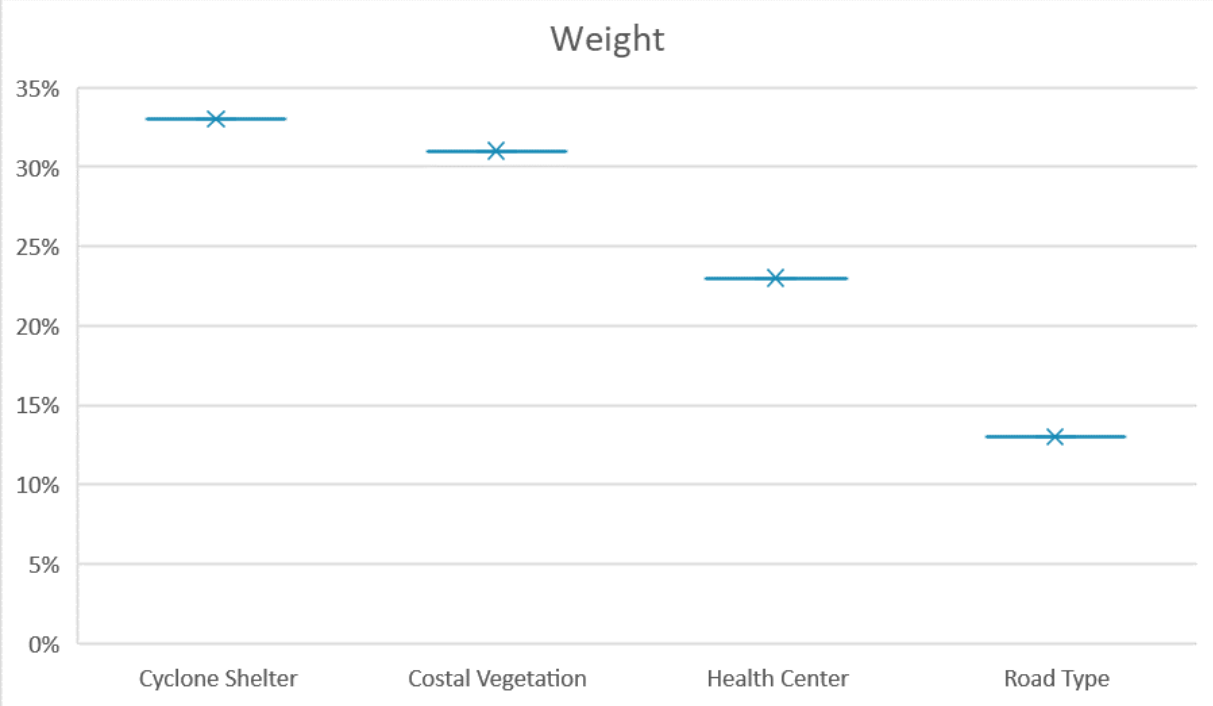

Fig 3.9: Weightage for Adaptive Capacity indicators

The map (Fig. 3.10) of the adaptive capacity shows that poor mitigation capacity was

found in the central and western zone. Almost all the coasts were highly adaptive to TCs in terms of the given parameters. The eastern district showed less preparedness compared to the western and central zones. The western part's high mitigation level was around the Sundarbans mangrove forest. (Fig. 3.10).

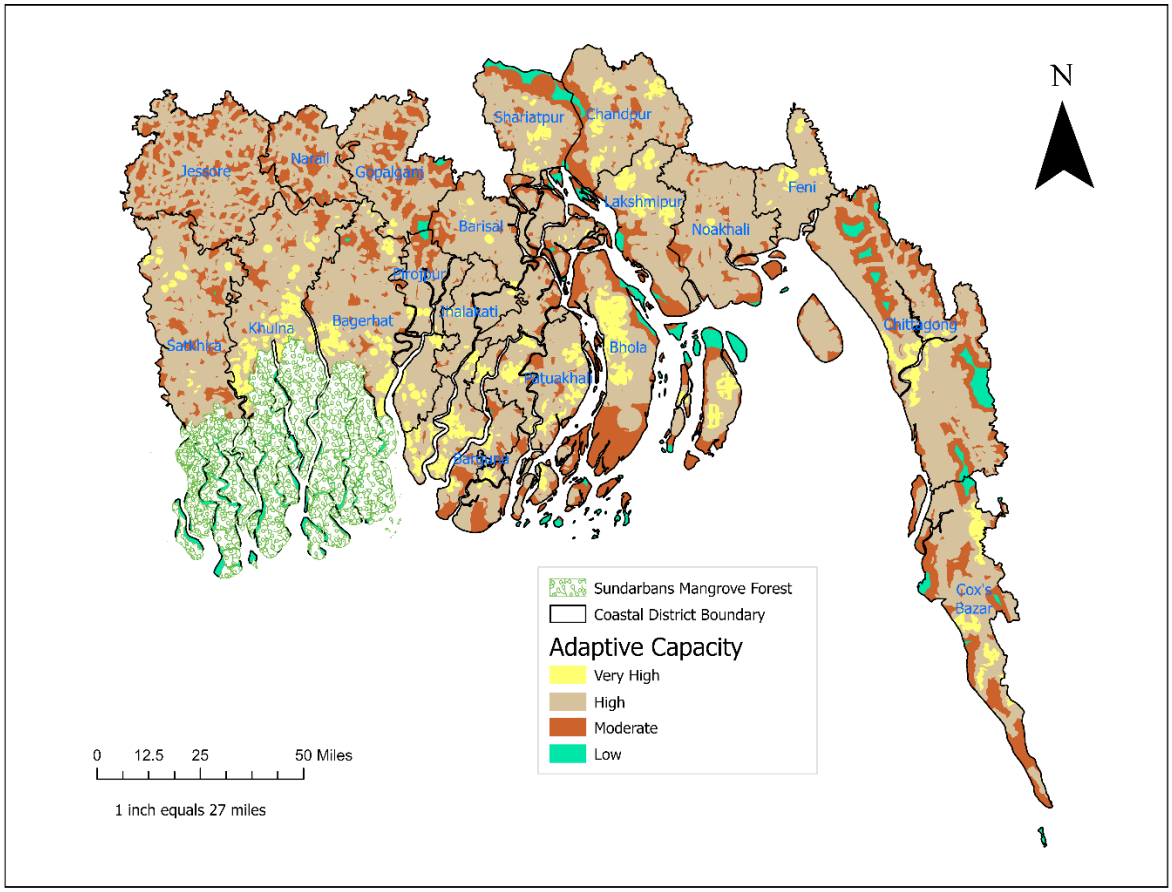

Fig. 3.10: Spatial distribution of Adaptive Capacity

3.3.4 Risk Assessment

Physical and social components are the two most important disciplines of vulnerability that are crucial to disaster risk assessment (Roberts et al., 2009). In order to generate the composite risk map for TCs, layers such as hazard, physical vulnerability, social vulnerability,

and adaptive capacity were incorporated into it. As shown in Fig. 3.11, a larger part of the central exposed coast and inland coast are at high to very high risk. Almost the entire Bhola district's risk varied from very high to high, which was also evident in the study of Quader et al. (2017).

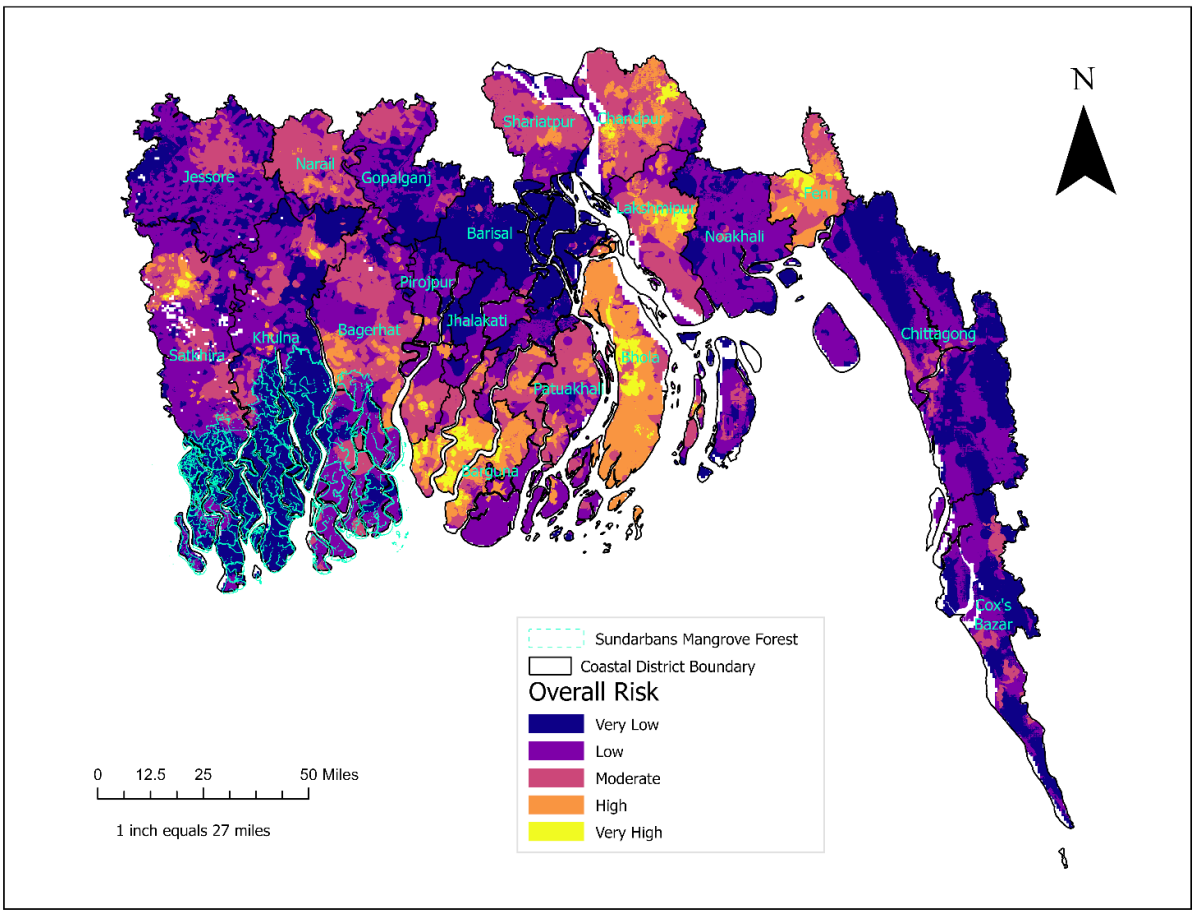

Fig. 3.11: Spatial distribution of overall TCs risk integrating social and physical vulnerability

On the other side, the eastern part is not in the high-risk zone, and this zone exhibited very low to moderate risk levels where most of the areas share low risk (Fig 3.11). The north-western part of the Satkhira district is at very high risk of tropical cyclones, whereby more than half of the Sundarbans Forest shows very low vulnerability. In addition, most parts of the Barguna district

showed a higher cyclonic risk, which also came out in the study by Hoque et al. (2021).

Its limitations include the use of 2011 data on housing and population because the latest census data for 2021 has not yet been published. This study tried to incorporate the most recent available data, but the social vulnerability layer includes information from 2011. Fig. 2.5 in Chapter 2 shows that almost all over the coast's population increased, including the areas with very low vulnerability in Fig. 3.11. It is assumed that with the increasing population, social vulnerability increased too. Hence, using social vulnerability data to show the overall coastal risk will influence the result significantly. To avoid the biasness, this study prepared a physical risk

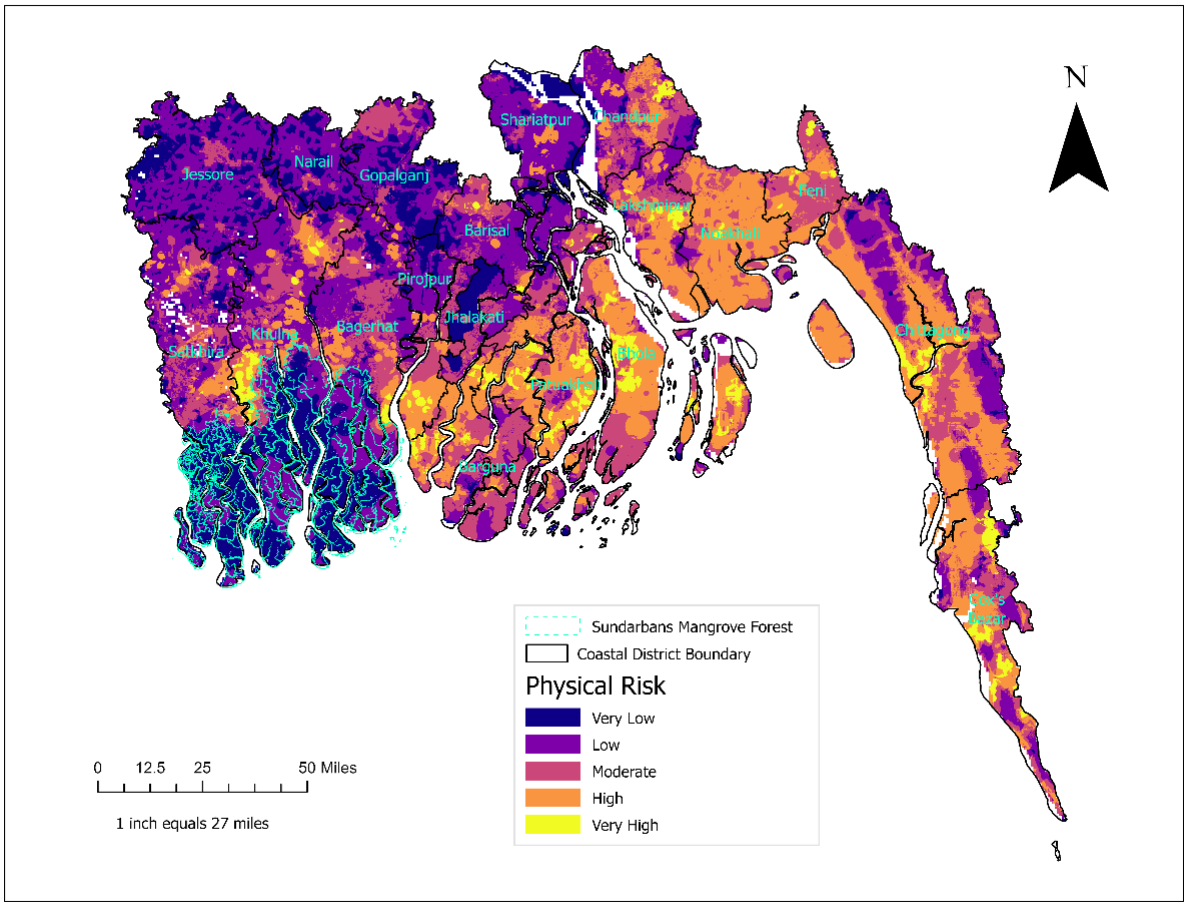

Fig. 3.12: Spatial distribution of TCs physical risk

map by excluding social vulnerability, shown in Fig. 3.12. Where the spatial distribution in Fig 3.11 marked the eastern coast as a high-risk area, Fig. 3.12 shows the opposite, where most of the areas are at high or very high risk of TCs. Noakhali occupies the most extensive area in the high risk level, followed by Laksmipur on the inland central coast, where the population density was also very high (Fig. 3.1c). Quader et al. (2017) found that the exposed coast of the Noakhali district was at very high physical risk, which is also displayed in Fig. 3.12. They also found Chandpur, Noakhali, and Feni districts in the western part of the central coast at low risk, which is ultimately the opposite of this study's finding, where it demonstrates very high to moderately high risk. However, Quader et al. (2017) analyzed physical risk based on only six parameters, while this study used 13 parameters. These disparity may be due to the inclusion of additional parameters in this study. Some areas near the Sundarbans mangrove forest show very risk (Fig 3.12), which matches their study. Khulna district in the western tidal plain exhibits high- or very high-risk levels near the Sundarbans area. This is one of the zones that are frequently hit by tropical cyclones (Fig 3.1e). Hoque et al. (2018) found very low to very high cyclonic risk for Sarankhola upazila in the Bagerhat district, which is also evident in this study (Fig 3.12). Almost all parts of the Swandip upazila in the Chittagong district demonstrates high cyclonic risk, which aligns with the finding of Hoque et al. (2019).

3.4 Conclusion

An overall cyclone risk map for the coastal region of Bangladesh was prepared in this study in order to assess the vulnerability of the country to tropical cyclones. Physical vulnerability assessment considered 13 variables under three broad categories: vulnerability and exposure, hazards, and mitigation. In addition, 19 socioeconomic and demographic indicators were selected to prepare the social vulnerability layer. The result indicates that vulnerability

along the coast increases without employing social vulnerability. Regardless of whether or not social vulnerability is considered, areas on the central coast are more susceptible to the negative effects of TCs. Compared to the western coast, where mangrove forest is abundant, and the eastern coast which is mainly high elevated land, the central coast is more vulnerable. Since other researchers assess risk and vulnerability differently, it becomes more challenging to compare the results with theirs since variables are selected differently and analyzed differently. A precise comparison was not possible for this study due to a lack of empirical research.

References

Adger, W. N. (2006). Vulnerability. *Global Environmental Change*, *16*(3), 268–281. https://doi.org/10.1016/j.gloenvcha.2006.02.006

Ahammad, R., Nandy, P., & Husnain, P. (2013). Unlocking ecosystem based adaptation opportunities in coastal Bangladesh. *Journal of Coastal Conservation*, *17*(4), 833–840. https://doi.org/10.1007/s11852-013-0284-x

Alam, A., Sammonds, P., & Ahmed, B. (2020). Cyclone risk assessment of the Cox's Bazar district and Rohingya refugee camps in southeast Bangladesh. *Science of the Total Environment*, *704*. https://doi.org/10.1016/j.scitotenv.2019.135360

Ali, S. A., Khatun, R., Ahmad, A., & Ahmad, S. N. (2020). Assessment of Cyclone Vulnerability, Hazard Evaluation and Mitigation Capacity for Analyzing Cyclone Risk using GIS Technique: A Study on Sundarban Biosphere Reserve, India. *Earth Systems and Environment*, *4*(1), 71–92. https://doi.org/10.1007/s41748-019-00140-x

Amin, S., Tamima, U., & Amador-Jiménez, L. E. (2019). Optimal pavement management: Resilient roads in support of emergency response of cyclone affected coastal areas. *Transportation Research Part A: Policy and Practice*, *119*, 45–61. https://doi.org/10.1016/j.tra.2018.11.001

Antinao, J. L., & Farfán, L. M. (2013). Occurrence of landslides during the approach of tropical cyclone Juliette (2001) to Baja California Sur, Mexico. *Atmósfera*, *26*(2).

Barua, D. K. (1991). The coastline of Bangladesh—An overview of processes and forms. *Coastal Zone'91*, 2284–2301.

Cardona, O.-D., Aalst, M. K. van, Birkmann, J., Fordham, M., McGregor, G., Perez, R., Pulwarty, R. S., Schipper, E. L. F., & Sinh, B. T. (2012). Determinants of risk: exposure

and vulnerability. *Managing the Risks of Extreme Events and Disasters to Advance Climate Change Adaptation*.

Dasgupta, S., Huq, M., Khan, Z. H., Murshed, M., Ahmed, Z., Mukherjee, N., Fida, M., Kiran, K., The, P., & Bank, W. (2010). Vulnerability of Bangladesh to Cyclones in a Changing Climate Potential Damages and Adaptation Cost. http://econ.worldbank.org.

Dewan, A. M. (2013). Floods in a Megacity: Geospatial Techniques in Assessing Hazards, Risk and Vulnerability. http://www.springer.com/series/10180

Dewan, A., Shahid, S., Bhuian, M. H., Hossain, S. M. J., Nashwan, M. S., Chung, E. S., Hassan, Q. K., & Asaduzzaman, M. (2022). Developing a high-resolution gridded rainfall product for Bangladesh during 1901–2018. *Scientific Data*, *9*(1). https://doi.org/10.1038/s41597-022-01568-z

Eckstein, D., Künzel, V., & Schäfer, L. (2021). Global Climate Risk Index 2021. Germanwatch e.V. https://www.germanwatch.org/en/19777

Emanuel, K., Ravela, S., Vivant, E., & Risi, C. (2006). Supplement to A Statistical Deterministic Approach to Hurricane Risk Assessment. *Bulletin of the American Meteorological Society*, *87*(3), S1–S5. https://doi.org/10.1175/bams-87-3-emanuel

Engle, N. L. (2011). Adaptive capacity and its assessment. *Global Environmental Change*, *21*(2), 647–656. https://doi.org/10.1016/j.gloenvcha.2011.01.019

Faruk, M., Ashraf, S. A., & Ferdaus, M. (2018). An analysis of inclusiveness and accessibility of Cyclone Shelters, Bangladesh. *Procedia Engineering*, *212*, 1099–1106. https://doi.org/10.1016/j.proeng.2018.01.142

Flanagan, B. E., Gregory, E. W., Hallisey, E. J., Heitgerd, J. L., & Lewis, B. (2011). A Social Vulnerability Index for Disaster Management. *Journal of Homeland Security and*

Emergency Management, *8*(1). https://doi.org/10.2202/1547-7355.1792

Füssel, H. M., & Klein, R. J. T. (2006). Climate change vulnerability assessments: An evolution of conceptual thinking. *Climatic Change*, *75*(3), 301–329. https://doi.org/10.1007/s10584-006-0329-3

Glick, Patricia., Stein, B. A., Edelson, N. A., & National Wildlife Federation. (2011). Scanning the conservation horizon : a guide to climate change vulnerability assessment. *National Wildlife Federation.* https://www.nwf.org/vulnerabilityguide

Hoque, M. A. A., Phinn, S., Roelfsema, C., & Childs, I. (2016). Assessing tropical cyclone impacts using object-based moderate spatial resolution image analysis: a case study in Bangladesh. *International Journal of Remote Sensing*, *37*(22), 5320–5343. https://doi.org/10.1080/01431161.2016.1239286

Hoque, M. A. A., Phinn, S., Roelfsema, C., & Childs, I. (2017). Tropical cyclone disaster management using remote sensing and spatial analysis: A review. *International Journal of Disaster Risk Reduction*, 22, 345–354. https://doi.org/10.1016/j.ijdrr.2017.02.008

Hoque, M. A. A., Phinn, S., Roelfsema, C., & Childs, I. (2018). Assessing tropical cyclone risks using geospatial techniques. *Applied Geography*, *98*, 22–33. https://doi.org/10.1016/j.apgeog.2018.07.004

Hoque, M. A. A., Pradhan, B., Ahmed, N., Ahmed, B., & Alamri, A. M. (2021). Cyclone vulnerability assessment of the western coast of Bangladesh. *Geomatics, Natural Hazards and Risk*, *12*(1), 198–221. https://doi.org/10.1080/19475705.2020.1867652

Hoque, M. A. A., Pradhan, B., Ahmed, N., & Roy, S. (2019). Tropical cyclone risk assessment using geospatial techniques for the eastern coastal region of Bangladesh. *Science of the Total Environment*, *692*, 10–22. https://doi.org/10.1016/j.scitotenv.2019.07.132

Karim, M. F., & Mimura, N. (2008). Impacts of climate change and sea-level rise on cyclonic storm surge floods in Bangladesh. *Global Environmental Change*, *18*(3), 490–500. https://doi.org/10.1016/j.gloenvcha.2008.05.002

Karra, K., Kontgis, C., Statman-Weil, Z., Mazzariello, J. C., Mathis, M., & Brumby, S. P. (2021). Global land use / land cover with Sentinel 2 and deep learning. *2021 IEEE International Geoscience and Remote Sensing Symposium IGARSS*, 4704–4707. https://doi.org/10.1109/IGARSS47720.2021.9553499

Kelman, I., Gaillard, J. C., Lewis, J., & Mercer, J. (2016). Learning from the history of disaster vulnerability and resilience research and practice for climate change. *Natural Hazards*, *82*, 129–143. https://doi.org/10.1007/s11069-016-2294-0

Khan, A., Chatterjee, S., & Weng, Y. (2021). UHI drivers and mapping the urban thermal environment. In *Urban Heat Island Modeling for Tropical Climates*, 69–115. https://doi.org/10.1016/b978-0-12-819669-4.00003-9

Li, K., & Li, G. S. (2013). Risk assessment on storm surges in the coastal area of Guangdong Province. *Natural Hazards*, *68*(2), 1129–1139. https://doi.org/10.1007/s11069-013-0682-2

Mahapatra, M., Ramakrishnan, R., & Rajawat, A. S. (2015). Coastal vulnerability assessment using analytical hierarchical process for South Gujarat coast, India. *Natural Hazards*, *76*(1), 139–159. https://doi.org/10.1007/s11069-014-1491-y

Mallick, B. (2014). Cyclone shelters and their locational suitability: An empirical analysis from coastal Bangladesh. *Disasters*, *38*(3), 654–671. https://doi.org/10.1111/disa.12062

Mallick, B., Ahmed, B., & Vogt, J. (2017). Living with the risks of cyclone disasters in the South-Western Coastal Region of Bangladesh. *Environments*, *4*(1), 1–17.

https://doi.org/10.3390/environments4010013

Mansour, S. (2019). Geospatial modelling of tropical cyclone risks to the southern Oman coasts. *International Journal of Disaster Risk Reduction*, *40*, 101151. https://doi.org/10.1016/j.ijdrr.2019.101151

MoEF. (2009). Bangladesh Climate Change Strategy and Action Plan 2009.

Mondal, M., Haldar, S., Biswas, A., Mandal, S., Bhattacharya, S., & Paul, S. (2021). Modeling cyclone-induced multi-hazard risk assessment using analytical hierarchical processing and GIS for coastal West Bengal, India. *Regional Studies in Marine Science*, *44*. https://doi.org/10.1016/j.rsma.2021.101779

Mullick, M. R. A., Tanim, A. H., & Islam, S. M. S. (2019). Coastal vulnerability analysis of Bangladesh coast using fuzzy logic based geospatial techniques. *Ocean and Coastal Management*, *174*, 154–169. https://doi.org/10.1016/j.ocecoaman.2019.03.010

Murali, R. M., Ankita, M., Amrita, S., & Vethamony, P. (2013). Coastal vulnerability assessment of Puducherry coast, India, using the analytical hierarchical process. *Natural Hazards and Earth System Sciences*, *13*(12), 3291–3311. https://doi.org/10.5194/nhess-13-3291-2013

Murty, P. L. N., Bhaskaran, P. K., Gayathri, R., Sahoo, B., Srinivasa Kumar, T., & SubbaReddy, B. (2016). Numerical study of coastal hydrodynamics using a coupled model for Hudhud cyclone in the Bay of Bengal. *Estuarine, Coastal and Shelf Science*, *183*, 13–27. https://doi.org/10.1016/j.ecss.2016.10.013

Neumann, B., Vafeidis, A. T., Zimmermann, J., & Nicholls, R. J. (2015). Future coastal population growth and exposure to sea-level rise and coastal flooding - A global assessment. *PLoS ONE*, *10*(3). https://doi.org/10.1371/journal.pone.0118571

Nicholls, R. J., Wong, P. P., Burkett, V., Codignotto, J., Hay, J., McLean, R., Ragoonaden, S., & Woodroffe, C. D. (2007). *Coastal systems and low-lying areas*.

Nikkanen, M., Räsänen, A., & Juhola, S. (2021). The influence of socioeconomic factors on storm preparedness and experienced impacts in Finland. *International Journal of Disaster Risk Reduction, 55*. https://doi.org/10.1016/j.ijdrr.2021.102089

Pathak, S., Panta, H. K., Bhandari, T., & Paudel, K. P. (2020). Flood vulnerability and its influencing factors. *Natural Hazards*, *104*(3), 2175–2196. https://doi.org/10.1007/s11069-020-04267-3

Qiu, Z., Yue, L., & Liu, X. (2019). Void filling of digital elevation models with a terrain texture learning model based on generative adversarial networks. *Remote Sensing*, *11*(23). https://doi.org/10.3390/rs11232829

Quader, M. A., Khan, A. U., & Kervyn, M. (2017). Assessing risks from cyclones for human lives and livelihoods in the coastal region of Bangladesh. *International Journal of Environmental Research and Public Health*, *14*(8). https://doi.org/10.3390/ijerph14080831

Rahman, M., Ningsheng, C., Islam, M. M., Dewan, A., Iqbal, J., Washakh, R. M. A., & Shufeng, T. (2019). Flood Susceptibility Assessment in Bangladesh Using Machine Learning and Multi-criteria Decision Analysis. *Earth Systems and Environment*, *3*(3), 585–601. https://doi.org/10.1007/s41748-019-00123-y

Rajakumari, S., Minnu, A., & Sarunjith, K. J. (2022). Determination of vulnerable zones along Brahmapur coast, Odisha using AHP and GIS with validation against multiple cyclones. *Environmental Monitoring and Assessment*, *194*(4). https://doi.org/10.1007/s10661-022-09886-w

Rana, M. S., Gunasekara, K., Kumar Hazarika, M., Samarakoon, L., & Siddiquee, M. (2010). Application of Remote Sensing and GIS for Cyclone Disaster Management in Coastal Area: A Case Stusy at Barguna District, Bangladesh.

Roberts, N. J., Nadim, F., & Kalsnes, B. (2009). Quantification of vulnerability to natural hazards. *Georisk*, *3*(3), 164–173. https://doi.org/10.1080/17499510902788850

Saaty, T. L. (1977). A Scaling Method for Priorities in Hierarchical Structures. *Journal 01: Mathematical Psychology, 15*.

Saaty, T. L. (1980). The Analytic Hierarchy Process.

Sahoo, B., & Bhaskaran, P. K. (2016). Assessment on historical cyclone tracks in the Bay of Bengal, east coast of India. *International Journal of Climatology*, *36*(1), 95–109. https://doi.org/10.1002/joc.4331

Sahoo, B., & Bhaskaran, P. K. (2018). Multi-hazard risk assessment of coastal vulnerability from tropical cyclones – A GIS based approach for the Odisha coast. *Journal of Environmental Management, 206*, 1166–1178. https://doi.org/10.1016/j.jenvman.2017.10.075

Sinaga, T. P. T., Nugroho, A., Lee, Y. W., & Suh, Y. (2011). GIS mapping of tsunami vulnerability: Case study of the Jembrana regency in Bali, Indonesia. *KSCE Journal of Civil Engineering*, *15*(3), 537–543. https://doi.org/10.1007/s12205-011-0741-8

Swain, D. (2022). Tropical Cyclones and Coastal Vulnerability: Assessment and Mitigation. 587–621. https://doi.org/10.1007/978-3-030-90479-1_30

Tempa, K. (2022). District flood vulnerability assessment using analytic hierarchy process (AHP) with historical flood events in Bhutan. *PLoS ONE, 17*(6). https://doi.org/10.1371/journal.pone.0270467

Thomas, K., Hardy, R. D., Lazrus, H., Mendez, M., Orlove, B., Rivera-Collazo, I., Roberts, J. T.,

Rockman, M., Warner, B. P., & Winthrop, R. (2019). Explaining differential vulnerability to climate change: A social science review. *Wiley Interdisciplinary Reviews: Climate Change, 10*(2). https://doi.org/10.1002/wcc.565

UNDRR. (2017). Understanding Disaster Risk.

UN-Spider. (2023). Step-by-Step: Use of Digital Elevation Data for Storm Surge Coastal Flood Modelling.

Viner, D., Ekstrom, M., Hulbert, M., Warner, N. K., Wreford, A., & Zommers, Z. (2020). Understanding the dynamic nature of risk in climate change assessments - A new starting point for discussion. *Atmospheric Science Letters*, *21*(4). https://doi.org/10.1002/asl.958

Westen, C. J. van, Castellanos, E., & Kuriakose, S. L. (2008). Spatial data for landslide susceptibility, hazard, and vulnerability assessment: An overview. *Engineering Geology*, *102*(3–4), 112–131. https://doi.org/10.1016/j.enggeo.2008.03.010

Wisner, B., Blaikie, P., Cannon, T., & Davis, I. (2003). At Risk: natural hazards, people's vulnerability and disasters Second edition 2003.

WorldPop. (2023). Open Spatial Demographic Data and Research.

Yin, J., Yin, Z., & Xu, S. (2013). Composite risk assessment of typhoon-induced disaster for China's coastal area. *Natural Hazards*, *69*(3), 1423–1434. https://doi.org/10.1007/s11069-013-0755-2

Zhou, M., Kuang, Y., Ruan, Z., & Xie, M. (2021). Geospatial modeling of the tropical cyclone risk in the Guangdong Province, China. *Geomatics, Natural Hazards and Risk, 12*(1), 2931–2955. https://doi.org/10.1080/19475705.2021.1972046

Zhu, J., Liu, K., Wang, M., Xu, W., Liu, M., & Zheng, J. (2022). An empirical approach for developing functions for the vulnerability of roads to tropical cyclones. *Transportation*

Research Part D: Transport and Environment, *102*. https://doi.org/10.1016/j.trd.2021.103136

Zhuang, Y., Xing, A., Jiang, Y., Sun, Q., Yan, J., & Zhang, Y. (2022). Typhoon, rainfall and trees jointly cause landslides in coastal regions. *Engineering Geology*, *298*. https://doi.org/10.1016/j.enggeo.2022.106561

CHAPTER 4

Tropical Cyclone's Impact on Sundarbans Mangrove Forest: A Case Study on Cyclone Amphan

4.1 Background

The mangrove forest is dominated by salt-tolerant halophytes, notably trees and shrubs, which are most commonly found between 30° N and 30° S latitude along the tropical and subtropical coastlines (Baishya et al., 2020; Donato et al., 2011; Lima et al., 2021; Reef & Lovelock, 2015). As of 2020, 14.8 million ha of the earth's surface was covered by mangrove forests which were distributed across 113 nations and territories (FAO, 2020). Asia was home to more than 37% of the world's mangrove forest, followed by Africa (~22%), North and Central America (~17%), South America (~14%), and Oceania (~9%) (FAO, 2020). These coastal biomes are of utmost significance as they are rich in biodiversity and provide a broad array of services, with a global annual value estimated to be approximately US $1.9 billion (Andersen, 2023). Aside from the economic worth of these forest resources, mangroves are a promising carbon sink that is capable of sequestering three to five times more carbon than traditional tropical forests (NOAA, 2023b). Due to its unique characteristics, the forest contributes to the stabilization of the shoreline by reducing erosion (Menéndez et al., 2020; Winterwerp et al., 2020). Furthermore, mangroves serve as a natural blockade against natural hazards like TCs, floods, and storm surges, and protect the community living near the sea and offshore islands (Hochard et al., 2019).

Mangrove protects more than 18 million global population from flooding annually and

saves 16% of global economic contraction (Beck et al., 2018). Although this coastal defense is rich in resources, it is paradoxical to say that it has been identified as one of the most endangered ecosystems in the world because of climate change-induced phenomena such as sea level rise, natural hazards, and human interference such as overexploitation of resources, aquaculture, and coastal development (Alongi, 2002; Feller et al., 2017; Friess et al., 2019). As a consequence, more than 1 out of 6 mangroves are in danger (Carugati et al., 2018; Ellison, 2015; IUCN, 2010a; Rahman et al., 2010; Segaran et al., 2023). Worldwide the mangrove forest coverage has shrunk by over 6% from 1990 to 2020, a reduction to around 14717 sq. ha from around 15759 sq. ha (FAO, 2020). While the greatest proportion of global mangroves was found in South and Southeast Asia, the highest (~13%) decline was also documented in this region over the past 31 years (1990-2020) (FAO, 2020).

TCs greatly threaten human lives and properties because of their association with high-velocity wind, tidal surge, and torrential rain (Krauss & Osland, 2019). Researchers project that tropical cyclones will become more intense, with an anticipated rise in category 4 and 5 cyclones, notwithstanding the lack of agreement on whether or not there will be an increase in tropical cyclone frequency as a result of climate change (Chand et al., 2022; C2ES, 2023; Knutson et al., 2021; Kossin et al., 2020). However, the physical structure of mangrove forests, specifically the canopy structure and deep aerial rooted network, help to attenuate the wind speed, wave actions, and storm surges height (Dutta et al., 2015; Massel et al., 1999; Zhang et al., 2012). As per the study of Spalding et al. (2014), Approximately 5-50 cm of storm surge can be reduced by a kilometer of mangroves, a significant amount that can prevent flooding of low-lying areas. Beck & Menéndez (2020) highlighted that the mangroves' presence protects lives in Southeast Asian countries such as Vietnam, India, and Bangladesh. In contrast, developed

countries like the United States, China, and Taiwan faces less economic damage because of mangrove forest. In spite of this, mangrove forests are particularly susceptible to disturbance by tropical cyclones regularly and globally due to their location along low-lying coastlines.

A UNESCO world heritage site, the Sundarbans mangrove forest is the largest continuous mangrove forest on earth (Dutta et al., 2015). Located in the Ganges, Brahmaputra, and Meghna delta, this mangrove shares the boundary of two countries- Bangladesh and India, extending between 21º 30′ to 22º 40′ N, 88º 05′ to 89º 55′ E, where approximately 60% is in Bangladesh and the remainder in India (Dutta et al., 2015; Gopal & Chauhan, 2006; Halder et al., 2021). Sundarbans fringing the BoB, a hotbed of tropical cyclones, recurrently confront severe tropical cyclones. From 1970 to 2021, 45 tropical cyclones traversed within 55 miles buffer zone of this mangrove area, among which 28 were in the tropical depression category, four were in

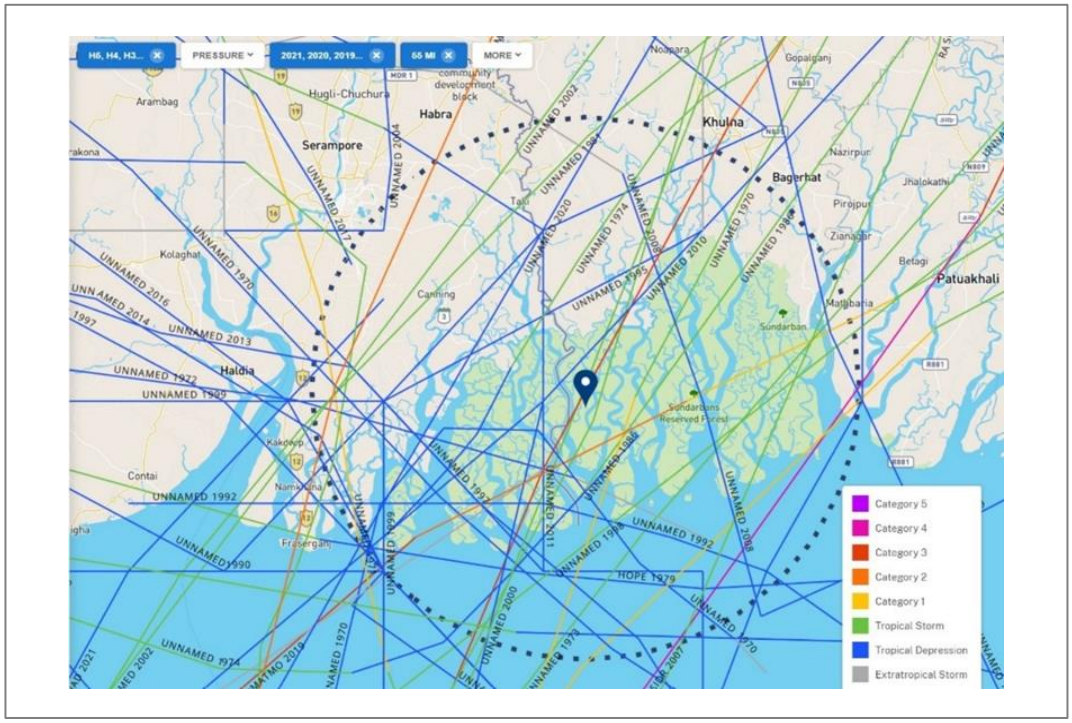

Fig. 4.1: Tropical cyclone tracks within 55 miles buffer zone of Sundarbans mangrove forest (Data derived from (NOAA, 2023b))

tropical storms, and 7 were hurricanes ranging from category 1 to category 4 (Fig 4.1). Among these, five of the seven tropical storms in the hurricane category crossed across the mangrove forest, and many slammed the forest. For instance, in Bangladesh, Sidr, a category four intensity storm of November 15, 2007, struck the eastern section of Sundarbans and caused severe damage to 30, 000 ha and partially damaged 80, 000 ha of the forest (Bhowmik& Cabral, 2013; Khan et al., 2016; MoEF, 2010). In accordance with Dutta et al. (2015), cyclone Sidr impacted more severely the Bangladeshi portion of the Sundarbans, near Bagerhat and Pirojpur, than the Indian portion. On the other hand, cyclone Ayla (category 1), which made landfall on May 25, 2009, adversely affected the social-economic condition of the coastal communities by rendering the agricultural land unproductive long term or for an extended period or permanently, which led to more exploitation and damage of the mangrove forest (Rahman & Khanum, 2017). After Sidr, cyclone Amphan wrought significant destruction to Sundarbans. Kumar & Kumar (2021) stated that around 3704 square km of forestland was impacted, among which ~37 km^2 of mangrove forest faced severe to very high degrees of damage from cyclone Amphan.

Despite being jeopardized, mangroves protect lives and properties in vulnerable coastal areas. As exemplified by Dasgupta et al. (2019), Valle et al. (2019), and Zhang et al. (2012), many researchers have attempted to demonstrate the contribution of mangrove forests to reducing storm surges and wind speeds during cyclones. Sundarbans mangrove also protected the coastal community by lowering the wind speed of cyclone Bulbul, a category- 2 hurricane, by 18km/hr from 148 km/h to 130 km/h (Gupta et al., 2019; Reliefweb, 2019). In order to determine the extent of damage caused by hazards in protected forest areas and inaccessible forest areas, a reliable evaluation of the disturbance regime is necessary for effective forest management (Dutta et al., 2015). A widespread and feasible method of monitoring changes in

mangrove ecosystems has emerged through remote sensing. With the availability of high-resolution remote sensing data and historical records, mangrove forests have been characterized, mapped, and monitored to a greater extent (Buitre et al., 2019; Giri, 2021). A number of indices have been developed that can be used to extract relevant information from satellite imagery to provide insight. This research uses optical and radar imagery to assess short-term and long-term changes in the Sundarbans mangrove forest in the wake of cyclone Amphan.

4.2 Materials and Methods

4.2.1 Data Required

The European Union Earth observation mission, Sentinel-2A Level-1C product, was used because of its high spatial and spectral resolution and frequent revisit time (ESA, 2023). The mission's multi-spectral instrument (MSI) comprises 13 spectral bands, including the range of visible, near-infrared, and short-wavelength infrared wavelengths, where visible bands and the near-infrared bands can be used to monitor vegetation health (Drusch et al., 2012; Guo et al., 2017; SentinelHub, 2023). On May 16, 2020, super cyclone Amphan formed over BoB and subsequently hit West Bengal, India, after landfall on May 20, 2020 (Ahmed et al., 2021). The normalized difference vegetation index (NDVI) was assessed for 21 days during the pre-Amphan period (80 images), from March 25, 2020, to April 15, 2020. For the post-Amphan period (58 images), images from October 25, 2020, to November 15, 2020, were collected for NDVI analysis. These were the closest sentinel 2A images available with less than 10% could coverage. A total of 241 and 232 images were collected to analyze the NDVI for 2019 and 2021, respectively.

Mangroves are mainly found in tropical and subtropical regions, which are cloud-cover-intensive regions, particularly during the monsoon season (Mitchell et al., 2017). Although

Sentinel-2A satellite has a shorter revisit time, getting cloud-free optical images is challenging for all seasons, especially during and after cyclones (Mondal et al., 2022). Radar data offers a benefit over optical imagery to overcome this issue as they can collect weather-independent imagery 24/7 (Kellndorfer, 2019; Thomas et al., 2017). In addition, the Sentinel-1 captures Earth's data in the C-radar band, and its polarity and dual-polarization capability allow quick data transmission from the satellite to the ground station (Sharifi et al., 2022). In this study, Sentinel 1C band data with vertical–vertical (VV) and vertical–horizontal (VH) in Interferometric Wide swath (IW) mode were used to assess the immediate change (Torres et al., 2012). First, it was downloaded from Copernicus Data Hub, available at https://scihub.copernicus.eu/dhus/#/home and later, the data was processed in SNAP software according to Çolak et al. (2021). Finally, ArcGIS Pro software was used for area calculation and mapping the output for both images (Segarra et al., 2022).

4.2.2. NDVI calculation

The Normalized Difference Vegetation Index (NDVI) is a widely used method to observe and measure the forest condition as well as changes caused by hazards like TCs (Cortés-Ramos et al., 2020). Therefore, it can be used as a critical indicator for remote sensing applications aimed at assessing forest disturbance. In general, NDVI values range from -1 to 1. NDVI values closer to +1 indicates healthier or dense vegetation. Conversely, a value close to 0 signifies scarce, or no vegetation, and negative NDVI values correspond to water areas (Delaporte et al., 2022). In this study, NDVI values were classified into 5 classes, also used in Aquino et al.'s (2018) study.

Analysis of satellite images became much more effective and efficient with the advent of Google Earth Engine, a powerful cloud computing platform (Çolak et al., 2021; Gorelick et al.,

2017). In this study, NDVI for Sundarbans mangrove forest was assessed in GEE using Sentinel-2A Level 1C product (Mondal et al., 2019). All the data were prepared before conducting NDVI analysis via atmospheric and radiometric correction. The areas of interest were selected using shapefiles to calculate NDVI for the required period. The NDVI was calculated using a year-over-year average (2019, 2021) in order to observe the gradual changes in the area of interest to obtain a better understanding of the health of the forest's vegetation before and after cyclone Amphan hit the Sundarbans. Fig. 4.2 illustrates the main steps followed in GEE where the required period

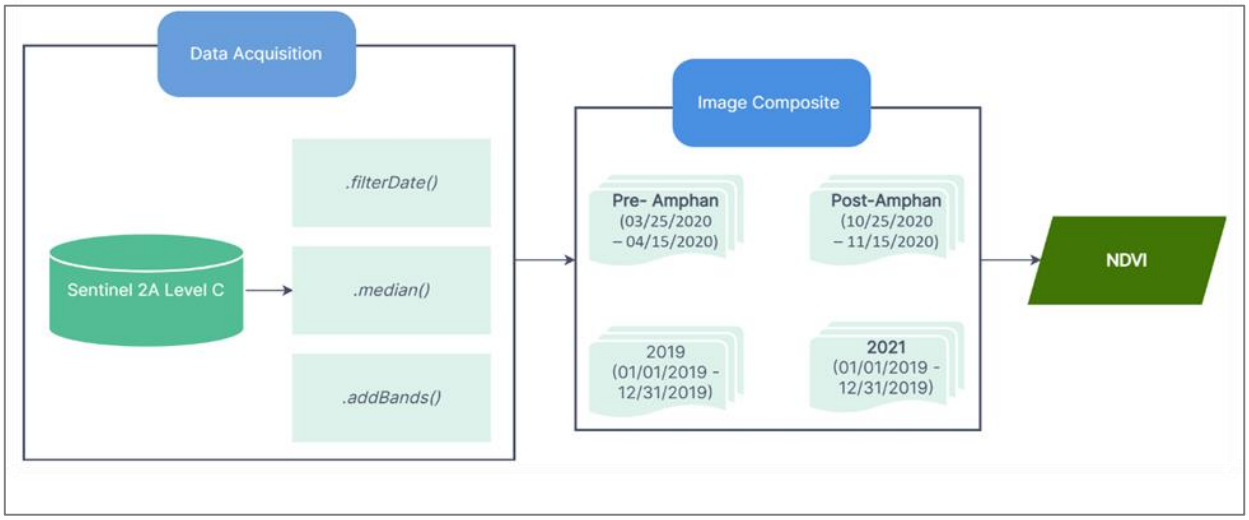

Fig. 4.2: Flowchart of NDVI analysis in GEE

images were filtered, and NDVI was performed for the Sundarbans mangrove forest using equation (1) (Rouse et al., 1974):

$$NDVI = \frac{NIR - RED}{NIR + RED} \quad (1)$$

For the Sentinel 2A satellite sensor, band 8 and band 4 are the NIR (near infrared) and RED bands.

4.2.3 mRFDI Calculation

The mRFDI is a revised version of the Radar Forest Degradation Index (RFDI), an approach used to track alteration in the composition and recovery in a forest (Chhabra et al., 2022; Çolak et al., 2021). Here sentinel 1 data was used to calculate mRFDI using the SNAP software, an open-source software developed by European Space Agency (Moskolaï et al., 2022). The data underwent preprocessing using the following steps in the graphic builder tool as depicted in Fig. 4.3. To correct the image edge noises caused by uneven topography during their generation; border noise was removed. Afterwards, it was calibrated in order to remove thermal noises and convert the data to Sigma-Not (σ°) value (Kumar, 2021). It was necessary to perform terrain correction in order to resolve distortion effects that were caused by the acquisition process. Values were converted from linear to decibel to enhance data visualization and analysis. Finally, the Subset tool in SNAP was selected to reduce the processing time (Fig 4.3). The following formula was employed for mRFDI (Çolak et al., 2021):

$$mRFDI = \frac{\sigma^{\circ}(VV) - \sigma^{\circ}(VH)}{\sigma^{\circ}(VV) + \sigma^{\circ}(VH)} \quad (2)$$

Here, this formula corresponds to the backscatter coefficient σ° (VV) for vertical polarization and the backscatter coefficient σ° (VH) for horizontal polarization.

In this study, pre-Amphan radar image was selected for May 7, 2020 and post-Amphan period image was collected for May 28, around one week before and after cyclone Amphan (May 16-21, 2020).

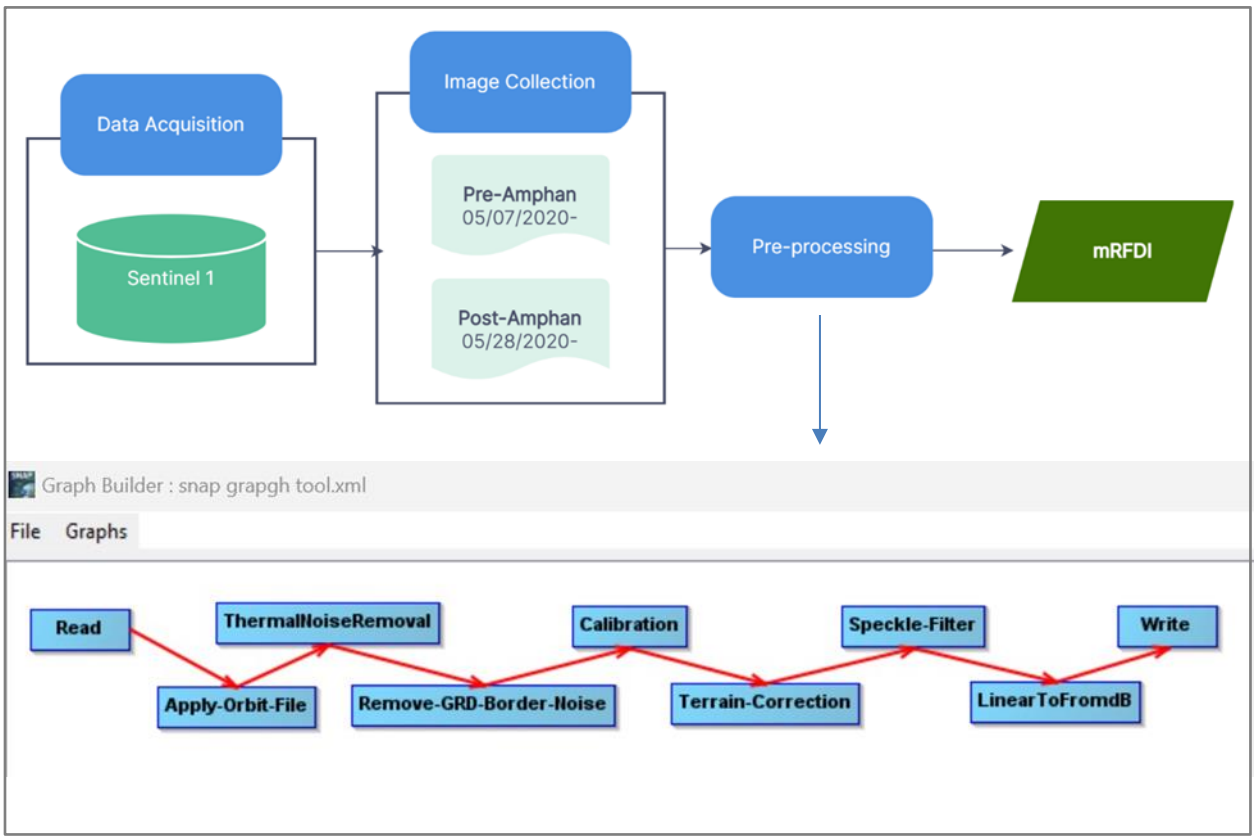

Fig 4.3: Flowchart of mRFDI analysis in SNAP

4.3 Results

4.3.1. Normalized Difference Vegetation Index (NDVI) in Sundarbans mangrove forest

4.3.1.1. Pre and post-Amphan NDVI

A composite value of 21 days was recorded for the NDVI during the pre-cyclonic period, ranging from -0.39 to 0.74. The northeastern part of the Sundarbans, which is located in Bangladesh, had reasonably healthy vegetation ($0.6 < NDVI \leq 0.8$). In contrast, the majority of the Sundarbans in India had notably lower NDVI values even before the landfall of cyclone Amphan. In the Sundarbans reserve forest in India, the vegetation was found to be of low health, with an NDVI value ranging from 0.2 to 0.4. On the other hand, the Khulna and Bagerhat districts of Bangladesh had a moderately high vegetation cover, with an NDVI value ranging

from 0.6 to 0.8 (Fig. 4.4).

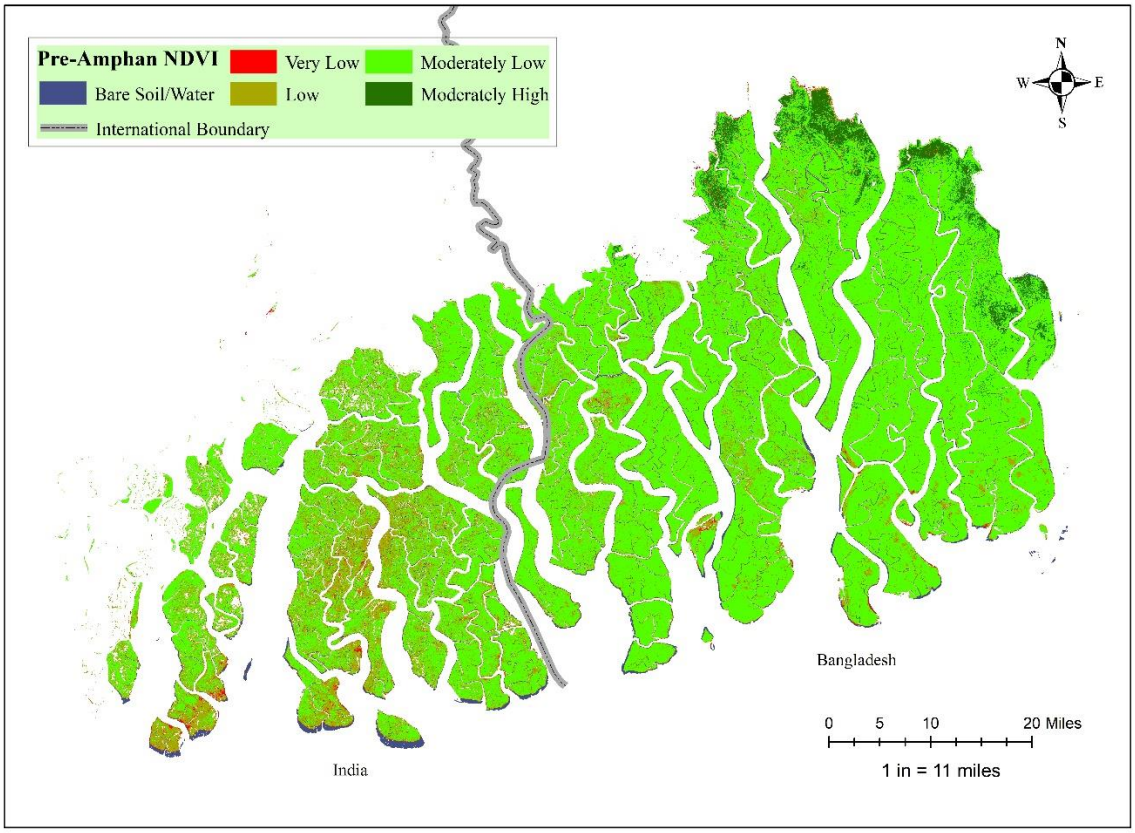

Fig 4.4: Pre-Amphan (03/25/2020 – 04/15/2020) period NDVI

The maximum area corresponded to Moderately Low NDVI, followed by Low NDVI, Bare Soil/ Water, Moderately High NDVI, and Very low NDVI (Table 4.1).

Table 4.1: Pre-Cyclonic period NDVI class areaa

Class Name	**NDVI Value**	**Area (sq. mi.)**
Bare soil/water	NDVI≤ 0	95.14
Very Low	0 <NDVI≤ 0.2	59.93
Low	0.2 <NDVI≤ 0.4	318.19

Moderately Low	0.4 <NDVI≤ 0.6	1802.28
Moderately High	0.6 <NDVI ≤ 0.8	78.32

Post-Amphan NDVI shows thriving vegetation in the Bangladesh part of the Sundarbans, mainly in the eastern part of Sundarbans (Fig 4.5). In the Indian part of the Sundarbans, although

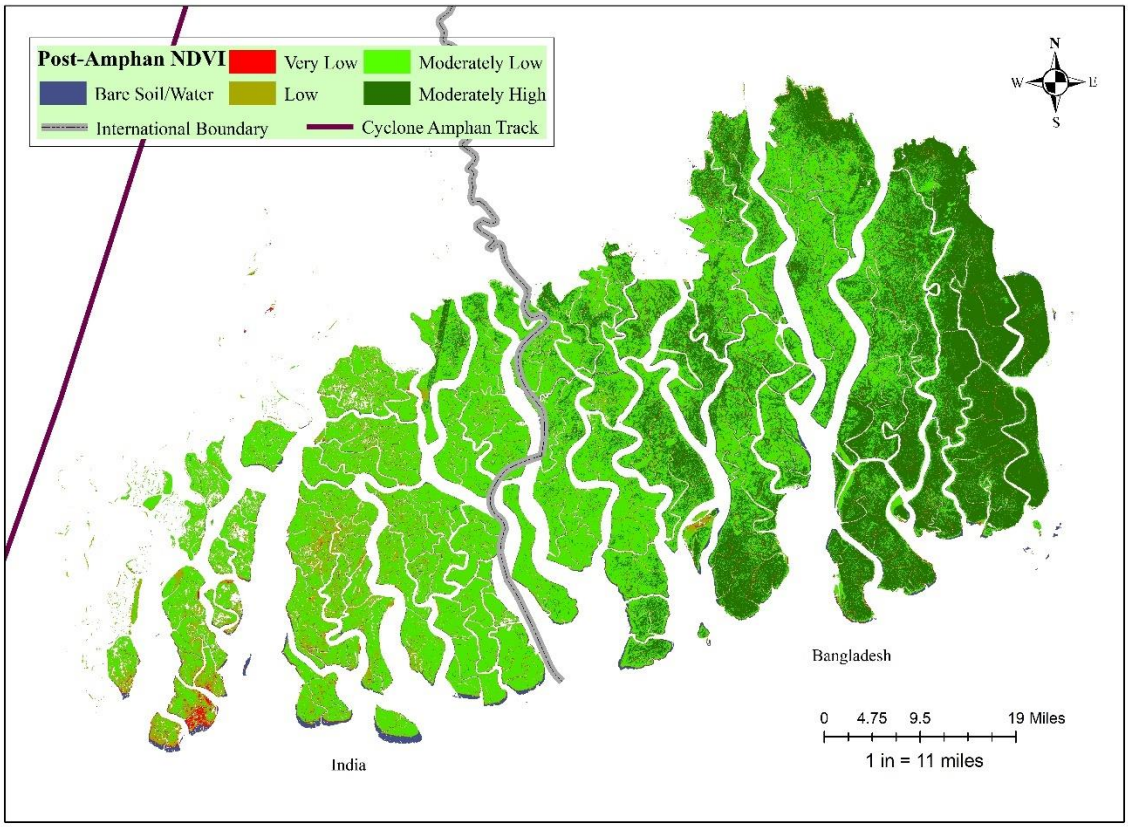

Fig 4.5: Post-Amphan (10/25/2020 – 11/15/2020) period NDVI

some improvement in vegetation health was noticed from the pre-Amphan period, NDVI value was still lower compared to the eastern part (Bangladesh part) of Sundarbans. The highest recorded NDVI value in the post-Amphan period was 0.76, which shows an increase from the pre-Amphan period. However, the lowest NDVI value was -0.39, the same as before the cyclone

hit Sundarbans. Near the cyclone track, degradation in vegetation was apparent. Almost the entire Sundarbans in the Pirojpur district, moderately high NDVI predominated (Fig. 4.5).

Table 4.2 indicates that most areas were occupied with moderately low vegetation, followed by moderately high, low, bare soil/water, and very low vegetation. Although a decrease in the area was noticed for bare soil, very low vegetation, low and moderately low vegetation, a sharp increase was observed in the moderately high NDVI class.

Table 4.2: Post-cyclonic period NDVI class area

Class Name	**NDVI Value**	**Area (sq. mi.)**
Bare soil/water	NDVI ≤ 0	78.29
Very Low	$0 < NDVI \leq 0.2$	57.08
Low	$0.2 < NDVI \leq 0.4$	136.52
Moderately Low	$0.4 < NDVI \leq 0.6$	1354.76
Moderately High	$0.6 < NDVI \leq 0.8$	754.25

Vegetation degradation was highly noticed in the thirty-mile buffer zone from the cyclone track (Fig. 4.6). While most of the forest remained unchanged, there was a visible loss near the track and places exposed to BoB. On the other hand, the density of moderately low vegetation has also increased remarkably because of the increase in low vegetation NDVI value. However, it was primarily in the eastern part, away from the track, and not exposed to BoB (Fig. 4.6).

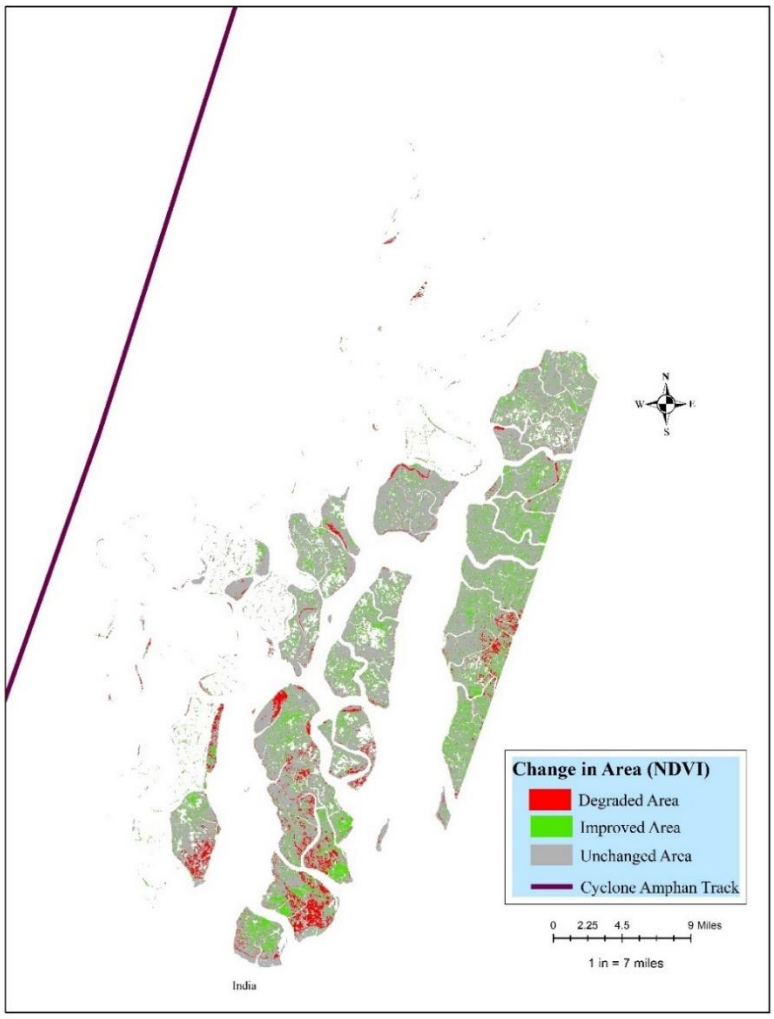

Fig 4.6: Change in NDVI from pre-Amphan to post-Amphan period

Table 4.3 represents the change in the area 30 miles away from the cyclone track. Although the results above showed that the vegetation health improved in 6 months, the overall damage was observed near the track. Roughly 17 sq miles of the area experienced degradation, and 42 sq miles of the area's vegetation showed an improvement within 30 sq miles from the cyclone path. The maximum degradation was recorded in moderately low vegetation, covering approximately 12 sq miles. However, a noticeable improvement of about 34% was seen in the low NDVI class after the cyclone (Table 4.3).

Table 4.3: Areal change in 30 miles from pre-Amphan to post-Amphan period

Change Type	**Total Area (sq. mi.)**	**Improvement/Degradation**
Very low- Low	4.8373	**Improvement**
Very low- Moderately Low	0.3635	
Low- Moderately High	0.0004	
Low- Moderately Low	34.2654	
Moderately Low- Moderately High	0.2410	
Bare soil/Water- Low	0.0184	
Bare soil/Water- Very Low	2.5349	
Bare soil/Water- Moderately Low	0.0004	
Total	**42.2613**	
Very low- Bare soil/Water	0.4888	**Degradation**
Low- Very low	3.7458	
Low- Bare soil/Water	0.0669	
Moderately Low- Low	12.1084	
Moderately Low- Very Low	0.6318	
Moderately Low- Bare soil/Water	0.0172	
Moderately High- Low	0.0038	
Moderately High- Very Low	0.0003	
Moderately High- Moderately Low	0.0594	
Total	**17.1224**	

4.3.1.4. Long-term Change in NDVI (2019 and 2021)

The annual average NDVI was calculated for the years 2019 and 2021. In both years, moderately low vegetation with an NDVI value of 0.4 - 0.6 dominated in Sundarbans, followed by an NDVI value of 0.2 -0.4, which represents unhealthy vegetation (Fig. 4.7). Fig. 4.7 represents that the low vegetation increased significantly. In contrast, moderately high vegetation showed a decline in 2021. The northeastern part of Bangladesh had moderately healthy biomass. However, in the later period, most of its area with an NDVI value of 0.6 - 0.8 was not identifiable in the NDVI map for 2021 because of a sharp decline. In both periods, Sundarbans mangrove was mostly moderately low NDVI dominated forest. Amphan struck this forest in 2020, and 1 year after the cyclone, most of the Indian Sundarbans part showed a decline in vegetation health, shifting from moderately low to low vegetation health.

The area coverage by different NDVI values in 2019 and 2021 are calculated and presented in Table 4.4. In 2019 and 2021, the largest area of the Sundarbans was attributed to moderately low vegetation. In 2019 moderately low NDVI was visible at 1,952 sq. mi., whereas in 2021, after the cyclone, it became 1,871 sq. mi. approximately (Table 4.4). An increase was noticed in very low and low vegetation too, after Amphan. However, a sharp decline was recorded in 2021, where moderately high vegetation decreased by around 93% compared to 2019, which has likely experienced severe damage.

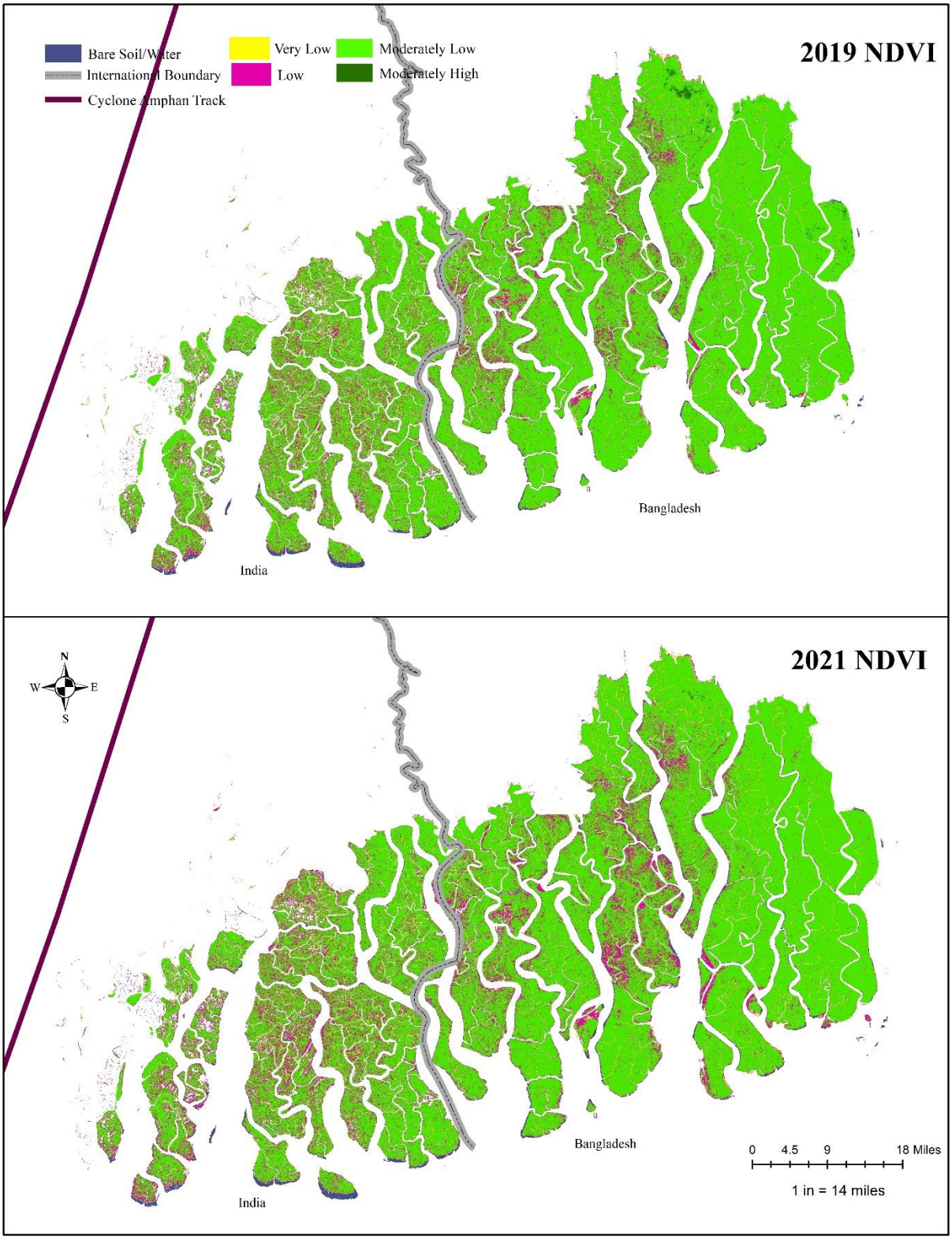

Fig 4.7: Yearly Average of NDVI (2019 and 2021)

Table 4.4: Annual Average of NDVI (2019 and 2021)

Class Name	**NDVI Value**	**2019 Area (sq. mi.)**	**2021 Area (sq. mi.)**
Bare soil/water	NDVI ≤ 0	80.8959	75.2760
Very Low	0 <NDVI ≤0.2	60.2108	73.2170
Low	0.2 <NDVI ≤0.4	271.3737	351.4841
Moderately Low	0.4 <NDVI ≤ 0.6	1951.5958	1871.3115
Moderately High	0.6 <NDVI ≤0.8	7.7794	0.5494

4.3.2. mRFDI

4.3.2.1. Pre-Amphan mRFDI

As seen in Figure 4.7, the May 20, 2020, image captured that most of the Sundarbans mangrove forest was degraded. Furthermore, it is evident that deforestation predominated in the Bangladesh part of northern Sundarbans, fringing the locality (Fig 4.8).

Table 4.5 shows that prior to when Amphan hit Sundarbans, the existing degraded forest area was around 1799 sq. mi., experiencing significant deforestation. A negligible portion of dense forest (~24%) was there within the mangrove region.

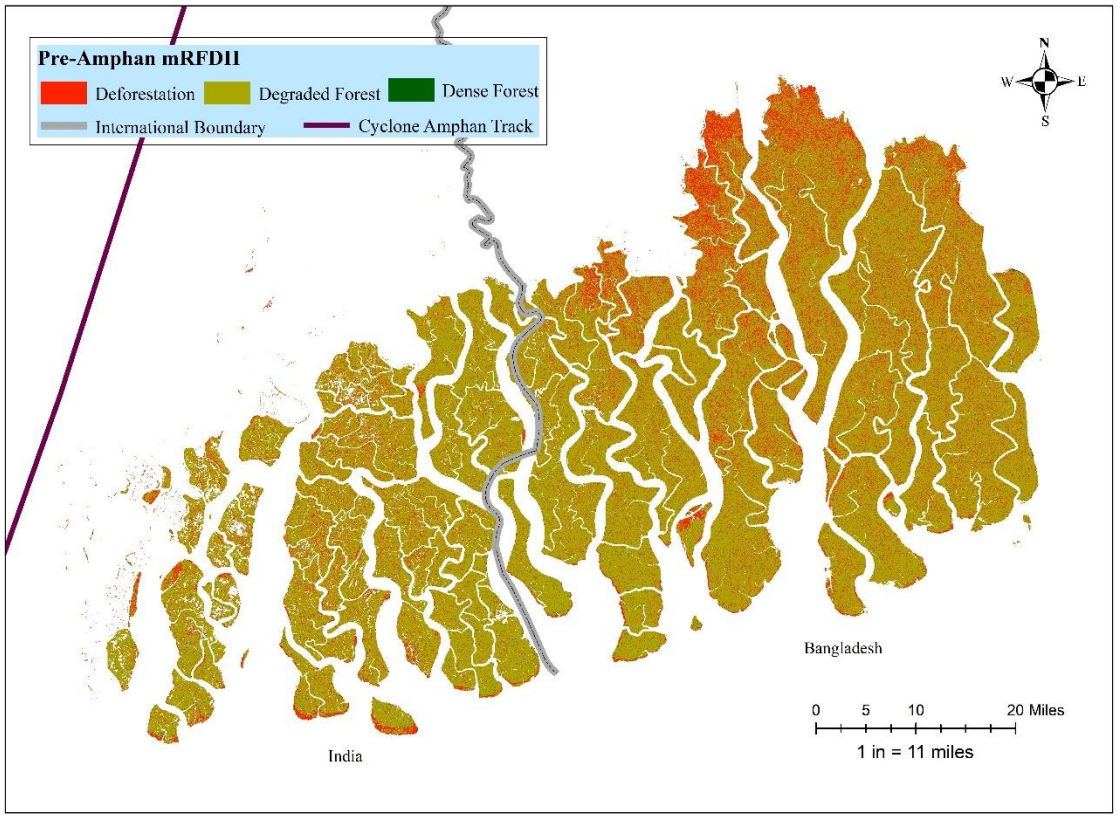

Fig 4.8: Pre-Amphan mRFDI

Table 4.5: Pre-Cyclonic period mRFDI class area

Class Name	**mRFDI Value**	**Area (sq. mi.)**
Dense Forest	< 0.3	23.7874
Degraded Forest	0.4 to 0.6	1798.9822
Deforestation	> 0.6	481.1357

4.3.2.2. Post-cyclonic mRFDI

Post- cyclonic index also shows a similar pattern to the pre-cyclonic period (Fig. 4.9).

The deforestation scenario was still existing in Bangladesh, but clusters of forested areas were more scattered than at the time before the cyclone hit. However, an increase in deforestation was observed near the cyclone's track in Figure 4.9, suggesting that the cyclone may have had a localized impact on the forest in that area.

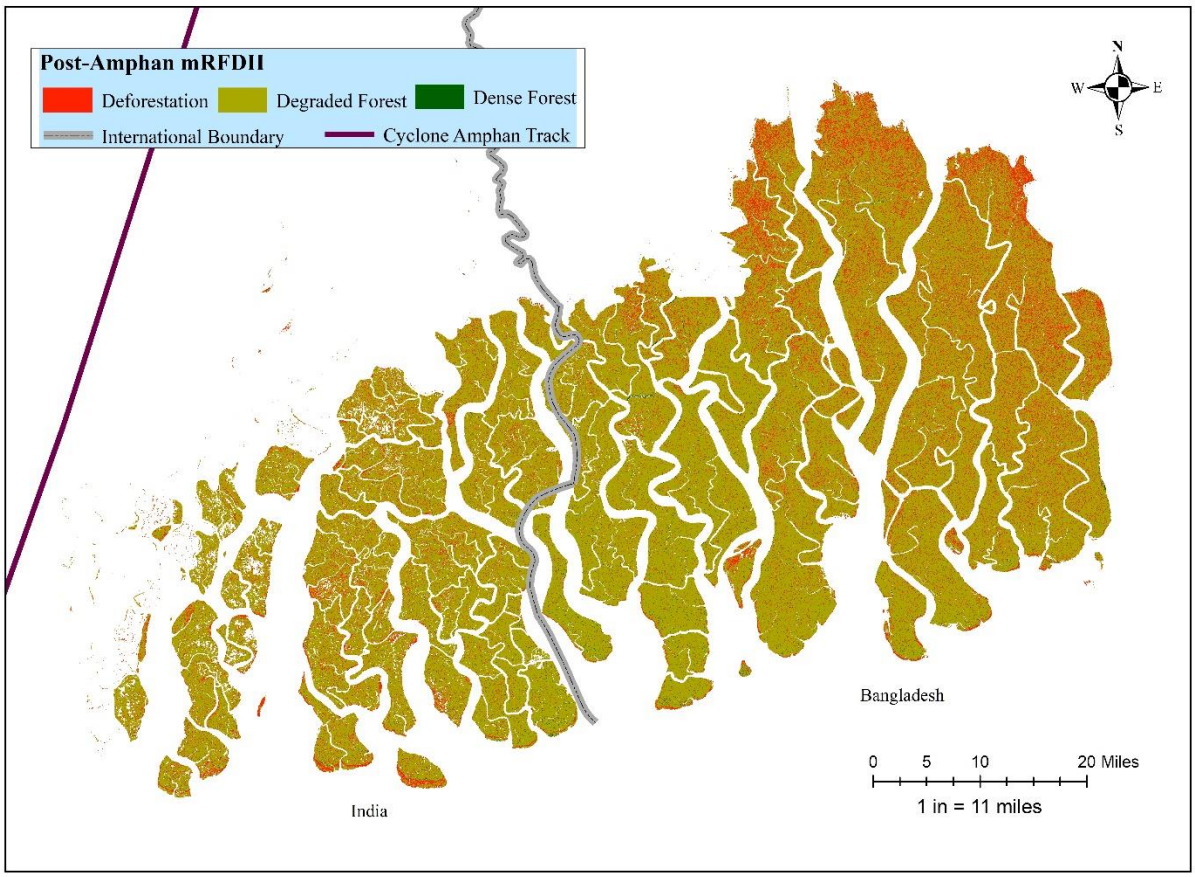

Fig 4.9: Post-Amphan mRFDI

Although the dense forest increased by ~10 sq miles and deforestation decreased by ~18%, around 75 sq mi. of forest were degraded in just 21 days (Table 4.6). Likewise pre-Amphan, most of the dominant area in the Sundarbans mangrove forest was attributed to the degraded forest, which was around 1874 sq. mi.

Table 4.6: Post-Cyclonic period mRFDI class area

Class Name	mRFDI Value	Area (sq. mi.)
Dense Forest	< 0.3	34.0159
Degraded Forest	0.4 to 0.6	1874.2471
Deforestation	> 0.6	395.8243

4.3.2.3. Change in the Forest in mRFDI Analysis

The north-western part of Sundarbans residing in Bangladesh showed some improvement in the forest condition. However, the northeastern part of Bangladesh still exhibited alarming

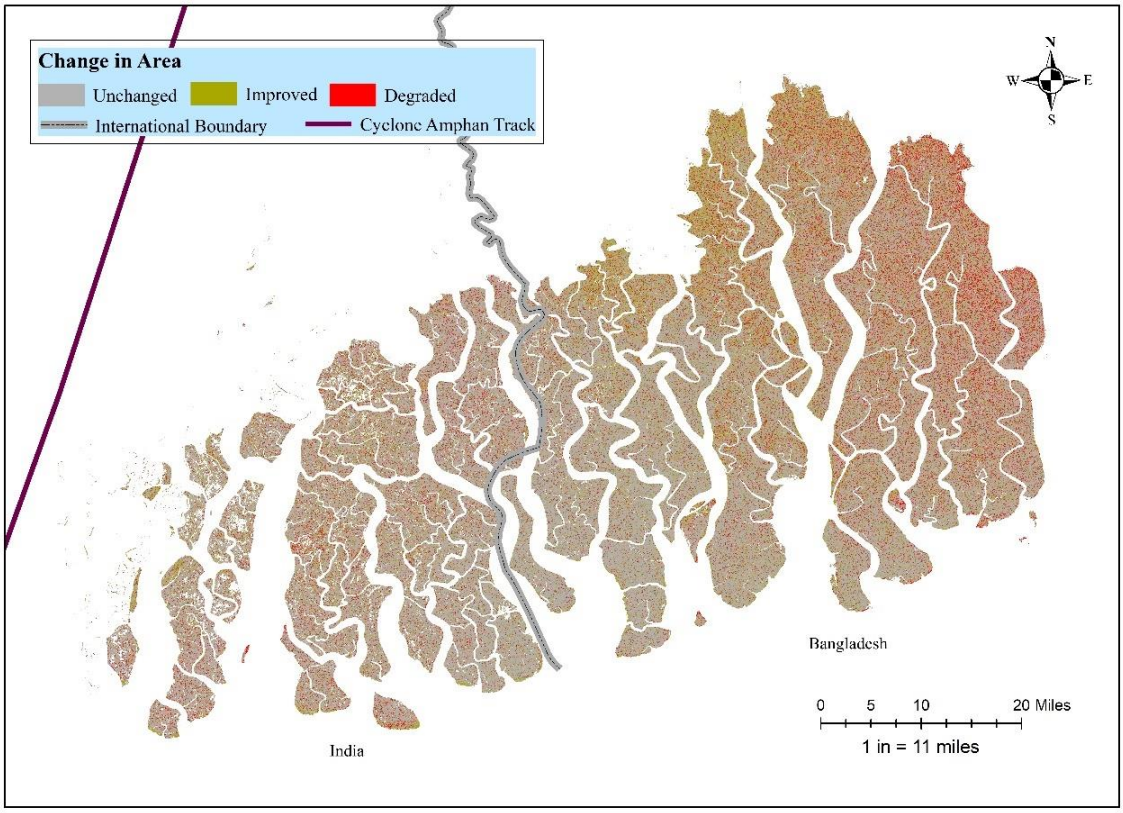

Fig 4.9: Change in mRFDI from Pre-Amphan to Post-Amphan period

results. Damage was scattered throughout the Indian part of Sundarbans; however, some areas experienced a substantial loss after cyclone Amphan (Fig. 4.9) but most of the areas remained unchanged.

From the pre-Amphan to post-Amphan period, there was some improvement in the forest, particularly the growth of degraded vegetation noticed in the deforested area (Table 4.7). However, while the deforested area showed some improvement, a decrease was also noticed in the existing degraded forest (Table 4.7).

Table 4.7: Areal change in 30 miles buffer from pre-Amphan to post-Amphan period

Change Type	**Total Area (sq. mi.)**	**Improvement/Degradation**
Degraded - Dense	26.9353	**Improvement**
Deforestation - Dense	5.5868	
Deforestation - Degraded	352.5475	
Total	**385.0696**	
Degraded - Deforestation	270.8826	**Degradation**
Dense- Degraded	19.7502	
Dense- Deforestation	2.7490	
Total	**293.3818**	

4.4 Discussion

4.4.1. Vegetation Health Analysis (NDVI)

The closest available satellite image for the pre-Amphan period with less than 10% cloud was from 03/25/2020 to 04/15/2020, one month before the cyclone hit Sundarbans. The post-

Amphan scenario showed an increase in vegetation health, and the image acquisition date was from 10/25/2020 to 11/15/2020, which was five months after cyclone Amphan. This significant time gap (6 months) is due to the unavailability of cloud-free images, which was also seen in the study of Mishra et al. (2021).

NDVI (Fig. 4.4) revealed that before Amphan, major mangrove vegetation cover in Sundarbans was in the class range of $0.4 < NDVI \leq 0.6$, which is consistent with the finding of Mishra et al. (2021). In addition, their study analyzed the immediate impact of Amphan on Sundarbans and found around 68% reduction in higher NDVI class value to lower NDVI. However, this study presents a contrasting result as the post-Amphan period was over four months compared to their post-Amphan period. Furthermore, more significant fragmentation happened in areas with moderately low NDVI values (Table 4.1 and 4.2), which signifies that sparse to less dense vegetation could not withstand the damage. Sen (2020) estimated that around 618 sq mi of Sundarbans was damaged, which validates the NDVI analysis for this study's pre and post-Amphan period, where the quantified forest damage was around 649 sq mi.

It is clearly seen from Fig. 4.6 that although there was some improvement after six months of the first analysis (pre-Amphan NDVI), the place near the cyclone track faced notable damage. A sharp increase was noticed in dense vegetation in the post-monsoon result. The monsoon period lasts in Bangladesh from June to October and June to September in India (NOAA, 2023a; World Bank, 2023). This might promote favorable conditions for regeneration. Gang et al. (2020) studied forest regeneration capability after several hurricanes struck, where they found that damaged canopy recovered after approximately one month of experiencing the hurricane. The season and time gap might influence the NDVI result significantly after six months of observing the Amphan impact on the forest.

The NDVI analysis is also influenced by soil moisture, which was lower during the pre-monsoon period than the post-monsoon period. During the high tide, if the land is inundated, an increase in soil moisture will occur. The post-monsoon period, when the second image was acquired, typically has higher soil moisture levels due to increased rainfall, which can lead to higher NDVI values. Therefore, the vegetation health in the catchment area of the cyclone trajectory, mainly in the southwestern part of the study area, deteriorated severely, which represents the damage where the cyclone's wind speed was 95 knot (NOAA, 2023b). Delaporte et al. (2022) also found a similar result where the damage was severe when the cyclonic wind speed was over 75 m/s and negligible at the place with 50 m/s cyclonic wind. Cortés-Ramos et al. (2020) found that NDVI value decreased in the heavy precipitation zone during TCs which can be another reason for this degradation. Figure 4.4 represents the presence of moderately high vegetation in Khulna and Bagerhat districts, where the tall mangrove trees are dominant and low NDVI dominating in the Sundarbans reserve forest in India, with canopy height ranging from 3-4 meters. An increase in very low NDVI value near the cyclone track was noticed after the cyclone, which indicates fragmentation due to the cyclone.

The long-term NDVI findings of this study reveal that the impact of cyclone Amphan was more evident in the long term. The year 2021 showed more abundance in low vegetation than the year before Amphan. A drastic decrease in healthy vegetation indicates the impact of cyclone Amphan. Moreover, all Indian parts of the Sundarbans showed degradation in long-term analysis.

4.4.2. Forest Degradation Analysis

As a prerequisite for rapid assessments, a high-resolution image from daily to monthly time scales is required as well as a high proportion of observations under clear skies but

Sundarbans have very high cloud cover associated with tropical climates, which is a critical factor (Islam, 2021). To address this challenge, the modified Radar Forest Degradation Index was analyzed using Sentinel 1 SAR image to detect changes due to cyclone Amphan in forest areas from 05/07/2020 to 05/28/2020. Both pre-and post Amphan image shows deforestation in northern and eastern Sundarbans in Bangladesh, which are *Heritiera fomes* and *Excoecaria agallocha* dominated zone, with the former being more susceptible to cyclonic wind and pressure than the latter in Sundarbans (Ghosh et al., 2016; Halder et al., 2021). The overall damage in Sundarbans was prevalent in the zones that are dominated by *Heritiera fomes*, *Excoecaria agallocha*, *Ceriops decandra* species which are overexploited because of timber, newspaper, match, and fuelwood, respectively (Gani, 2023; Ghosh et al., 2016).

The decline in degraded vegetation in 21 days from the pre-Amphan period to the post-Amphan period was noticed, which indicates the damage caused by the gusty wind, heavy rainfall, and storm surge of cyclone Amphan (Table 4.4 and 4.5). A positive result was noticed in dense forest and deforestation classes. This improvement is likely due to the monsoon season and less human intervention during the cyclone and COVID-19 period. No study was available on Sundarbans mangrove forest using mRFDI, which makes this novel, as well as challenging to compare the result.

4.5 Limitations of the Study

This study's approach, including the timeline, type of imagery used, and the extent of the study area, differs from those of other researchers who have investigated the impact of Cyclone Amphan on the Sundarbans mangrove forest. Consequently, it is not easy to directly compare the results of other studies, although many of the findings from the pre-Amphan period are consistent with previous research. It should be noted that validation is a critical component of

remotely sensed data, but in this case, ground truthing was not feasible due to time constraints. However, the study attempted to compare its results with those of other published studies. Furthermore, stating the forest was damaged solely because of cyclone Amphan is not possible because, before this event, many cyclones struck and damaged this forest, which will alter the result. Mangroves are a slow-growing ecosystem, so recovering the previous damage will take a considerable amount of time.

4.6. Conclusion

The Sundarbans mangrove forest not only plays a critical role in efforts to battle against climate change but also protects many marginalized people from extreme weather and provides them with a source of food and income. Unfortunately, because of its unique geographic position and ecological characteristics, the Sundarbans is especially susceptible to the destructive effects of severe storms. Throughout the study period, the Indian mangrove forest consistently displayed poor conditions than the Bangladesh part, which was also seen in the study of GMW, where the mangrove in Bangladesh has expanded by about 14 sq mi, and in India, the extent of mangrove shrunk by around 17 sq mi. between 2019-2020. The damage caused by Cyclone Amphan highlights the vulnerability of mangrove forests to tropical cyclones and the importance of remote sensing techniques in monitoring and assessing the damage. Even though several conservation planning initiatives have been undertaken by governmental organizations (e.g., the Bangladesh Forest Department) to protect mangrove ecosystems, Sundarbans are being deforested due to a lack of law enforcement in both countries. The result of mRFDI with Sentinel-1 SAR data can be valuable in detecting human intervention and disturbance. Using these approaches, sustainable development strategies can be improved, and conservation initiatives can be improved to lessen the impact of cyclones in the future.

References

Ahmed, R., Mohapatra, M., Dwivedi, S., & Giri, R. K. (2021). Characteristic features of Super Cyclone 'AMPHAN'- observed through satellite images. *Tropical Cyclone Research and Review*, *10*(1), 16–31. https://doi.org/10.1016/j.tcrr.2021.03.003

Alongi, D. M. (2002). Present state and future of the world's mangrove forests. *Environmental Conservation*, *29*(3), 331–349. https://doi.org/10.1017/S0376892902000231

Andersen, M. (2023). Loss of Mexico's Valuable Mangrove Forests.

Aquino, D. do N., Neto, O. C. da R., Moreira, M. A., Teixeira, A. dos S., & de Andrade, E. M. (2018). Use of remote sensing to identify areas at risk of degradation in the semi-arid region. *Revista Ciencia Agronomica*, *49*(3), 420–429. https://doi.org/10.5935/1806-6690.20180047

Baishya, S., Banik, S. K., Choudhury, M. D., Das Talukdar, D., & Das Talukdar, A. (2020). Therapeutic potentials of littoral vegetation: an antifungal perspective. *Biotechnological Utilization of Mangrove Resources*, 275–292). https://doi.org/10.1016/B978-0-12-819532-1.00011-1

Beck, M., & Menéndez, P. (2020). Protecting Mangroves Can Prevent Billions of Dollars in Global Flooding Damage Every Year.

Beck, M. W., Narayan, S., Trespalacios, D., Pfliegner, K., Losada, I. J., Menéndez, P., Espejo, A., Torres, S., Díaz-Simal, P., Fernandez, F., Abad, S., Mucke, P., & Kirch, L. (2018). *The Global Value of Mangroves for Risk Reduction*. https://doi.org/10.7291/V9930RBC

Bhowmik, A. K., & Cabral, P. (2013). Cyclone Sidr Impacts on the Sundarbans Floristic Diversity. *Earth Science Research*, *2*(2). https://doi.org/10.5539/esr.v2n2p62

Buitre, M. J. C., Zhang, H., & Lin, H. (2019). The mangrove forests change and impacts from

tropical cyclones in the philippines using time series satellite imagery. *Remote Sensing*, *11*(6). https://doi.org/10.3390/RS11060688

C2ES. (2023). Hurricanes and Climate Change.

Carugati, L., Gatto, B., Rastelli, E., Lo Martire, M., Coral, C., Greco, S., & Danovaro, R. (2018). Impact of mangrove forests degradation on biodiversity and ecosystem functioning. *Scientific Reports*, *8*(1). https://doi.org/10.1038/s41598-018-31683-0

Chand, S. S., Walsh, K. J. E., Camargo, S. J., Kossin, J. P., Tory, K. J., Wehner, M. F., Chan, J. C. L., Klotzbach, P. J., Dowdy, A. J., Bell, S. S., Ramsay, H. A., & Murakami, H. (2022). Declining tropical cyclone frequency under global warming. *Nature Climate Change*, *12*(7), 655–661. https://doi.org/10.1038/s41558-022-01388-4

Chhabra, A., Rüdiger, C., Yebra, M., Jagdhuber, T., & Hilton, J. (2022). RADAR-Vegetation Structural Perpendicular Index (R-VSPI) for the Quantification of Wildfire Impact and Post-Fire Vegetation Recovery. *Remote Sensing*, *14*(13). https://doi.org/10.3390/rs14133132

Çolak, E., Chandra, M., & Sunar, F. (2021). The use of sentinel 1/2 vegetation indexes with gee time series data in detecting land cover changes in the sinop nuclear power plant construction site. *International Archives of the Photogrammetry, Remote Sensing and Spatial Information Sciences - ISPRS Archives*, *43*(B3-2021), 701–706. https://doi.org/10.5194/isprs-archives-XLIII-B3-2021-701-2021

Cortés-Ramos, J., Farfán, L. M., & Herrera-Cervantes, H. (2020). Assessment of tropical cyclone damage on dry forests using multispectral remote sensing: The case of Baja California Sur, Mexico. *Journal of Arid Environments*, *178*. https://doi.org/10.1016/j.jaridenv.2020.104171

Dasgupta, S., Islam, M. S., Huq, M., Khan, Z. H., & Hasib, M. R. (2019). Quantifying the protective capacity of mangroves from storm surges in coastal Bangladesh. *PLoS ONE*, *14*(3). https://doi.org/10.1371/journal.pone.0214079

Delaporte, B., Ibanez, T., Despinoy, M., Mangeas, M., & Menkes, C. (2022). Tropical Cyclone Impact and Forest Resilience in the Southwestern Pacific. *Remote Sensing*, *14*(5). https://doi.org/10.3390/rs14051245

Donato, D. C., Kauffman, J. B., Murdiyarso, D., Kurnianto, S., Stidham, M., & Kanninen, M. (2011). Mangroves among the most carbon-rich forests in the tropics. *Nature Geoscience*, *4*(5), 293–297. https://doi.org/10.1038/ngeo1123

Drusch, M., Del Bello, U., Carlier, S., Colin, O., Fernandez, V., Gascon, F., Hoersch, B., Isola, C., Laberinti, P., Martimort, P., Meygret, A., Spoto, F., Sy, O., Marchese, F., & Bargellini, P. (2012). Sentinel-2: ESA's Optical High-Resolution Mission for GMES Operational Services. *Remote Sensing of Environment*, *120*, 25–36. https://doi.org/10.1016/j.rse.2011.11.026

Dutta, D., Das, P. K., Paul, S., Sharma, J. R., & Dadhwal, V. K. (2015). Assessment of ecological disturbance in the mangrove forest of Sundarbans caused by cyclones using MODIS time-series data (2001–2011). *Natural Hazards*, *79*(2), 775–790. https://doi.org/10.1007/s11069-015-1872-x

Ellison, J. C. (2015). Vulnerability assessment of mangroves to climate change and sea-level rise impacts. *Wetlands Ecology and Management*, *23*(2), 115–137. https://doi.org/10.1007/s11273-014-9397-8

ESA. (2023). SENTINEL-2 MISSION GUIDE.

FAO. (2020). Global Forest Resources Assessment 2020: Main report. *Global Forest Resources*

Assessment 2020. https://doi.org/10.4060/ca9825en

Feller, I. C., Friess, D. A., Krauss, K. W., & Lewis, R. R. (2017). The state of the world's mangroves in the 21st century under climate change. *Hydrobiologia*, *803*(1). https://doi.org/10.1007/s10750-017-3331-z

Friess, D. A., Rogers, K., Lovelock, C. E., Krauss, K. W., Hamilton, S. E., Lee, S. Y., Lucas, R., Primavera, J., Rajkaran, A., & Shi, S. (2019). The State of the World's Mangrove Forests: Past, Present, and Future. *Annual Review of Environment and Resources*, *44*(1), 89–115. https://doi.org/10.1146/annurev-environ-101718-033302

Gang, C., Pan, S., Tian, H., Wang, Z., Xu, R., Bian, Z., Pan, N., Yao, Y., & Shi, H. (2020). Satellite observations of forest resilience to hurricanes along the northern Gulf of Mexico. *Forest Ecology and Management*, *472*. https://doi.org/10.1016/j.foreco.2020.118243

Gani, M. O. (2023). Tree Stand Improvement Initiatives for Increasing Tree Resources of Bangladesh Ssundarbans.

Ghosh, M. K., Kumar, L., & Roy, C. (2016). Mapping long-term changes in mangrove species composition and distribution in the Sundarbans. *Forests*, *7*(12). https://doi.org/10.3390/f7120305

Giri, C. (2021). Recent advancement in mangrove forests mapping and monitoring of the world using earth observation satellite data. *Remote Sensing*, *13*(4), 1–6). https://doi.org/10.3390/rs13040563

Gopal, B., & Chauhan, M. (2006). Biodiversity and its conservation in the Sundarban mangrove ecosystem. *Aquatic Sciences*, *68*(3), 338–354. https://doi.org/10.1007/s00027-006-0868-8

Gorelick, N., Hancher, M., Dixon, M., Ilyushchenko, S., Thau, D., & Moore, R. (2017). Google

Earth Engine: Planetary-scale geospatial analysis for everyone. *Remote Sensing of Environment*, *202*, 18–27. https://doi.org/10.1016/j.rse.2017.06.031

Guo, Y., Jia, X., & Paull, D. (2017). Superpixel-Based Adaptive Kernel Selection for Angular Effect Normalization of Remote Sensing Images With Kernel Learning. *IEEE Transactions on Geoscience and Remote Sensing*, *55*(8), 4262–4271. https://doi.org/10.1109/TGRS.2017.2689798

Gupta, J., Basu, J., & Soeb, Z. R. (2019). Bangladesh: Sundarbans Mangroves Save Bengal from Cyclone Bulbul. *UNDRR*.

Halder, N. K., Merchant, A., Misbahuzzaman, K., Wagner, S., & Mukul, S. A. (2021). Why some trees are more vulnerable during catastrophic cyclone events in the Sundarbans mangrove forest of Bangladesh? *Forest Ecology and Management*, *490*, 119117. https://doi.org/10.1016/j.foreco.2021.119117

Hochard, J. P., Hamilton, S., & Barbier, E. B. (2019). Mangroves shelter coastal economic activity from cyclones. *Proceedings of the National Academy of Sciences of the United States of America*, *116*(25), 12232–12237. https://doi.org/10.1073/pnas.1820067116

Islam, A. M. (2021). Tracking Cyclonic (Sidr) Impact and Recovery Rate of Mangrove Forest Using Remote Sensing: A Case Study of the Sundarbans, Bangladesh. Kent State University.

IUCN. (2010). Mangrove forests in worldwide decline.

Kellndorfer, J. (2019). Using SAR Data for Mapping Deforestation and Forest Degradation. *The Synthetic Aperture Radar (SAR) Handbook: Comprehensive Methodologies for Forest Monitoring and Biomass Estimation*.

Khan, Z. H., Environment, B., Zakir, M., & Khan, H. (2016). Disaster Impact on Sundarbans -A

Case Stusy on Sidr Affected Area. 5–12. https://www.researchgate.net/publication/310446619

Knutson, T. R., Chung, M. V, Vecchi, G., Sun, J., Hsieh, T.-L., & Smith, A. J. P. (2021). Climate change is probably increasing the intensity of tropical cyclones.

Kossin, J. P., Knapp, K. R., Olander, T. L., & Velden, C. S. (2020). Global increase in major tropical cyclone exceedance probability over the past four decades. *Atmospheric, And Planetary Sciences*, *117*(22). https://doi.org/10.1073/pnas.1920849117/-/DCSupplemental

Krauss, K. W., & Osland, M. J. (2019). Tropical cyclones and the organization of mangrove forests: a review. *Annals of Botany*. https://doi.org/10.1093/aob/mcz161

Kumar, D. (2021). Urban objects detection from C-band synthetic aperture radar (SAR) satellite images through simulating filter properties. *Scientific Reports*, *11*(1). https://doi.org/10.1038/s41598-021-85121-9

Kumar, S., Lal, P., & Kumar, A. (2021). Influence of Super Cyclone "Amphan" in the Indian Subcontinent amid COVID-19 Pandemic. *Remote Sensing in Earth Systems Sciences*, *4*(1–2), 96–103. https://doi.org/10.1007/s41976-021-00048-z

Lima, B. de N. G., Cunha-Lignon, M., & Galvani, E. (2021). Microclimatic analysis of mangroves in two distinct categories of Protected Areas and conserved status. *Sociedade & Natureza*, *33*. https://doi.org/10.14393/SN-v33-2021-57483

Massel, S. R., Furukawa, K., & Brinkman, R. M. (1999). Surface wave propagation in mangrove forests. *Fluid Dynamics Research*, *24*, 219–249. http://www.iop.org/journals/FDR

Menéndez, P., Losada, I. J., Torres-Ortega, S., Narayan, S., & Beck, M. W. (2020). The Global Flood Protection Benefits of Mangroves. *Scientific Reports*, *10*(1).

https://doi.org/10.1038/s41598-020-61136-6

Mishra, M., Acharyya, T., Santos, C. A. G., Silva, R. M. da, Kar, D., Mustafa Kamal, A. H., & Raulo, S. (2021). Geo-ecological impact assessment of severe cyclonic storm Amphan on Sundarban mangrove forest using geospatial technology. *Estuarine, Coastal and Shelf Science*, *260*. https://doi.org/10.1016/j.ecss.2021.107486

Mitchell, A. L., Rosenqvist, A., & Mora, B. (2017). Current remote sensing approaches to monitoring forest degradation in support of countries measurement, reporting and verification (MRV) systems for REDD+. *Carbon Balance and Management*, *12*(1). https://doi.org/10.1186/s13021-017-0078-9

MoEF. (2010). Integrated Resources Management Plan for the Sundarbans. http://bfis.bforest.gov.bd/library/integrated-resource-management-plans-for-the-sundarbans-2010-2020-volume-1/

Mondal, P., Dutta, T., Qadir, A., & Sharma, S. (2022). Radar and optical remote sensing for near real-time assessments of cyclone impacts on coastal ecosystems. *Remote Sensing in Ecology and Conservation*, *8*(4), 506–520. https://doi.org/10.1002/rse2.257

Mondal, P., Liu, X., Fatoyinbo, T. E., & Lagomasino, D. (2019). Evaluating combinations of sentinel-2 data and machine-learning algorithms for mangrove mapping in West Africa. *Remote Sensing*, *11*(24). https://doi.org/10.3390/rs11242928

Moskolaï, W. R., Abdou, W., Dipanda, A., & Kolyang. (2022). A Workflow for Collecting and Preprocessing Sentinel-1 Images for Time Series Prediction Suitable for Deep Learning Algorithms. *Geomatics*, *2*(4), 435–456. https://doi.org/10.3390/geomatics2040024

NOAA. (2023a). Indian summer monsoon.

NOAA. (2023b). HISTORICAL HURRICANE TRACKS.

Rahman, M. M., Rahman, M. M., & Islam, K. S. (2010). The Causes of Deterioration of Sundarban Mangrove Forest Ecosystem of Bangladesh: Conservation and Sustainable Management Issues. https://www.researchgate.net/publication/210196055

Rahman, S., & Khanum, R. (2017). The impact of cyclone aila on the sundarban forest ecosystem. www.ceserp.com/cp-jour

Reef, R., & Lovelock, C. E. (2015). Regulation of water balance in Mangroves. *Annals of Botany*,*115*(3), 385–395. https://doi.org/10.1093/aob/mcu174

Reliefweb. (2019). Cyclone Bulbul a month on: the impact on Bangladesh's coastal communities.

Rouse, J. W., Haas, Jr. R. H., Schell, J. A., & Deering, D. W. (1974). Monitoring Vegetaiton Systems in the Great Plains with Erts. https://ntrs.nasa.gov/citations/19740022614

Segaran, T. C., Azra, M. N., Lananan, F., Burlakovs, J., Vincevica-Gaile, Z., Rudovica, V., Grinfelde, I., Rahim, N. H. A., & Satyanarayana, B. (2023). Mapping the Link between Climate Change and Mangrove Forest: A Global Overview of the Literature. *Forests*, *14* (2). https://doi.org/10.3390/f14020421

Segarra, J., Araus, J. L., & Kefauver, S. C. (2022). Farming and Earth Observation: Sentinel-2 data to estimate within-field wheat grain yield. *International Journal of Applied Earth Observation and Geoinformation*, *107*. https://doi.org/10.1016/j.jag.2022.102697

Sen, S. (2020). Sundarbans Mangroves, Post Amphan: An Overview. www.ijcrt.org

SentinelHub. (2023). Sentinel-2 L1C.

Sharifi, A., Felegari, S., & Tariq, A. (2022). Mangrove forests mapping using Sentinel-1 and Sentinel-2 satellite images. *Arabian Journal of Geosciences*, *15*(20).

https://doi.org/10.1007/s12517-022-10867-z

Spalding, M., McIvor, A., Tonneijck, F. H., Tol, S., & van, E. P. (2014). Mangroves for coastal defence. Guidelines for coastal managers & policy makers. www.nature.org.

Thomas, N., Lucas, R., Bunting, P., Hardy, A., Rosenqvist, A., & Simard, M. (2017). Distribution and drivers of global mangrove forest change, 1996-2010. *PLoS ONE*, *12*(6). https://doi.org/10.1371/journal.pone.0179302

Torres, R., Snoeij, P., Geudtner, D., Bibby, D., Davidson, M., Attema, E., Potin, P., Rommen, B., Floury, N., Brown, M., Traver, I. N., Deghaye, P., Duesmann, B., Rosich, B., Miranda, N., Bruno, C., L'Abbate, M., Croci, R., Pietropaolo, A., Rostan, F. (2012). GMES Sentinel-1 mission. *Remote Sensing of Environment*, *120*, 9–24. https://doi.org/10.1016/j.rse.2011.05.028

Valle, A. del, Eriksson, M., Ishizawa, O. A., & Miranda, J. J. (2019). Mangroves protect coastal economic activityfrom hurricanes. *PNAS*, *117*(1), 265–270. https://doi.org/https://doi.org/10.3886/E115611V1

Winterwerp, J. C., Albers, T., Anthony, E. J., Friess, D. A., Mancheño, A. G., Moseley, K., Muhari, A., Naipal, S., Noordermeer, J., Oost, A., Saengsupavanich, C., Tas, S. A. J., Tonneijck, F. H., Wilms, T., Van Bijsterveldt, C., Van Eijk, P., Van Lavieren, E., & Van Wesenbeeck, B. K. (2020). Managing erosion of mangrove-mud coasts with permeable dams – lessons learned. *Ecological Engineering*, *158*. https://doi.org/10.1016/j.ecoleng.2020.106078

World Bank. (2023). Current Climate.

Zhang, K., Liu, H., Li, Y., Xu, H., Shen, J., Rhome, J., & Smith, T. J. (2012). The role of mangroves in attenuating storm surges. *Estuarine, Coastal and Shelf Science*, *102–103*,

11–23. https://doi.org/10.1016/j.ecss.2012.02.021

CHAPTER 5

SUMMERY AND CONCLUSION

5.1 Conclusions

TCs are a global threat, particularly for the communities residing along the coastal areas. The study analyzes the detailed spatial pattern of tropical cyclone risk with the most up-to-date available data for the entire coast of Bangladesh. The study employed a range of techniques to build the composite risk map, including the PCA analysis, which was used to construct a social vulnerability index to assess social vulnerability. The physical vulnerability was quantified by the AHP method and geospatial techniques to construct an integrated tropical cyclone risk map in the coastal areas of Bangladesh. Additionally, vegetation indices (NDVI, mRFDI) were performed to detect the change induced by a tropical cyclone in the Sundarbans mangrove forest of Bangladesh. This social and physical vulnerability assessment incorporated a wide range of variables.

The significant outcomes from this research were: both the inland and exposed coast communities are socially vulnerable. At the county level, vulnerability varied more on the western and central coast than on the eastern coast. The study highlights that around 8% of upazilas (same as the county in the US) along the coast were in a range of high to very high vulnerability, and cyclonic risk all along the coast increased without considering social vulnerability parameters. However, with and without incorporating social vulnerability, areas on the central coast were at higher risk of the adverse impact of TCs, which highlights the contribution of Sundarbans mangrove forest as a bio-shield on the western coast. Social

vulnerability for Feni upazila was very high, whereas the risk considering only physical criteria in that place varied from moderate to very high. On the contrary, another upazila with very high social vulnerability, namely Narail, showed very low to low physical risk, the Indian mangrove forest consistently exhibited poor conditions than the Bangladesh portion, and the short-term radar data and long-term optical data indicated the damage done by cyclone Amphan.

5.2 Limitations of the Study

The key constraint of this study is the unavailability of the updated census data which was used to construct the social vulnerability index. Further, the study area lacks information regarding the spatial distribution of rainfall and storm surge height triggered by tropical cyclones. Also, the information regarding the capacity and facilities of cyclone shelters and health centers is not up to date. Moreover, no drone data was available for the Sundarbans mangrove forest which could be of great use to analyze the destruction of cyclone Amphan.

Notwithstanding these limitations, this work certainly contributes to existing knowledge in the field of TCs by providing insight into the degree of individual risk components and the integrated spatial distribution of TCs risk in the coastal settings of Bangladesh. As far as the author is aware, this is the only empirical study for the entire coast that examines the comprehensive distribution of tropical cyclone risks with regard to both social and physical vulnerability using a multi-criteria decision-making technique.

5.3 Recommendations

Although this study has some limitations, it provides a realistic depiction of the existing vulnerability of coastal Bangladesh. The probable cyclone mitigation measure can be used to increase the cyclone shelter and health facility and promote afforestation initiatives in more vulnerable and exposed zones. Unlike the developed world, property insurances in developing

countries are not a common practice, which increases the suffering in the post-cyclone period. This study can help identify the risky areas to implement possible mitigation measures. The misery of the coastal communities of Bangladesh because of natural disasters like tropical cyclones can be mitigated through proper relief distribution during the post-cyclonic period. Unfortunately, three warehouses to store reliefs are in Khulna district (western coast), Chittagong district (eastern coast), and Dhaka (outside coast). This study's spatial information can help establish relief warehouses in the more vulnerable areas, particularly on the central coast. Furthermore, the findings of this study can serve as a guideline for mapping coastal vulnerability, and risk. Emergency responders and authorities could utilize the information in preparing effective cyclone mitigation plans. Future works may include more mitigation capacity indicators and quantitative analysis on the role of Sundarbans mangrove forest in attenuating tropical cyclones intensity.